國 立 交 通 大 學

工學院精密與自動化工程學程

碩 士 論 文

操控性橢圓理論於兩足機器人步態規劃之
應用研究

The Study on the Gait Generation of Biped Robot Using the
Manipulability Ellipsoid Algorithm

研 究 生 ： 李 駿 榮

指導教授 ： 鄭 璧 瑩 博士

中華民國 九十五 年 六 月

操控性橢圓理論於兩足機器人步態規劃之應用研究

The Study on the Gait Generation of Biped Robot Using the Manipulability Ellipsoid Algorithm

研 究 生：李駿榮　　　　Student：Jiung-Rong Lee

指導教授：鄭璧瑩 博士　Advisor：Dr. Pi-Ying Cheng

國 立 交 通 大 學

工學院精密與自動化工程學程

碩 士 論 文

A Thesis
Submitted to Degree Program of Automation and Precision Engineering
College of Engineering
National Chiao Tung University
in Partial Fulfillment of the Requirements
for the Degree of
Master of Science
in
Automation and Precision Engineering
November 2005
Hsinchu, Taiwan, Republic of China

中華民國九十五年六月

操控性橢圓理論於兩足機器人步態規劃之應用研究

研究生：李駿榮　　　　　　　　　　　　指導教授：鄭 璧 瑩 博士

國立交通大學工學院精密與自動化工程學程

摘要

本論文以具有十個自由度之空間並聯式機構模擬 KHR-1 兩足機器人之下半身，並以操控性橢圓理論為核心，設計並模擬兩足機器人由蹲姿轉換至直立站姿及由站立姿態開始完成以兩左右跨步為一基礎步伐組之關節運動軌跡做為範例，進行電腦輔助軌跡規劃法的研發。在以程式完成軌跡設計後，透過控制器的數據傳輸介面將關節運動軌跡數據轉入 KHR-1 兩足機器人控制系統中，並藉由機器人執行動作範例以驗證理論推導之關節運動軌跡之實用性與穩定性。本研究所建立的兩足機器人步態規劃之流程，可簡化傳統程序的繁瑣耗時，同時提供一較為穩定可靠之動作模式。本研究所提出的方法為先推導出終端效應器特定點在卡氏座標中之線速度單位圓與關節角速度橢圓之對應轉換模型，經由計算找出終端效應器在往某特定方向移動時所對應各關節驅動器之最小角速度組合，以此最小角速度組合做為機械手作動規劃時之依據。本研究所採用的原理，在靜力學之觀點來看，每一單位時間間隔之角加速度變化較小。這

使得兩足機器人運作時能獲得較高之穩定性。在機器人的姿態平衡的維持方面，關節角位移的計算規劃時輔以零矩點理論(Zero-Moment Point)建立機器人平衡機制。應用零矩點理論在兩足機器人的運動平衡控制方面，為維持機器人姿態對地面形成之合作用力向量通過零矩點且作用力接觸座標落在單腳腳底或雙腳間區域內便能使機器人獲得穩定的運動與姿態。本論文提出以操控性橢圓理論及零矩點理論作為核心概念建立輔助規劃與模擬系統規劃出兩足機器人之動作並進行穩定性與效率之分析。此外，本研究也實際組裝 KHR-1 多關節人形兩足機器人，經傳入所規劃的控制軌跡數據，進行作動測試。經實作測試，可確信本研究成果不僅可將多自由度的兩足機器人的控制軌跡規劃過程系統化與簡化，同時也可經由理論與模擬方法進行最佳化的規劃與應用。

關鍵字：操控性橢圓理論、兩足機器人、步態規劃、零矩點理論

The Study on the Gait Generation of Biped Robot Using the Manipulability Ellipsoid Algorithm

Student：Jiung-Rong Lee   Advisor：Dr. Pi-Ying Cheng

Department of Automation and Precision Engineering

National Chiao Tung University

ABSTRACT

Based on the manipulability ellipsoid algorithm, the research develops a gait planning system to generate the gait for the spatial parallel/serial type manipulator with ten or more degree of freedom. The research develops systematic methods for joint trajectory planning and simulation of the biped robot motion. The proposed methodology can be successfully applied to generate but not limited to the gaits of squat to stand and two walking strides.

The desired joint trajectory of biped robot produced by developed program with the kernel of the manipulability ellipsoid algorithm. An appropriate procedure has been set up to transform the generated joint trajectory data to the control unit of the KHR-1 biped robot, after the simulation to test and verification of the robot on the motion stability. This proposed method can save the cycle-time on trajectory generation of the biped robot. The velocity ellipsoid method is currently adopted for finding the minimum combination of angular velocity of the joints of the robot. Based on the static kinematics, the manipulability ellipsoid method can provide the choice of the minimum variation of the joint velocity for the biped robot to reach the more stable motion status. Furthermore, Zero-Moment point algorithm is applied as the constraint of the restriction area of the projection point of the mass center of the robot in the state of trajectory planning, thus the high stability of the robot can be afforded. A

biped robot KHR-1 with ten more degree of freedom has also been assembled and installed for proving the advantage and usefulness of the proposed method. The illustrated examples have demonstrated the benefit and the advantage on the gait planning of biped robot.

KEY WORDS: Manipulability Ellipsoid Algorithm, Biped Robot, Gait Generation, Zero-Moment Point Algorithm

Acknowledgement

I would like to express the gratitude to my advisor, Dr. Pi-Ying Cheng, for his excellent guidance in my research and his sincere concern about my personal life throughout these years. Dr. Pi-Ying Cheng is an amiable and decent professor, and he is also a person who has integrity and responsibility. His outstanding personality gives me a deep impression, and he is a role of model for me.

There are so many teachers who gave me the precious advices and guidance so that I can have the continuously improvement and progress with my research and study in Chaio Tung University. The NCTU has been instructed me the most valuable knowledge.

The absolute support and constant encouragement from my family and my girlfriend, Debby, keep me move on whether my mind was weighed down or up. I would like to dedicate this thesis to my parents and my girlfriend for their consistent care and the sacrifice that they made for me in the past years.
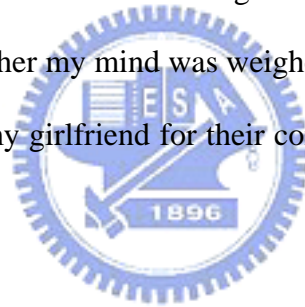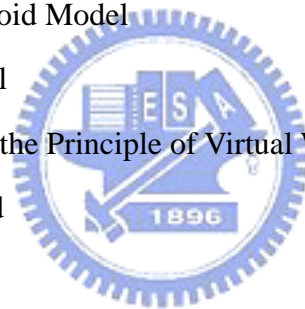
Table of Contents

List of Tables

List of Figures

Nomenclature

a_1, a_2, a_3	= Length of link in physical model
a_i	= The displaced $(i-1)$th coordinate system is translated along the x_i axis a distance
α_i	= The displaced $(i-1)$th coordinate system is rotated about the x_i axis an angle
$^0A_1$	= The transformation matrix of link one respected with base
$^1A_2$	= The transformation matrix of link two respected link one
$^2A_3$	= The transformation matrix of link three respected link two
$^{i-1}A_i$	= The transformation matrix of link i respected with link i-1
c	= Condition number
C_1	= Initial configuration in procedure of design motion
C_N	= Goal configuration in procedure of design motion
C_r	= Reasonable configuration in procedure of design motion
CH_i	= The number of servo motor of KHR-1 robot
d_i	= The $(i-1)$th coordinate system is translated along the z_{i-1} axis a distance
$e_j(t_i)$	= Compound estimate function
g	= The velocity of gravity
H_g	= The rate of change of angular momentum at center of mass of a robot
J	= Jacobain matrix of physical model which define the relation of velocity of End-effector and the angular velocity of each joint
K	= Arbitrary point on sole of robot
λ_1	= Eigenvalue of $J^T J$
λ_2	= Eigenvalue of $J^T J$
M	= Joint two of Physical model
$M_K^f n$	= Moment of friction force
$M^P n$	= Moment of pressure force

n	= Unit vector which is normal to the sole
O	= Joint one (base) of Physical model
O_i	= The origin of link i
P	= Joint three of Physical model
$\dot{P}_x$	= The linear velocity of joint two in x coordinate
$\dot{P}_y$	= The linear velocity of joint two in y coordinate
$\dot{q}$	= N dimensional velocity vector mapped by Jacobian matrix
^0q	= Position vector of Q respected to the base coordinate system
^3q	= Position vector of end-effector coordinate system
Q	= End-effector of Physical model
Q_x	= Position of end-effector in x coordinate
Q_y	= Position of end-effector in y coordinate
$\dot{Q}_x$	= Linear velocity of end-effector in x coordinate $\left(V_{qx}\right)$
$\dot{Q}_y$	= Linear velocity of end-effector in y coordinate $\left(V_{qy}\right)$
$R^P n$	= Pressure force
$R^f n$	= Friction force
θ_1, θ_2, θ_3	= Angle of links respected with its coordinate system in physical model
θ_{1b}	= The θ_1 value on boundary
θ_{2b}	= The θ_2 value on boundary
θ_{1c}	= The current θ_1 in time t_i
θ_{2c}	= The current θ_2 in time t_i
θ_{1v}	= The next θ_1 value in time t_{i+1}
θ_{2v}	= The next θ_2 value in time t_{i+1}
$\theta_{1\min}$	= The boundary of minimum θ_1
$\theta_{1\max}$	= The boundary of maximum θ_1
$\theta_{2\min}$	= The boundary of minimum θ_2
$\theta_{2\max}$	= The boundary of maximum θ_2
θ_i	= Angle of arbitrary link respected with its coordinate system in physical model or KHR-1 robot

θ_{iHOME} = The data value of home position in

θ_{iKHR} = The actual data value executed by KHR-1

$\theta_{imotion}$ = The data value of motion file

$\dot{\theta}_i$ = Angular velocity of arbitrary link with its coordinate system in physical

model or KHR-1 robot

$\Delta\theta_1$ = The displacement of θ_1 in time t_i

$\Delta\theta_2$ = The displacement of θ_2 in time t_i

Δt = The segment of time constant

$T(z,d)$ = The transformation matrix of distance d_i

$T(z,\theta_i)$ = The transformation matrix of angle θ_i

$T(z,a)$ = The transformation matrix of angle a_i

$T(z,\alpha)$ = The transformation matrix of angle α_i

τ_c = The constraint output force of each joint

τ_i = The output force of arbitrary joint in physical model of KHR-1 robot

τ_{max} = The maximum output force supported of each joint

τ_1, τ_2, τ_3 = The output force of arbitrary joint in physical model

X_0, Y_0 = Coordinate system of base in physical model

X_1, Y_1 = Coordinate system of joint two in physical model

X_2, Y_2 = Coordinate system of joint three in physical model

Y_{14}, Z_{14} = Coordinate system of servo motor number 14 (left thigh on KHR-1)

Y_{15}, Z_{15} = Coordinate system of servo motor number 15 (left thigh on KHR-1)

Y_{16}, Z_{16} = Coordinate system of servo motor number 16 (left thigh on KHR-1)

Y_{20}, Z_{20} = Coordinate system of servo motor number 20 (right thigh on KHR-1)

Y_{21}, Z_{21} = Coordinate system of servo motor number 21 (right thigh on KHR-1)

Y_{22}, Z_{22} = Coordinate system of servo motor number 22 (right thigh on KHR-1)

CHAPTER 1

Introduction

1.1 Literature Reviews

The Biped robot motion design and trajectory planning based on novel and various theories had developed for more complex motion requirement. For optimal control of biped robots, Fujimoto [1] proposed a general formulation of optimal control for biped robots based on numerical representation of motion equation, which can solve exactly the minimum energy consumption trajectory for a biped running motion. The main contribution of his idea is: it is useful to know the lower boundary of the consumption energy when we design the biped robot and select actuators. He fined input joint torques and initial posture that minimize input energy.

Tang, Zhou and Sun [2] adopted third-order spline interpolation based trajectory planning and zero moment point method which is aiming to achieve smooth biped swing leg trajectory by reducing the instant velocity change which occurs at the time of collision of the biped swing leg with the ground.

McGeea and Spong [3] discuss the control of the biped robot which consists of two legs connected to a cylindrical torso by DC-motors. A key problem that exists with this design is the generation of stable gaits while simultaneously guarantee bounded torso velocity. He presented a solution to this problem by controlling the velocity of the hub through design of the leg trajectory, which in turn determines the zero dynamics governing the hub velocity. In the manipulability ellipsoids implementation research, such as Chiacchio [4] proposed a formal definitions of force and velocity manipulability ellipsoids for multiple cooperative arms are established according to the global task space formulation that regards the

closed-chain system as a whole, at the object level and then independently from the number of arms involved in the cooperation. The proposed manipulability ellipsoids can be conveniently utilized to determine optimal postures for redundant multiple arm systems. Furthermore, the formulation adopted in this work allows the derivation of a dynamic manipulability ellipsoid. Tao [5] developed the optimal force distribution under the known posture. Two separate coordinating robots whose end-effectors firmly grasp a common inertial load, from a closed-chain structure. In these closed kinematical chains, the two robots must observe a set of constraint conditions on end-effectors' position, orientation, linear and angular velocities, as well as the forces and torques inserted onto the end-effectors by the load.

Although the manipulability ellipsoid, force and velocity ellipsoid are widely used technique in visualizing the dexterousness of robot motion, it has some problems that it does not transform the exact joint constraints into end-effector space. Therefore, Lee [6] explored the relation between manipulability ellipsoid and manipulability polytope for handling this problem. Another implementation of manipulability ellipsoid is adopted for developing the multi coordinates of robotic system, Lee [7] presented the static characteristics of a three degrees of freedom in parallel actuated manipulator and its desired static actuator characteristics for clamping and bracing applications. In his paper, highlights the influences of the over constraining forces on the manipulator performance using the presentation of the velocity, and force ellipsoids which were often employed in robotics for prediction of singularity, graphical representation of static characteristics, and for optimization of task performance.

In terms of robotic motion design, except the various trajectory planning methods, Yamamoto [8] presented the global dynamics, which include two kernels: zero moment point and passive dynamics. He pointed out most commonly used strategy for trajectory generation, the high-gain servo method [9] is basically playing back of the predefined ideal trajectory.

Then if we expect a robot to behave as various as the human, almost infinite number of ideal trajectory may be required. Yamamoto's global dynamics theory is base on the explored phase space of robot motion. In the phase space, the envelopes of motion are connected by an unstable region which is called node. The unstable region is the exchanging point between motions transitions, then the controlling parameters can input into the node the cause the motion change from current to next one. The particular contribution of global dynamics is to minimize the control parameter and to simply the procedure of motion design.

In legged robots development, especially the biped robots, the balance control is the particular and the first affected problem. Zero moment point is just the concept to explore the balance control issue. Goswani [10] studied the fundamental mechanics of rotational stability of multi-body systems with the goal to identify a general stability criterion. He focused on H_g, the rate of change of angular momentum in center of mass of a robot, as the physical quantity containing its stability information. He proposed three control strategies using H_g that can be used for stability recapture of biped robot.
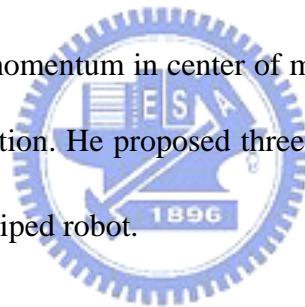
1.2 Motive

In various theory of trajectory planning for biped robot motion we can see different complexity in mathematical model and experimental procedure. In terms of a specific motion design, the complexity depends on the number of parameters of the desired motion, the more parameters the more difficult to accomplish it. There are several theories such as impedance control, torque control, zero moment point, energy control, are developed for a long period. A biped robot problem comes out first is the balance maintenance, a loss of stability might result in a fall with potentially disastrous consequence for both robots and animals.

Furthermore, a procedure of design robot motion will be another issue when the degree of freedom is steamily high so that the cycle-time of trajectory planning can not be reduced.

Due to these reasons, we proposed a velocity ellipsoid theory, in terms of the static kinematics, study the better procedure which can provide the shorter cycle-time for motion design, can produced a stable manipulating environment and produced the less executing force of each joint .

1.2.1 Target of Research

(1) Developing a biped robotic gait generation procedure which can provide a shorter cycle-time for specific robotic motion design.

(2) Based on the static kinematics, the manipulability ellipsoid method can provide the choice of the minimum variation of the joint rate to reach the more stable motion status for the biped robot gait.

(3) Reducing the executing force of each joint. A valuable advantage of using manipulability ellipsoid is eliminating the energy consumption when manipulating.

1.2.2 Assumption and Basic Constraint of Research

Several necessary assumption and constraint need to be defined before we discuss the main object in this thesis, and they are:

(1) Base on static kinematics to study the biped gait generation issue, and do not consider the effects of dynamic parameters such as inertial force, linear acceleration, angular acceleration and so on. Trying to extend the limitation of manipulability ellipsoid algorithm in static kinematics sphere.

(2) By first assumption, according to manipulability ellipsoid algorithm, dividing the entire process of biped locomotion to infinity of interval of time, let the angular velocity in arbitrary interval is defined by the minimum combination of angular velocity from last configuration.

(3) Only consider how to design desired joint trajectories and ignore the parameters of servo motor control system such as rotation rate and output torque.

(4) The kinematical model in this thesis is a spatial parallel type manipulator, for the purpose to reduce the kinematical model to two planer serial type manipulators, first we calculate the coordinate of end-effector from leg A, where the end-effecotor is also belong to another leg B, and obtain the configuration of leg B through inverse kinematics.

1.2.3 Kernel Conception

Manipulability ellipsoid algorithm content velocity ellipsoid and force ellipsoid, these two sub algorithm were adopted to implement and produce joint trajectories in most process of locomotion.

In this thesis we design continuously biped gaits which include three envelopes [8], as shown in Fig. 1.1. The first envelop is from initial posture, squat, to goal posture, stand. In this envelop, we implement both the velocity ellipsoid and force ellipsoid algorithm to obtain a stable and less energy consumption gait. The second envelop is from initial posture, stand, to goal posture, first stride; and the third envelop is also the second stride, from the initial posture, stride, to the goal posture, stand. The two strides in last two envelops defined as a humanoid biped robot is walking slowly as human being.

When a joint trajectory is produced by programming, next we have to do is transfer the trajectory data and implement into KHR-1 biped robot. When find out the invalid or unstable situation, trying to modify the program code and execute the experiment again until the situation of experiment is satisfied the principle we set. The entire procedure of biped gait generation is described in Fig.1.2.

1.3 Thesis Overview

   This thesis is base on the manipulability ellipsoid theory to develop a simply procedure of biped robot motion design. The construction of our experimentation includes derive the manipulability ellipsoid model of planar serial manipulator, producing the desired joint trajectory by program, implement the desired joint trajectory by KHR-1 simulation and finally analysis the θ_i, $\dot{\theta}_i$, τ_i of each joint. The content of each chapter are described below:

(1) Chapter one is the introduction of research background, targets of research, assumption of research, review the relative literatures and a brief chapter by chapter of this thesis.

(2) In the first part of chapter two, we discuss the kinematical model of KHR-1 biped robot. The KHR-1 robot system is presented with its hardware, software, communication interface and procedure of motion design. Through this chapter, one can realize the whole picture of practical KHR-1 robot, the virtual model which used for simulating the KHR-1 robot in programming, and how equilibrium of these two objects constructed. The second part of this chapter is to derive the mathematical equation of kinematical model.

(3) In chapter three, there are three main algorithms to be introduced. The manipulability ellipsoid equation, which include velocity and force ellipsoid. And base on this theory we can define the arbitrary coordination on the unity velocity circle is corresponding to the specific coordination of angular velocity on the velocity ellipsoid, or on the unity output force circle is corresponding to the specific coordination of joint torque on the joint torque ellipsoid. The second algorithm is inverse kinematics, which defined the configuration of manipulator by a given location and direction of end-effector. The third algorithm is Zero-Moment point algorithm, which used to constraint the location of projection which belongs to center of mass of biped upper body on the single or double support phase, so that the resultant moment affect on center of mass of biped upper body will be zero, and the stability of biped motion will be guaranteed.
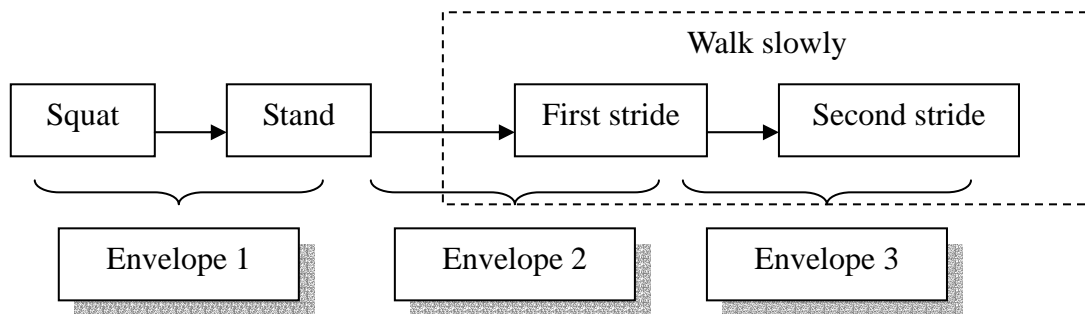
Fig.1.1 The envelops of biped gait.
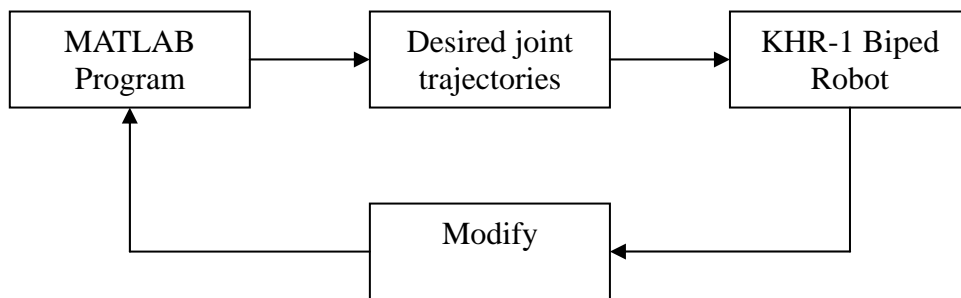
Fig.1.2 The procedure of gait generation.

(4) In chapter four, we present the result of experimentation envelops by envelop. In first envelop we compare the two different method of designing the gait, squat to stand. In second and the third envelop we compare the difference between the motion which design by KONDO company and by this thesis.

(5) In chapter five, we integrate the main target of research, kernel of algorithm, procedure of gait generation to construct a complete picture, conclude the differences and advantage in these objects. Besides, several new vision of research in the future will be presented for extending the current progress of research to more and better achievements.

CHAPTER 2

The Kinematical Model of KHR-1 Biped Robot

2.1 Introduction

In this chapter we are going to present the KHR-1 biped robot system which includes hardware, software, control system and procedure of motion design. Furthermore, the kinematical model of KHR-1 biped robot which is a simulator of KHR-1 biped robot in the programming is introduced too.

The desired joint trajectories are based on the kinematical model and produced by MATLAB programming which is shown in Fig. 1.2. We use this virtual kinematical model as an intermediary; all programs were designed according to this kinematical model.

2.2 KHR-1 Robot System
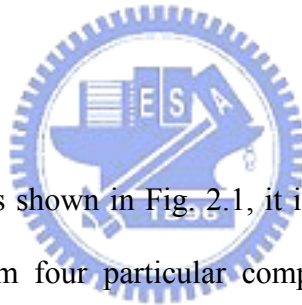
The KHR-1 biped robot is shown in Fig. 2.1, it is manufactured by Kondo Kagaku Co. Japan. It was constructed from four particular components, servo motors, RCB-1 circuit boards, plastic passive transmission parts and aluminum alloy supporting skeleton parts. We will have the detail discuss in next section about these particular components. One of objects of this research is develop an ideal joint trajectory planning procedure, which is evaluated by the simulation of KHR-1. Via the practical experimentation that include visualize observation on moving robot, the stability and efficiency can be guarantee to proof.

2.2.1 Hardware Interface

In this section we are going to introduce the particular hardware components of KHR-1. All of the components are manufactured by Kondo Kagaku Co. Japan. There are four particular hardware components: servo motors, RCB-1 circuit boards, plastic passive

(a)
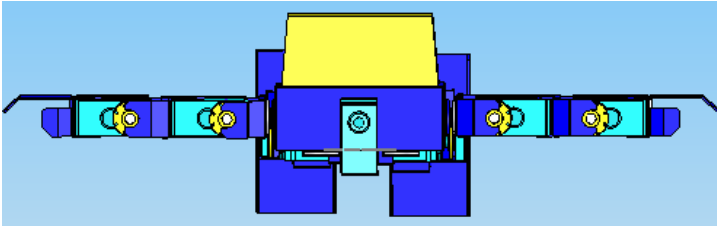
(b)
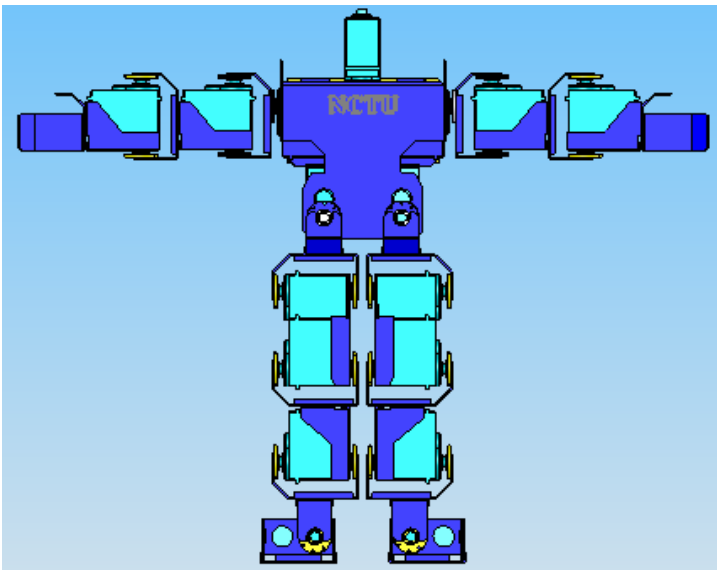
(c)
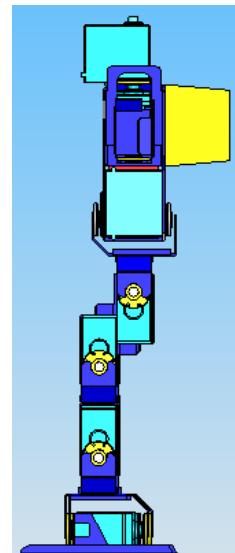
Fig.2.1 (a) KHR-1 biped robot top view.

(b) KHR-1 biped robot front view.

(c) KHR-1 biped robot right view.

transmission parts and aluminum alloy supporting skeleton parts.

2.2.1.1 KRS-784ICS Servo Motors

KRS-784ICS servo motor is shown in Fig.2.2 (a), it is the digital FET (Field Effect Transtor) servo motor. It has been developed to drive joint of robot. Here are the specifications of KRS-784ICS:

Size: 41×35×21(mm) excluded projections

Weight: 45g

Torque: 8.7 kg/cm (using 5N600 power cell)

Speed: 0.17 sec/60 degree (using 5N600 power cell)

Reasonable Voltage: 6V

2.2.1.2 RCB-1 Circuit Boards

RCB-1 is shown in Fig.2.2 (b), it has been developed for KHR-1 kit as the robot control board. A board can control twelve servo motors. It can control using all functions of the robot servo motors as KRS-784ICS. Since KHR-1 constructed from seventeen servo motors, in other words, there are necessary two pieces of RCB-1 boards for link the motors. Note that the number of motors link to RCB-1 is higher than the exactly number content of KHR-1, therefore, there are few non function I/O on RCB-1 without linking with servo motor. Here are the specifications of RCB-1:

Size: 45×35 (mm)

Weight: 12 g (one board)

Possible number of servo motors: 12

Reasonable Voltage: 6V

There is an EEPROM (Electrically Erasable Programmable ROM) embedded in the RCB-1,

all the command data will be saved in the EEPROM. The topology of command data is:

The maximum a hundred position data accomplished a motion.

The maximum two hundred motion data accomplished a scenario.

The maximum four scenario data could be edited and saved in EEPEROM.

2.2.1.3 Passive Transmission Parts

The passive transmission parts is shown in Fig.2.2 (c), when assemble KHR-1, there should be transmission parts for delivering the power which produced from servo motors into the supporting skeleton parts and accomplishing the motion.

2.2.1.4 Supporting Skeleton Parts

The skeleton parts support the servo motors and other components so that all the different components will be located at the fixed position on robot. The other function of skeleton parts are endowed the robot a humanoid body and be brawnier.
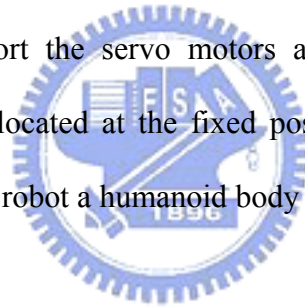
2.2.2 Communicated Interface

A RS232C cable transmits the command signal from the software in computer into the RCB-1, then a motion command is executed and a new motion is produced. The RS232C cable is shown in Fig.2.2 (d).

2.2.3 Software Interface

The Heart to Heart is used to produce the motion command which defined by adjusting the rotational value of joint, and the motion commands transmit by the RS232C cable into the RCB-1. It is shown in Fig. 2.3, each channel determines the rotational angle of servo motor of KHR-1, when a new angle value is produced by adjusting the angle bar, a new configuration

(a)

(b)

(c)

(d)
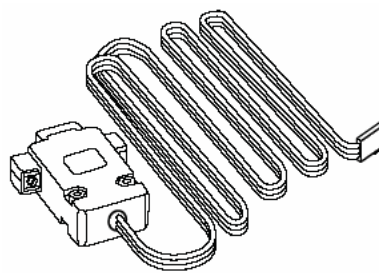
Fig.2.2 (a) KRS-784ICS Servo Motor.

(b) RCB-1 Circuit Boards.

(c) Passive Transmission Parts.

(d) RS232C cable.

of robot is produced. Besides, one can adjust the desired speed by choosing the button zero to seven, which the smaller number determine the higher speed.

2.2.4 The Control System of KHR-1

The RCB-1 can connect maximum twenty four servo motors, the particular function is motion command processor, all of the command signal will be send out there and receive by chip on RCB-1. The result of motion depends on the command which defined by modifying the angle value of motor in Heart to Heart. Therefore, different command causes the different motion. The Fig.2.4 (a), (b) and (c) determine the complete circuit configuration of servo motors with signal cables and power cables. Due to only seventeen motors used in KHR-1, there are several I/O do not connect with motors and act as no function I/O.

2.2.5 Procedure of Motion design

A robot motion is produced by user who adjusts the configuration of robot through the Heart to Heart. A complete configuration is determined by a group value include seventeen angular magnitudes of servo motors. Unfortunately, this inefficiently and non-systematic procedure will be the serious obstruct when we develop the biped gait. The current procedure of design the robot motion is shown in Fig.2.5, because a group value include seventeen angular magnitudes of servo motors as previous description, it means, one has to adjusts the each value one by one until all the motors are in the new position.

One can easy to perceive that from step two to step five are presented a try and error process. The result brings from this try and error process is procrastinate and tardy progress when design a robot motion. Besides, there is no other way can guarantee the stability, reliability and efficiency of the new motion except execute the motion and observe it.

Since there are several drawbacks in the current procedure of motion design for biped
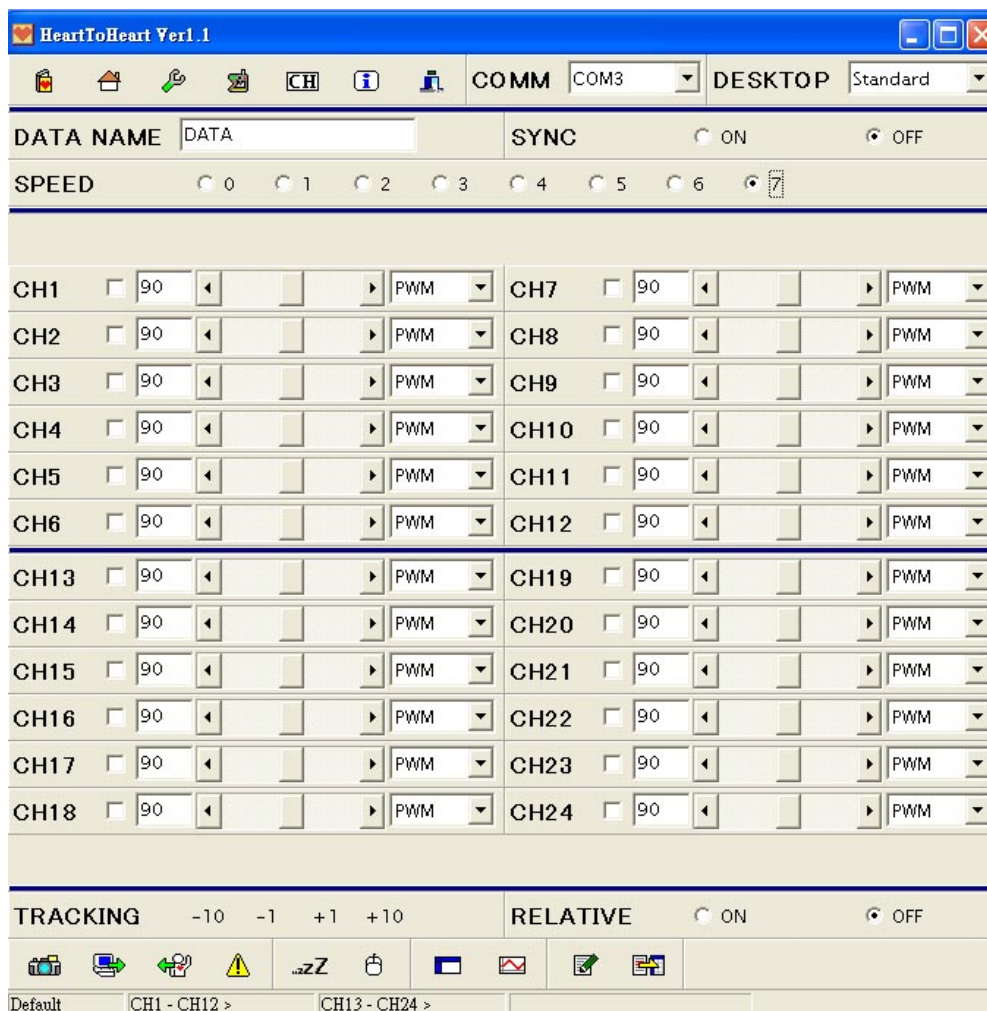
Fig.2.3 Communicated software, Heart to Heart.

robot locomotion, we have to develop a new procedure which can eliminate these drawbacks and make the stability, reliability and efficiency to be guaranteed. The procedure we develop in this research will be discussed in next chapter.

2.2.6 Example of Motion Create by Try and Error

Here we are going to introduce the sample of motion which is created by the current procedure, try and error. The motion is called prostrate to stand up, which include several postures transmission. When the motion is very complicated or involve the transmission between several different motions, it will cause the difficulty of designing procedure to be more and more complex.

The initial posture is shown in Fig.2.6 (a), the robot lies on the ground, the first transmission between motions is shown in Fig.2.6 (b), swing the arms and prop body by arms support on the ground. The second transmission is shown in Fig.2.6 (c), cower the thighs and legs towards the body so that the robot can try to make the center of mass moves to the lower body. The third transmission is shown in Fig.2.6 (d), when the thighs and legs are moving toward the body and the soles are supporting on the ground, the reaction force present the kinetic energy and the robot starts moving body and its body becomes backward, the arms are more and more distant from the ground. We called the posture in this moment, squat. The last transmission is shown in Fig.2.6 (e) and (f), the position of center of mass is located in lower body so that the robot can ascend the body into the goal posture, stand.

(a)
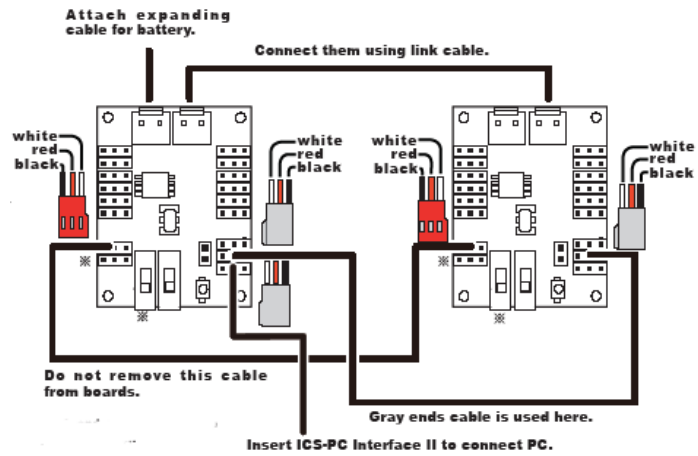
(b)
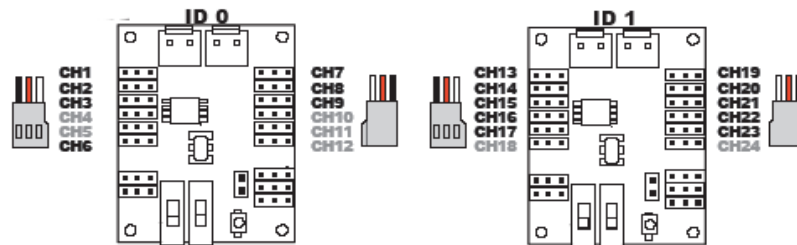
(c)
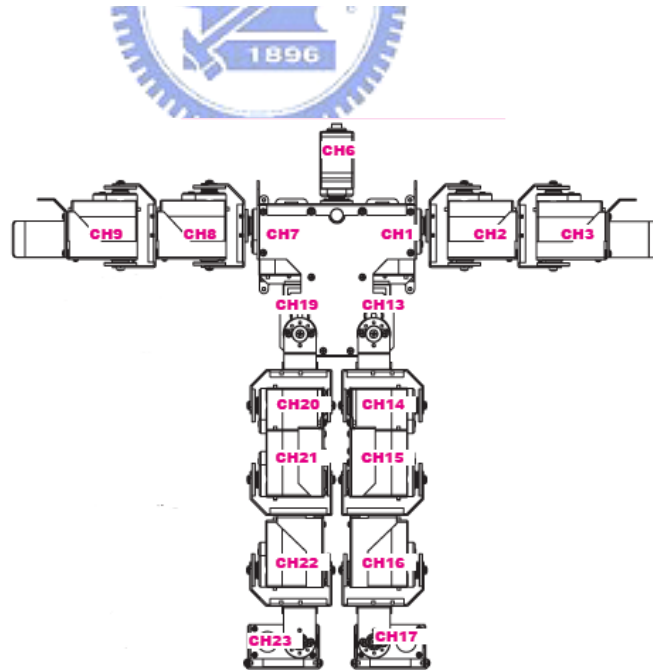
Fig.2.4 (a) The circuit I/O set configuration on RCB-1.
(b) The comparison of number of servo motors and I/O on RCB-1.
(c) The comparison of number of servo motors and the location on KHR-1.

```
┌─────────────────────┐
│ (1)Define initial posture │
│    and goal posture      │
└─────────────────────┘
          ↓
┌─────────────────────┐
│ (2) Adjust configuration │
│  1, $C_1$  with group value, │
│    $CH1_1 \sim CH24_1$    │
└─────────────────────┘
          ↓
┌─────────────────────┐
│ (3) Add the group      │
│ value of $C_1$ to motion │
│      editor            │
└─────────────────────┘
          ↓
┌─────────────────────┐
│ (4) Adjust configuration │
│  N, $C_N$  with group value, │
│    $CH1_N \sim CH24_N$   │
└─────────────────────┘
```

(9) Back to adjust C_r

(5) Add the group value of C_N to motion editor

(8) Check which configuration is reasonable, C_r

(6) Produce the motion, M_1.

(7) Experiment Check if the motion M_1 is desired target.

No

Yes

(10) Produce the desire trajectory

Fig 2.5 Current procedure of design motion.

18

Fig 2.6 Example motion, prostrate to stand up, created by try and error.
    (a) Initial posture.
    (b) Support by arms.
    (c) Curling the thigh towards to body.
    (d) Support by arms and thigh.
    (e) Arms getting away from ground.
    (f) Goal posture, stand up.

2.3 Kinematical Model of KHR-1 Robot

A kinematical model has been considered as a spatial parallel type manipulator, which is adopted to simplify the KHR-1 biped robot system. This kinematical model is an intermediary when design the joint trajectories by programming. We constraint the upper body of KHR-1 robot is immobile; therefore we need not consider the upper body in the kinematical model. Besides, via appropriate assumptions to simplify the kinematical model, the original characteristic of model will transform to planar serial type manipulator. We are going to present appropriate assumptions in chapter three.

A serial type manipulator consists of several links connected in series by various types of joints, typically revolute and prismatic joints. One end of the manipulator is attached to the ground and the other end is free to move in space. For this reason a serial type manipulator is sometimes called an open-loop manipulator. We call the fixed link the base, and the free end where a gripper or a mechanical hand is attached, the end-effector. We use this planar serial type manipulator, is shown in Fig. 2.7 (a), which has three degree of freedom to be a kinematical model and simulate a KHR-1 biped robot which is introduced in next section.

The object of making analogy between this three link serial manipulator and KHR-1 biped robot are:

(1) Simplifying the multi rigid body of KHR-1 biped robot and replace it by an extremely simple constitution to be the kinematical model in the whole experimentation. The contribution of this vehicle can produce the higher efficiency when design the robot motion.

(2) Via solving the direct kinematics and inverse kinematics problem of serial type manipulator, we can find a solution of producing ideal trajectory for robotic motion planning. In solving the inverse kinematics problems, we often interested in obtaining a closed-form solution that is, in reducing the problem to an algebraic equation relating the

end-effector location to a single joint variable. The number of possible inverse kinematics solutions depends on the type and location of a robot manipulator. In general, closed-form solutions can be found for manipulators with simple geometry, such as manipulators with three consecutive joint axes intersecting at the common point or three consecutive joint axes parallel to another. For a manipulator of general geometry, the inverse kinematics problem becomes a very difficult task. Therefore, we use the Denavit and Hartenberg's method to solve the inverse kinematics problem in this research.

2.3.1 Denavit-Hartenberg Homogeneous Transformation Matrices

The method created by Denavit and Hartenberg in year 1955 is systematic in nature and more suitable for the kinematics analysis of serial manipulator. First of all we have to take a look for the basic conception of D-H method. We are going to establish a coordinate system to each link of a manipulator, a 4×4 transformation matrix relating two successive coordinate systems can be established. The definition of link parameters is shown in Fig.2.8.
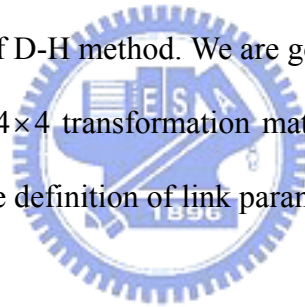
2.3.2 Link Parameter and Link Coordinate System

Here are the 4×4 transformation matrix of D-H method:

(1) The $(i-1)$th coordinate system is translated along the z_{i-1} axis a distance d_i. This brings the origin O_{i-1} into coincidence with H_{i-1}. This corresponding transformation matrix is

$$T(z,d) = \begin{bmatrix} 1 & 0 & 0 & 0 \\ 0 & 1 & 0 & 0 \\ 0 & 0 & 1 & d_i \\ 0 & 0 & 0 & 1 \end{bmatrix}$$

(2) The displaced $(i-1)$th coordinate system is rotated about the z_{i-1} axis an angle θ_i, which brings the x_{i-1} axis. The corresponding transformation matrix is
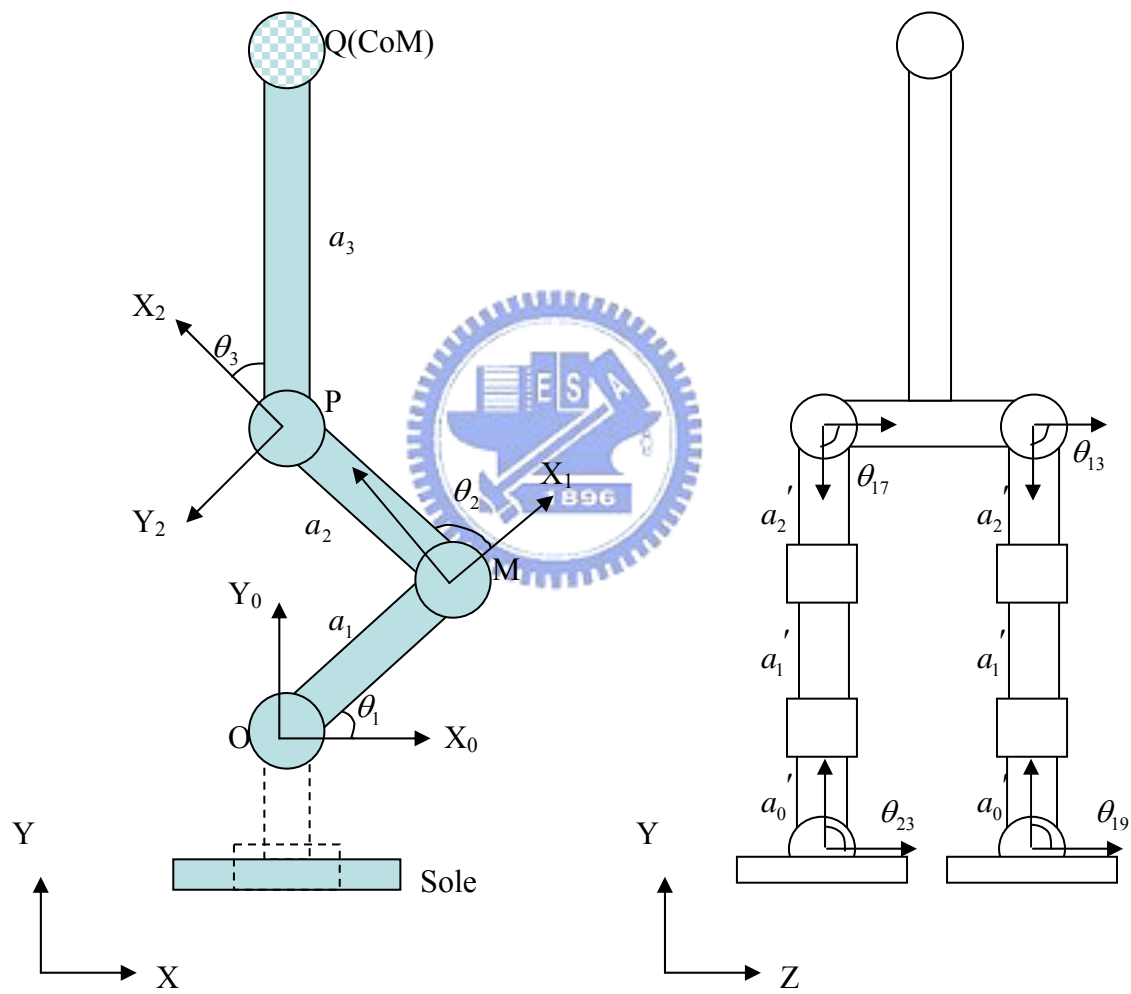
Fig.2.7 A three link planar serial type manipulator.
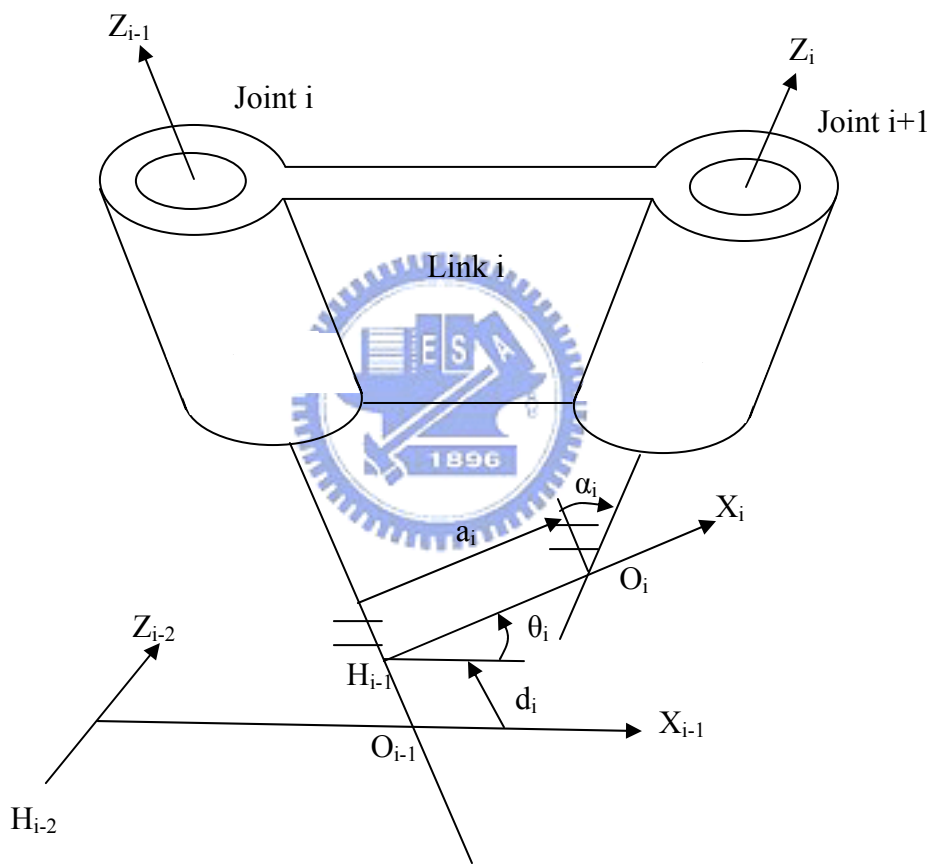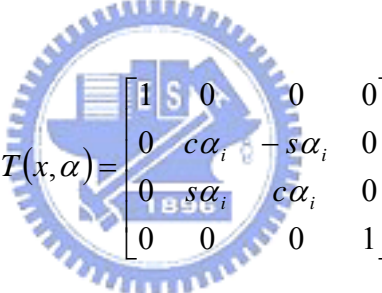
Fig.2.8 Definition of link parameters.

$$T(z,\theta)=\begin{bmatrix} c\theta_i & -s\theta_i & 0 & 0 \\ s\theta_i & c\theta_i & 0 & 0 \\ 0 & 0 & 1 & 0 \\ 0 & 0 & 0 & 1 \end{bmatrix}$$

(3) The displaced $(i-1)$th coordinate system is translated along the x_i axis a distance a_i. This brings the origin O_{i-1} into coincidence with O_i. The corresponding transformation matrix is

$$T(x,a)=\begin{bmatrix} 1 & 0 & 0 & a_i \\ 0 & 1 & 0 & 0 \\ 0 & 0 & 1 & 0 \\ 0 & 0 & 0 & 1 \end{bmatrix}$$

(4) The displaced $(i-1)$th coordinate system is rotated about the x_i axis an angle α_i, which brings the two coordinate system into complete coincident. The corresponding transformation matrix is

$$T(x,\alpha)=\begin{bmatrix} 1 & 0 & 0 & 0 \\ 0 & c\alpha_i & -s\alpha_i & 0 \\ 0 & s\alpha_i & c\alpha_i & 0 \\ 0 & 0 & 0 & 1 \end{bmatrix}$$

We may think of the transformations above as four basic transformations about the moving coordinate axes. Therefore, the resulting transformation matrix, $^{i-1}A_i$, is given by

$$^{i-1}A_i = T(z,d)T(z,\theta)T(x,a)T(x,\alpha). \tag{2.1}$$

Expanding Eqs. (2.1), we obtain

$$^{i-1}A_i = \begin{bmatrix} c\theta_i & -c\alpha_i s\theta_i & s\alpha_i s\theta_i & a_i c\theta_i \\ s\theta_i & c\alpha_i c\theta_i & -s\alpha_i c\theta_i & a_i s\theta_i \\ 0 & s\alpha_i & c\alpha_i & d_i \\ 0 & 0 & 0 & 1 \end{bmatrix} \tag{2.2}$$

where $^{i-1}A_i$ define arbitrary link with the four parameters, d_i, θ_i, a_i, α_i. Equation (2.2) is called Denavit-Hartenberg (D-H) transformation matrix.

2.3.3 Closure-loop Equation

In this section we are going to formulate the entire coordinated system of three link planar serial type manipulator by D-H method. According to the definition of D-H method, we can list out the D-H parameters of a 3 link manipulator is shown in Table 2.1. Substituting the D-H parameters in to Eqs. (2.2), we obtain

$$
{}^{0}A_{1} = T(Z_{0},0)R(Z_{0},\theta_{1})T(X_{1},a_{1})R(X_{1},0) = \begin{bmatrix} c\theta_{1} & -s\theta_{1} & 0 & a_{1}c\theta_{1} \\ s\theta_{1} & c\theta_{1} & 0 & a_{1}s\theta_{1} \\ 0 & 0 & 1 & 0 \\ 0 & 0 & 0 & 1 \end{bmatrix} \tag{2.3}
$$

$$
{}^{1}A_{2} = T(Z_{1},0)R(Z_{1},\theta_{2})T(X_{2},a_{2})R(X_{2},0) = \begin{bmatrix} c\theta_{2} & -s\theta_{2} & 0 & a_{2}c\theta_{2} \\ s\theta_{2} & c\theta_{2} & 0 & a_{2}s\theta_{2} \\ 0 & 0 & 1 & 0 \\ 0 & 0 & 0 & 1 \end{bmatrix} \tag{2.4}
$$

$$
{}^{2}A_{3} = T(Z_{2},0)R(Z_{2},\theta_{3})T(X_{3},a_{3})R(X_{3},0) = \begin{bmatrix} c\theta_{3} & -s\theta_{3} & 0 & a_{3}c\theta_{3} \\ s\theta_{3} & c\theta_{3} & 0 & a_{3}s\theta_{3} \\ 0 & 0 & 1 & 0 \\ 0 & 0 & 0 & 1 \end{bmatrix} \tag{2.5}
$$

Furthermore, we can use the loop-closure Equation

$$
{}^{0}A_{1}\,{}^{1}A_{2}\,{}^{2}A_{3} = {}^{0}A_{3} \tag{2.6}
$$

then substituting the Eqs. (2.3), (2.4) and (2.5) to (2.6), we obtain

$$
{}^{0}A_{3} = \begin{bmatrix} c\theta_{123} & -s\theta_{123} & 0 & a_{1}c\theta_{1}+a_{2}c\theta_{12}+a_{3}c\theta_{123} \\ s\theta_{123} & c\theta_{123} & 0 & a_{1}s\theta_{1}+a_{2}s\theta_{12}+a_{3}s\theta_{123} \\ 0 & 0 & 1 & 0 \\ 0 & 0 & 0 & 1 \end{bmatrix} \tag{2.7}
$$

One can compute the position of the end-effector point by using the Eqs. (2.7), which is direct kinematics as

$$
\begin{bmatrix} q_{x} \\ q_{y} \\ q_{z} \\ 1 \end{bmatrix} = {}^{0}A_{3} \begin{bmatrix} 0 \\ 0 \\ 0 \\ 1 \end{bmatrix} = \begin{bmatrix} a_{1}c\theta_{1}+a_{2}c\theta_{12}+a_{3}c\theta_{123} \\ a_{1}s\theta_{1}+a_{2}s\theta_{12}+a_{3}s\theta_{123} \\ 0 \\ 1 \end{bmatrix} \tag{2.8}
$$

where $\begin{bmatrix} q_x & q_y & q_z & 1 \end{bmatrix}^T = {}^0q$ is position vector of Q with respect to the base coordinate system; and the position vector of the end-effector coordinate system is given by ${}^3q = \begin{bmatrix} 0,0,0,1 \end{bmatrix}^T$. Suppose given θ_1, θ_2 and θ_3, the position of point Q can be computed by Eqs. (2.8).

2.4 Jacobian Analysis of Three Links Planar Serial Type Manipulator

In the last section we have discussed about the position analysis of the three links planar serial type manipulator. This knowledge enables us to bring the end-effector to some desired locations in space. In this section we are going to extend the position analysis problem with our kinematical model, the three links serial type manipulator, to a velocity analysis problem of serial manipulator.

For our trajectory planning, it is necessary to move the end effector of a manipulator along some desired paths with a prescribed speed. To achieve this goal, the motion of the individual joints of a manipulator must be carefully coordinated. For the robot manipulators, the Jacobian matrix is defined as the matrix that transforms the joint rates in the actuator space to the velocity state in the end-effector space. The Jacobian matrix is a critical component for generating trajectories of prescribed geometry in the end-effector space.

2.4.1 Mathematical model of Jacobian Matrix

According to the three links planar serial manipulator is shown in Fig. 2.7, the position of end effector, Q, can the determined as

$$Q_x = a_1 c\theta_1 + a_2 c\theta_{12} + a_3 c\theta_{123} \tag{2.9}$$

$$Q_y = a_1 s\theta_1 + a_2 s\theta_{12} + a_3 s\theta_{123} \tag{2.10}$$

$$Z_0 = Z_1 = Z_2 = \begin{bmatrix} 0 \\ 0 \\ 1 \end{bmatrix} \tag{2.11}$$

From Eqs. (2.9) and (2.10), take the derivative with respect to the time, we obtain

$$\frac{d\hat{Q}_x}{dt} = \dot{Q}_x = V_{qx} = -a_1 s\theta_1 \dot{\theta}_1 - a_2 s\theta_{12} \dot{\theta}_{12} - a_3 s\theta_{123} \dot{\theta}_{123} \qquad (2.12)$$

$$\frac{d\hat{Q}_y}{dt} = \dot{Q}_y = V_{qy} = a_1 c\theta_1 \dot{\theta}_1 + a_2 c\theta_{12} \dot{\theta}_{12} + a_3 c\theta_{123} \dot{\theta}_{123} \qquad (2.13)$$

Write the Eqs. (2.12) and (2.13) into the matrix form as

$$\begin{bmatrix} \dot{Q}_x \\ \dot{Q}_y \\ \dot{Q}_z \end{bmatrix} = \begin{bmatrix} V_{qx} \\ V_{qy} \\ \omega_{qz} \end{bmatrix} = \begin{bmatrix} -a_1 s\theta_1 - a_2 s\theta_{12} - a_3 s\theta_{123} & -a_2 s\theta_{12} - a_3 s\theta_{123} & -a_3 s\theta_{123} \\ a_1 c\theta_1 + a_2 c\theta_{12} + a_3 c\theta_{123} & a_2 c\theta_{12} + a_3 c\theta_{123} & a_3 c\theta_{123} \\ 1 & 1 & 1 \end{bmatrix} \begin{bmatrix} \dot{\theta}_1 \\ \dot{\theta}_2 \\ \dot{\theta}_3 \end{bmatrix} \quad (2.14)$$

$$\begin{bmatrix} V_{qx} \\ V_{qy} \\ \omega_{qz} \end{bmatrix} = J \begin{bmatrix} \dot{\theta}_1 \\ \dot{\theta}_2 \\ \dot{\theta}_3 \end{bmatrix} \qquad (2.15)$$

where the J determined the Jacobian matrix.

Table.2.1. D-H parameters of a three link planar serial type manipulator.

| Joint i	α_i	a_i	d_i	θ_i
1	0	a_1	0	θ_1
2	0	a_2	0	θ_2
3	0	a_3	0	$-\theta_3$

2.5 The Transforming Procedure with KHR-1

The purpose of using transforming procedure is transform the coordinate system of kinematical model as same as KHR-1 biped robot. Due to there are differences of construction between KHR-1 biped robot and kinematical model , it is necessary to transform the data of desired joint trajectory to a proper data file of KHR-1.

### 2.5.1 The Coordinate System Transformation

The three links planar serial manipulator is adopted to be a kinematical model to simulate the KHR-1 robot, and we have been introduced the kinematical model in section 2.3. A serious problem after the desired trajectory design is how we transform the data file of desired trajectory into KHR-1 robot by an exact, correct and simple procedure. The first part of this issue is transforming the coordinate system between the kinematical model and KHR-1 robot. The KHR-1 robot constructed from seventeen servo motors, and each motor marked with an individual number, which is shown in Fig.2.9 (a), and we has the analogy of kinematical model to the right thigh of KHR-1, which is shown in Fig.2.9 (b), and the left thigh in Fig.2.9 (c).

Comparing the kinematical model and right thigh of KHR-1, we can find out that the coordinate system of motor number twenty one and twenty of right thigh, and link two, link three of kinematical model are quite different from each other. The comparison result is shown in Fig.2.10. In terms of link one of kinematical model, coordinate system $x_0 - y_0$ is completely the same with coordinate system $x_{22} - y_{22}$ of motor number twenty two, so that need not any transformation between these two coordinate systems. In terms of link two of kinematical model, the coordinate system $x_1 - y_1$ needs to be rotated 90 degree to meet the coordinate system $x_{21} - y_{21}$, in terms of link three of kinematical model; coordinate system $x_2 - y_2$ needs to be rotated 90 degree to meet coordinate system $x_{20} - y_{20}$.

(a)
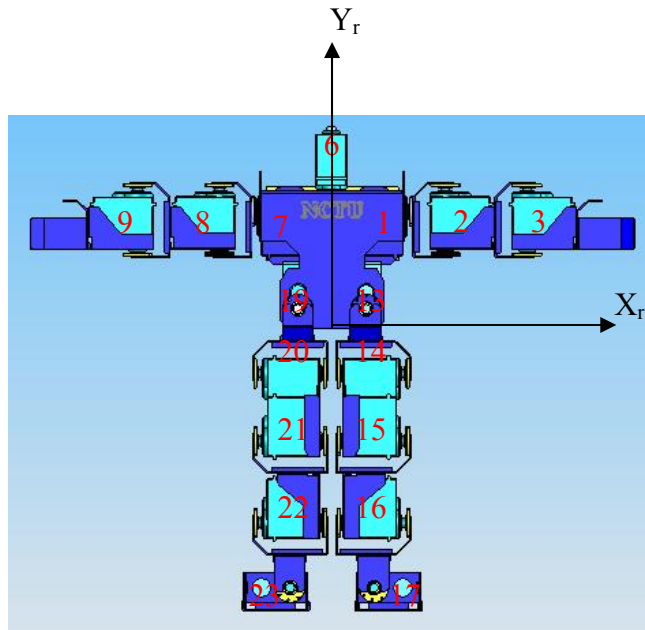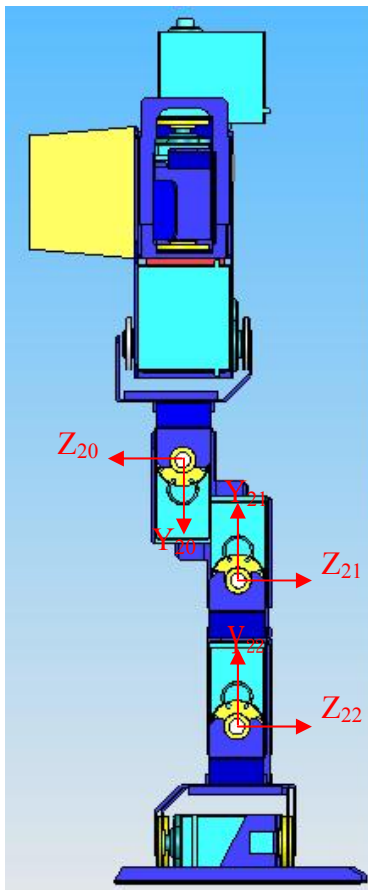
(b)   (c)
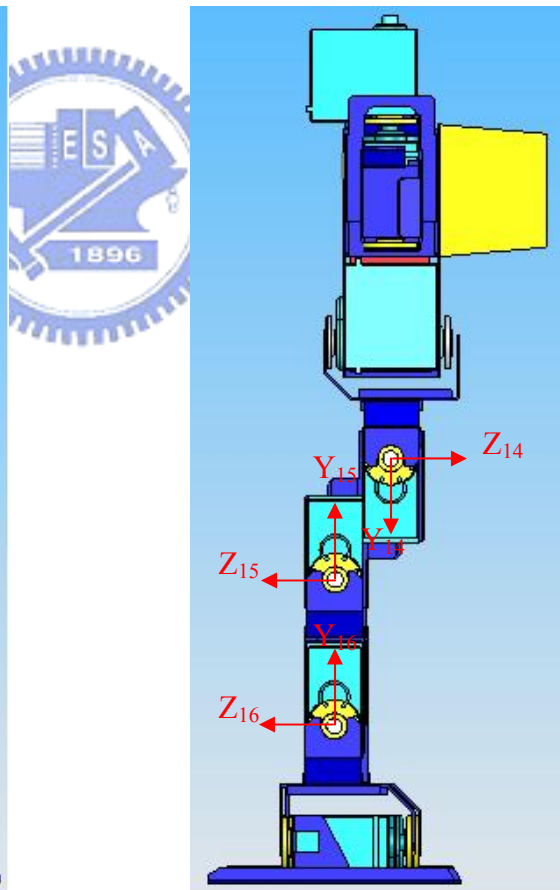
Fig.2.9 (a) Complete order number of each servo motor on KHR-1 robot.
        (b) The coordinate system of right thigh (No.20~22 motors) of robot.
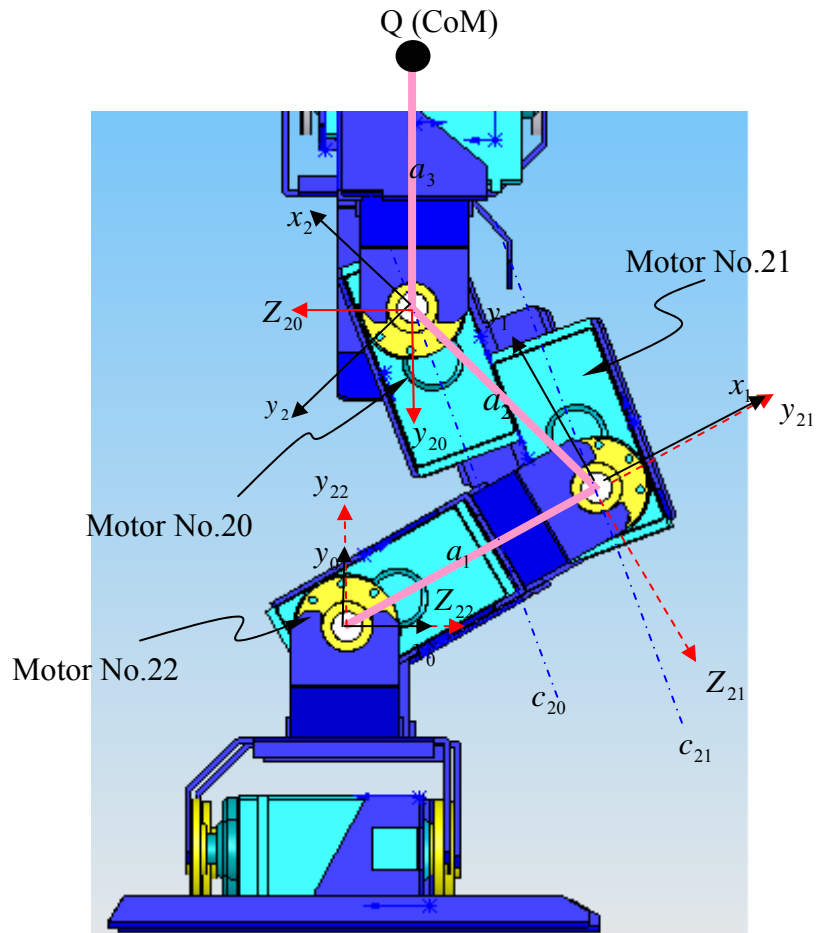   (c) The coordinate system of left thigh (No.14~16 motors) of robot.

Fig.2.10 The coordinate system comparison of physical model and KHR-1

Besides, a shift angle is produced by the arrangement distance when assemble the motors number twenty one and twenty. Therefore, we must consider the shift angle and find the mathematical relation between link two and these two motors. In Fig.2.11, the shift angle is calculated with distance between joints of the motors and is $27.78°$. This shift angle cause the link two constructed with the conceal distance from joint of motor number twenty one to twenty. For this reason, we can integrate the coordinate system and describe them as Table 2.2. According to Table 2.2, the data file of desired trajectory transformation can be accomplished.

2.5.2 Definition of Link Three of Kinematical Model

The shift angle we discussed in last section cause the conceal distance, and the distance is actually determined the link two of kinematical model. In terms of kinematical model, link three is a special case when match the configuration with KHR-1 robot. Because we constraint the configuration of upper body is fixed during the biped gait is manipulating, therefore, we can simplify the upper body of KHR-1 biped robot to a particle as the end-effector. In other words, the definition of link three of kinematical model is determined as the distance from joint of motor number twenty to center of mass of upper body. The canter of mass can be calculated is shown in Fig.2.12, measured the vector from joint of motor twenty to global origin of KHR-1, and measured the vector from center of mass of upper body to global origin. We can obtain the distance between joint of motor twenty to CoM of upper body.

Table 2.2 Coordinate system transformation between kinematical model and KHR-1

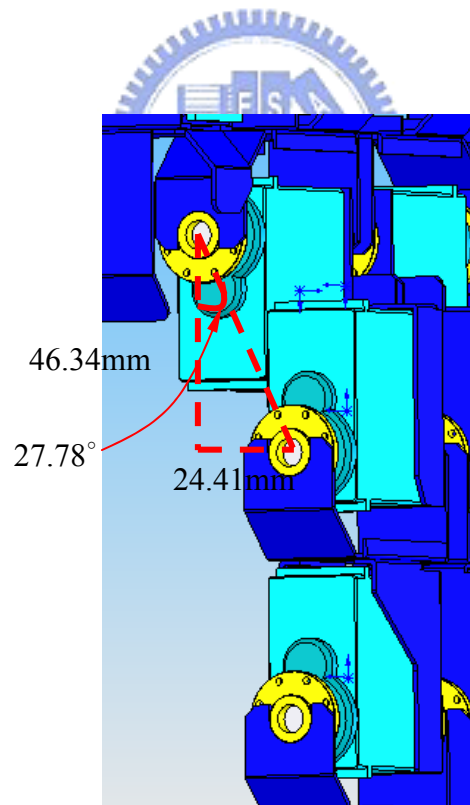| Physical Model	Coordinate System	Transform	Coordinate System	KHR-1
Link 1	$x_0 - y_0$	0	$z_{22} - y_{22}$	Motor 22
Link 2	$x_1 - y_1$	90-27.78=62.22	$z_{21} - y_{21}$	Motor 21
Link 3	$x_2 - y_2$	90-27.78=62.22	$z_{20} - y_{20}$	Motor 20

46.34mm

27.78°

24.41mm

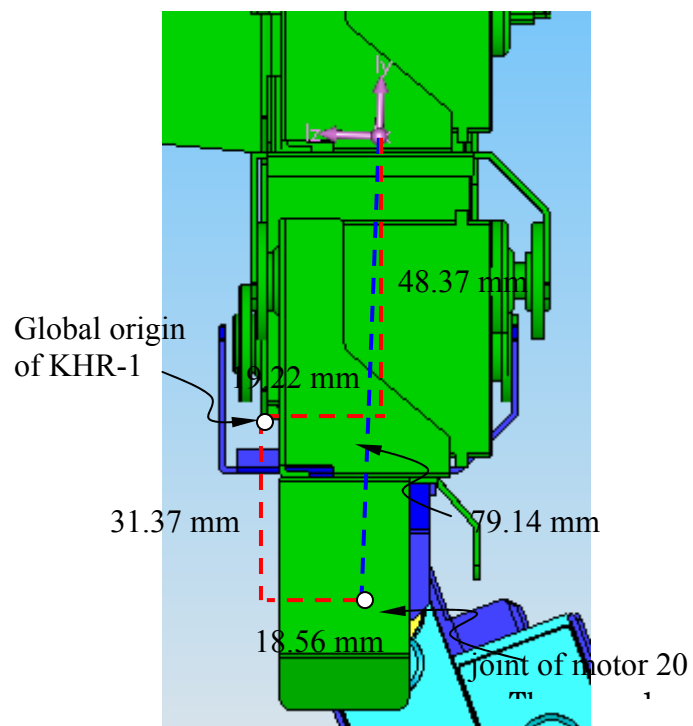Fig.2.11 The shift angle between motors number 21 and 20.

Fig.2.12 The distance between joint of motor number 20 and canter of
mass of upper body.

CHAPTER 3

Introduction of Main Algorithm

3.1 Introduction

In this chapter we are going to introduce the main algorithms and the assumptions of simplify the kinematical model in the research. There are three different algorithms were adopted for designing the joint trajectory. Manipulability ellipsoid algorithm which includes velocity ellipsoid and force ellipsoid, ZMP (Zero-Moment Point) algorithm and inverse kinematics. For the purpose of simplifying the kinematical model of KHR-1 robot, we must set several assumptions which associate with these algorithms.

3.2 Manipulability Ellipsoid Algorithm

The manipulability ellipsoid algorithm is a kernel of research for developing stable condition of biped robot gait, where velocity ellipsoid is for creating the stable locomotion by defining the minimum combination of angular velocity of each joint in arbitrary interval of time, and the force ellipsoid is for reducing the output force consumption. We develop a new strategy which can improve the stability and reduce the energy consumption via establishing both two ellipsoids.

3.2.1 Condition Number

In Last chapter we have discussed about the Jacobian matrix of three links serial manipulator. The Jacobian matrix, J, transform the joint rate in n-dimensional space into the end-effector velocity in m-dimensional space. We have the kinematical model which includes all joint are revolute, therefore the first three rows of Jacobian matrix, J, have the dimension of length, whereas the last three rows are dimensionless. For those manipulators with only one type of joint and for one type of task, either point positioning or body orienting but not both,

the Jacobian matrix can be characterized by a measure called the condition number, c [11].

The condition number of a matrix A is defined as

$$c = \|A\| \|A^{-1}\|$$ (3.1)

Where the norm of A is defined as

$$\|A\| = \max_{x \neq 0} \frac{\|Ax\|}{\|x\|}$$ (3.2)

In other word, the norm of A bounds the amplifying power of the matrix:

$$\|Ax\| \leq \|A\| \|x\| \qquad \text{for all vector x,}$$ (3.3)

The condition number of the Jacobian matrix depends on the link lengths and the manipulator

configuration. As the end-effector moves from location to location, the condition number will

assume different values. The minimum condition number of any matrix is 1. Those points in

the works space of a manipulator where the condition number of the Jacobian matrix is equal

to 1 are called isotropic points [12].
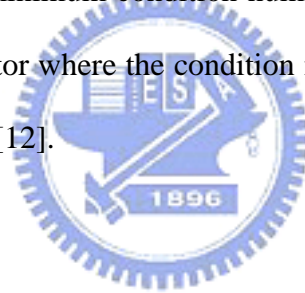
3.2.2 Velocity Ellipsoid Model

For the target of comparing the characteristics to compare the joint rates required to

produce a unit end-effector velocity in all possible directions. To achieve this goal, we confine

the end-effector velocity vector on an m-dimensional unit sphere,

$$\dot{x}^T \dot{x} = 1$$ (3.4)

Where

$$\dot{x} = J\dot{q}$$ (3.5)

and $\dot{q}$ is an n-dimensional velocity vector which mapped by Jacobian matrix into

m-dimensional velocity vector $\dot{x}$. Compare the corresponding joint rates in the n-dimensional

joint space. Substituting Eq. (3.5) into (3.4) yields

$$\dot{q}^T J^T J \dot{q} = 1 \tag{3.6}$$

Equation (3.6) represents an ellipsoid in the n-dimensional joint space. Because the product $J^T J$ is symmetric positive semi definite, its eigenvectors are orthogonal, The principle axes of the ellipsoid coincide with the eigenvectors of $J^T J$, and the length of its principle axes are equal to the reciprocals of the square roots of the eigenvectors of $J^T J$.

Since the Jacobian matrix is configuration dependent, the ellipsoid is also configuration dependent. As the end-effector moves from one location to another, the shape and orientation of the ellipsoid will also change accordingly. The closer the velocity ellipsoids to a sphere, the better the transformation characteristics are. The transformation is said to be isotropic when the principle axes are all of equal length. At an isotropic point, a unit sphere in the n-dimensional joint space. On the other hand, at a singular point, one or more of the principle axes becomes infinitely long and the ellipsoid degenerates into a cylinder. Under such a condition, the end-effector will not be able to move in some directions.

Consider a three links planar serial manipulator is shown in Fig.2.7, apply the restricted condition which present in chapter one, reduce the Jacobian matrix of Eq.(2.14) to

$$J = \begin{bmatrix} -a_1 s\theta_1 - a_2 s\theta_{12} & -a_2 s\theta_{12} \\ a_1 c\theta_1 + a_2 c\theta_{12} & a_2 c\theta_{12} \end{bmatrix} \tag{3.7}$$

and

$$J^T J = \begin{bmatrix} a_1^2 + a_2^2 + 2a_1 a_2 c\theta_2 & a_1 a_2 c\theta_2 + a_2^2 \\ a_1 a_2 c\theta_2 + a_2^2 & a_2^2 \end{bmatrix} \tag{3.8}$$

Substituting the length of link one $\sqrt{2}$ m and link two 1 m into Eq.(3.8), we obtain

$$J^T J = \begin{bmatrix} 3 + \sqrt{2} c\theta_2 & \sqrt{2} c\theta_2 + 1 \\ \sqrt{2} c\theta_2 + 1 & 1 \end{bmatrix} \tag{3.9}$$

Let us assume the $\theta_2 = \dfrac{\pi}{2}$, then the matrix product $J^T J$ becomes

$$J^T J = \begin{bmatrix} 3 & 1 \\ 1 & 1 \end{bmatrix} \tag{3.10}$$

The eigenvalues of $J^T J$ are

$$\lambda_1 = 0.5858, \quad \lambda_2 = 3.4142$$

and the eigenvector is

$$\begin{bmatrix} 0.3827 & -0.9238 \\ -0.9238 & 0.3827 \end{bmatrix}$$

Substituting Eq. (3.10) to (3.6) yields

$$3\dot{\theta}_1^2 + 2\dot{\theta}_1\dot{\theta}_2 + \dot{\theta}_2^2 = \frac{\left(0.3827\dot{\theta}_1 - 0.9238\dot{\theta}_2\right)^2}{1.3065^2} + \frac{\left(0.9238\dot{\theta}_1 + 0.3827\dot{\theta}_2\right)^2}{0.5415^2}$$

$$= 1 \tag{3.11}$$

Equation (3.12) represents an ellipse is shown in Fig.3.1 (b), the joint rates required to produce a unity end-effector velocity are $\left(\dot{\theta}_1, \dot{\theta}_2\right) = \left(-0.500, 1.207\right)$ rad/s along the major axis, and $\left(\dot{\theta}_1, \dot{\theta}_2\right) = \left(0.500, 0.207\right)$ rad/s along the minor axis.

Without loss the generality, we assume that $\theta_1 = 0$. Then the Jacobian matrix becomes

$$J = \begin{bmatrix} -1 & -1 \\ \sqrt{2} & 0 \end{bmatrix} \tag{3.12}$$

Hence the corresponding end-effector velocities are $\left(\dot{v}_x, \dot{v}_y\right) = \left(-0.707, -0.707\right)$ m/s along the major axis and $\left(\dot{v}_x, \dot{v}_y\right) = \left(-0.707, 0.707\right)$ m/s along the minor axis, respectively, is shown in Fig.3.1 (a). We notice that to produce the same end-effector speed along the principle axes, one requires the largest joint rates while the other requires the smallest joint rates.
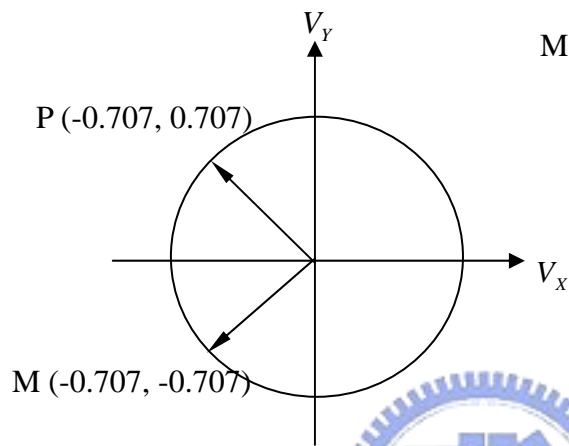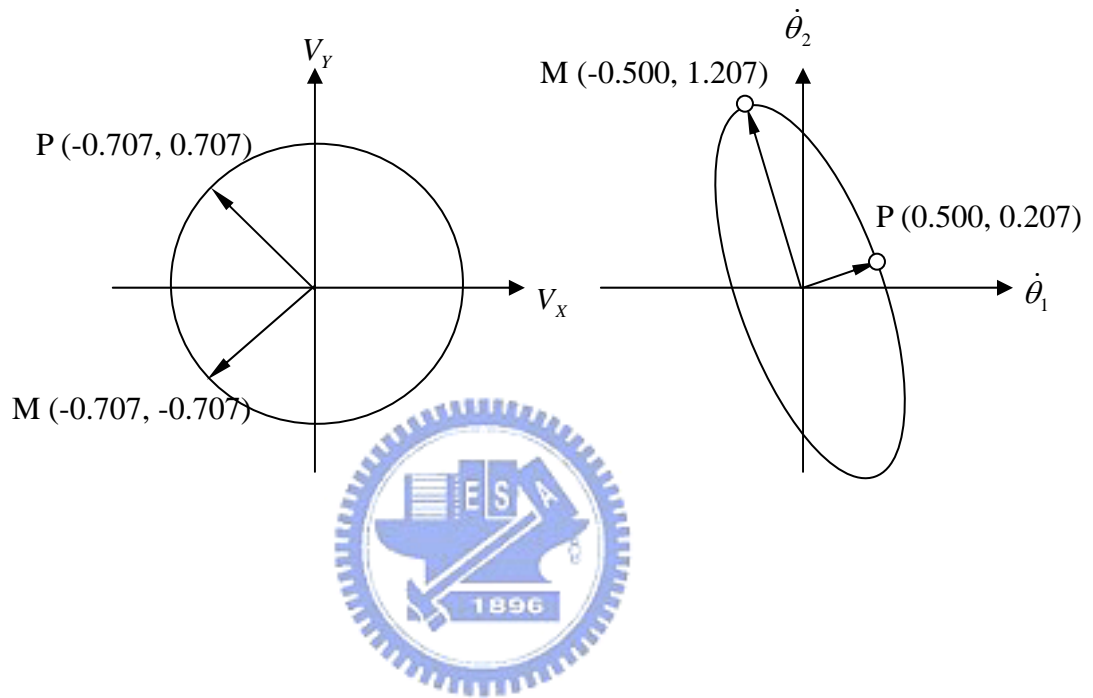
(a)   (b)

Fig.3.1 (a) Unity circle of velocity of end-effector in Cartesian coordinate.
(b) Velocity ellipsoid.

3.3 Force Ellipsoid Model

Similar to the transformation of velocities, the transformation of forces for manipulators with only one type of joints and for one type of tasks can be characterized by a comparison of the end-effector force produced by a unity joint torque.

3.3.1 Application of the Principle of Virtual Work

For a serial manipulator, the virtual displacements at the joints can be written as $\delta q = [\delta q_1, \delta q_2, \dots \delta q_n]^T$, and the virtual displacement of the end-effector can be expressed as $\delta x = [\delta x, \delta y, \dots \delta \psi]^T$. Let the end-effector output force and moment be denoted by

$$\mathbf{F} = \begin{bmatrix} f \\ n \end{bmatrix} \tag{3.13}$$

Also the vector of joint torques be denoted by

$$\tau = \begin{bmatrix} \tau_1 \\ \tau_2 \\ \vdots \\ \tau_n \end{bmatrix} \tag{3.14}$$

Assuming the frictional forces at the joints are negligible, the virtual work produced by the force of constraint at the joints is zero. Hence, by neglecting the gravitational effect, the virtual work, δW, define by all active forces is given by

$$\delta W = \tau^T \delta q - F^T \delta x \tag{3.15}$$

The principle of virtual work states that a system is under equilibrium if and only if the virtual work vanishes for any infinitesimal virtual displacement. This is true if the virtual displacements are compatible with the constraints imposed on the system. In Eq. (3.15), however, the virtual displacement δq and δx are not independent, In fact, they are related by the conventional Jacobian matrix as follows:

$$\delta q = J \delta q \tag{3.16}$$

40

Substituting Eq.(3.16) into (3.15) yields

$$\left(\tau^T - F^T J\right)\delta q = 0 \tag{3.17}$$

Since Eq.(3.17) holds for any arbitrary virtual displacement, δq, we conclude that

$$\tau^T - F^T J = 0 \tag{3.18}$$

Taking the transpose of Eq.(3.18) yields

$$\tau = J^T F \tag{3.19}$$

Equation (3.19) maps an m-dimensional end-effector output force into an n-dimensional joint torques. Since the Jacobian matrix is configuration dependent, the mapping is also configuration dependent.[11]

3.3.2 Force ellipsoid

Similar to transformation of velocities, the transformation of force for manipulators with only one type of joints and for one type of tasks can be characterized by a comparison of the end-effector force produced by a unit joint torque. Substituting Eq. (3.19) into $\tau^T \tau = 1$ yields

$$F^T J J^T F = 1 \tag{3.20}$$

At a given manipulator configuration, Eq. (3.20) represents an m-dimensional ellipsoid. Because the product JJ^T is symmetric positive semi definite, its eigenvectors are orthogonal. The principle axes of the ellipsoid coincide with the eigenvectors of JJ^T, and their lengths are equal to the reciprocals of the square roots of the eigenvalues.
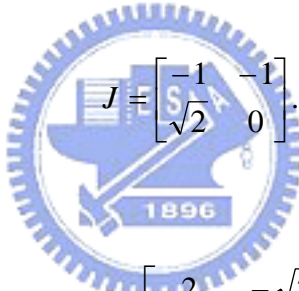
Since the Jacobian matrix is configuration dependent, the force ellipsoid is also configuration dependent. As the end-effector moves from one location to another, the shape and orientation of the force ellipsoid will also change accordingly. The closer the transmission is said to be isotropic when the principle axes are of equal lengths. At an isotropic point, an n-dimensional unit sphere in the joint torque space maps onto m-dimensional sphere in the end-effector force space. On the other hand, at a singular point, and n-dimensional unit sphere

in the joint torque space maps onto an m-dimensional cylinder in the end-effector force space. Thus the mechanical advantage of the manipulator becomes infinitely large in some direction.

Consider a three links planar serial manipulator is shown in Fig.2.7, apply the restricted condition which present in chapter one, reduce the Jacobian matrix of Eq.2.14 to Eq. (3.7), and yield a 2-dof manipulator. For this 2-dof manipulator, the end-effector output force and input joint torques can be written as $f = [f_x, f_y]^T$ and $\tau = [\tau_x, \tau_y]^T$, respectively. Substituting the Jacobain matrix, Eq. (3.7), into (3.19), we obtain

$$\begin{bmatrix} \tau_1 \\ \tau_2 \end{bmatrix} = \begin{bmatrix} -a_1 s\theta_1 - a_2 s\theta_{12} & a_1 c\theta_1 + a_2 c\theta_{12} \\ -a_2 s\theta_{12} & a_2 c\theta_{12} \end{bmatrix} \begin{bmatrix} f_x \\ f_y \end{bmatrix} \tag{3.21}$$

Let the link lengths be $a_1 = \sqrt{2}$ m and $a_2 = 1$ m. At the posture where $\theta_1 = 0$ and $\theta_1 = \pi/2$, the Jacobian matrix reduces to

$$J = \begin{bmatrix} \dfrac{-1}{\sqrt{2}} & -1 \\ 0 \end{bmatrix}.$$

Hence

$$JJ^T = \begin{bmatrix} 2 & -\sqrt{2} \\ -\sqrt{2} & 2 \end{bmatrix}.$$

The eigenvalues of JJ^T are $\lambda_1 = 2 - \sqrt{2} = 0.5858$ and $\lambda_2 = 2 + \sqrt{2} = 3.4142$. The corresponding eigenvectors, normalized to unit length, are (0.707, 0.707) and (-0.707, 0.707), respectively. These two eigenvectors are at $45°$ angles with the f_x and f_y axes, respectively, and they are lined up with the principle axes of the ellipse.

Substituting JJ^T into (3.20), we obtain

$$2f_x^2 - 2\sqrt{2}f_x f_y + 2f_y^2 = 0.5858\left(\frac{f_x}{\sqrt{2}} + \frac{f_y}{\sqrt{2}}\right)^2 + 3.4142\left(\frac{f_x}{\sqrt{2}} - \frac{f_y}{\sqrt{2}}\right)^2 = 1$$

Figure 3.2 shows the ellipse and its principal axes. The end-effector forces produced by a unit

joint torque are $(f_x, f_y) = (0.924, 0.924)$ N along the minor axis. The corresponding joint torques are $(\tau_1, \tau_2) = (0.383, -0.924) N \cdot m$ along the major axis and $(\tau_1, \tau_2) = (0.924, 0.383)$ $N \cdot m$ along the minor axis. We note that the mechanical advantage along the major axis is larger than that along the minor axis.

(a)

(b)

τ_y

P (0.924, 0.383)

P (-0.383, 0.383)

τ_x

M (0.383, -0.924)

f_y
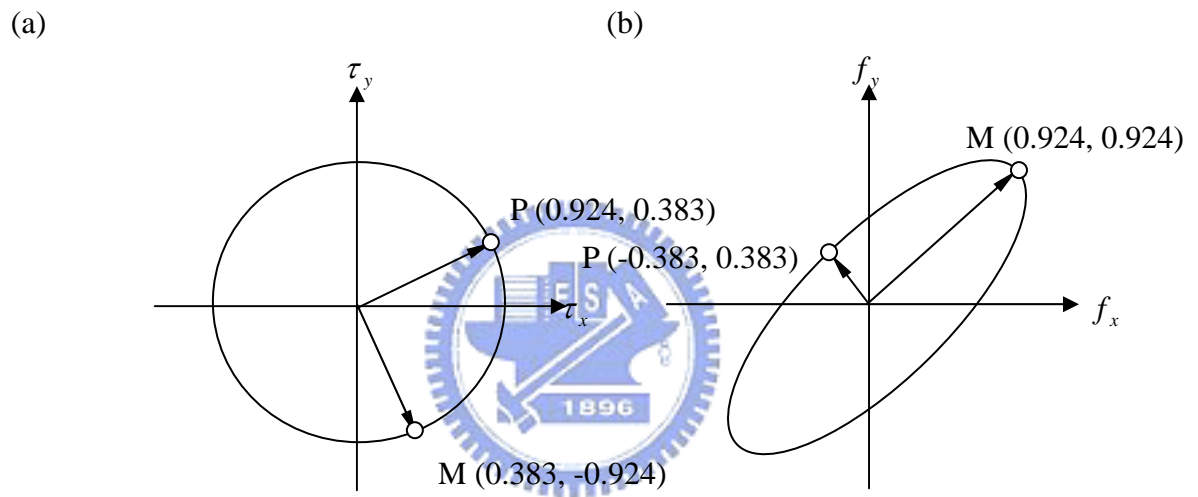
M (0.924, 0.924)

f_x

Fig.3.2 (a) Unity circle of joint torque.
(b) Force ellipsoid of end-effector.

3.4 Inverse Kinematics

For the inverse kinematics problem, the location of the end-effector is given and the problem is to find the joint angles θ_i, i = 1, 2, 3, necessary to bring the end-effector to the desired location. For a planar 3-dof manipulator, the end-effector can be specified in terms of the position of point Q and orientation angle Φ of the end-effector. Hence the overall transformation matrix from the end-effector coordinate system to the base coordinate system, $^0A_3$, is given by

$$^0A_3 = \begin{bmatrix} c\Phi & -s\Phi & 0 & q_x \\ s\Phi & c\Phi & 0 & q_y \\ 0 & 0 & 1 & 0 \\ 0 & 0 & 0 & 1 \end{bmatrix} \tag{3.21}$$

Inverse kinematics solution can be obtained by equating the elements of Eq. (2.7) to that of (3.21). To find the orientation of the end-effector, we equate the (1, 1) and (2, 1) elements of Eq. (2.7) to that of (3.21):

$$c\theta_{123} = c\Phi, \tag{3.22}$$

$$s\theta_{123} = s\Phi, \tag{3.23}$$

Hence

$$\theta_{123} = \theta_1 + \theta_2 + \theta_3 = \Phi \tag{3.24}$$

Next we equate the (1, 4) and (2, 4) elements of Eq. (2.7) to that of (3.21):

$$P_X = a_1 c\theta_1 + a_2 c\theta_{12}, \tag{3.25}$$

$$P_Y = a_1 s\theta_1 + a_2 s\theta_{12}, \tag{3.26}$$

where $P_X = q_X - a_3 c\Phi$ and $P_Y = q_Y - a_3 s\Phi$ denote the position vector of the point P located at the third joint axis is shown in Fig. 2.7. Note that by using this substitution θ_3 disappears from Eq. (3.25) and (3.26). From Fig. 2.7 we observe that the distance from point O to P is independent of θ_1. Hence we can eliminate θ_1 by summing the squares of Eq.

(3.25) and (3.26); that is,

$$P_X{}^2 + P_Y{}^2 = a_1{}^2 + a_2{}^2 + 2a_1a_2c\theta_2 \qquad (3.27)$$

Solving Eq. (3.27) for θ_2, we obtain

$$\theta_2 = \cos^{-1}k, \qquad (3.28)$$

where

$$k = \frac{P_X{}^2 + P_Y{}^2 - a_1{}^2 - a_2{}^2}{2a_1a_2}$$

Equation (3.28) yields (1) two real roots if $|k| < 1$, (2) one double root if $|k| = 1$, and (3) no real roots if $|k| > 1$, In general, if $\theta_2 = \theta_2{}^*$ is a solution, $\theta_2 = -\theta_2{}^*$ is also a solution, where $\pi \geq \theta_2{}^* \geq 0$. We call $\theta_2 = \theta_2{}^*$ the elbow-down solution and $\theta_2 = -\theta_2{}^*$ the elbow-up solution. If $|k| = 1$, the arm is in a fully stretched or folded configuration. If $|k| > 1$, the position is not reachable.
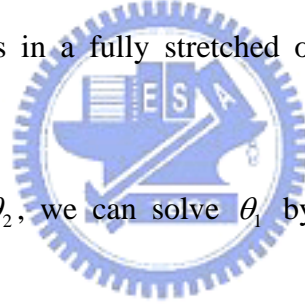
Corresponding to each θ_2, we can solve θ_1 by expending Eq. (3.25) and (3.26) as follows:

$$(a_1 + a_2c\theta_2)c\theta_1 - (a_2s\theta_2)s\theta_1 = p_X, \qquad (3.29)$$

$$(a_2S\theta_2)c\theta_1 + (a_1 + a_2c\theta_2)s\theta_1 = p_Y, \qquad (3.30)$$

Solving Eq.(3.29) and (3.30) for $c\theta_1$ and $s\theta_1$, yields

$$c\theta_1 = \frac{p_X(a_1 + a_2c\theta_2) + P_Ya_2s\theta_2}{\Delta},$$

$$s\theta_1 = \frac{-P_Ya_2s\theta_2 + p_y(a_1 + a_2c\theta_2)}{\Delta},$$

where $\Delta = a_1{}^2 + a_2{}^2 + 2a_1a_2c\theta_2$. Hence, corresponding to each θ_2, we obtain a unique solution for θ_1:

$$\theta_1 = A\tan2(s\theta_1, c\theta_1). \qquad (3.31)$$

In a computer program we may use the function $A\tan 2(x,y)$ to obtain a unique solution for θ_1. However, the solution may be real or complex. A complex solution corresponds to an end-effector location that is not reachable by the manipulator. Once θ_1 and θ_2 are known, Eq. (3.24) yields a unique solution for θ_3. Hence, corresponding to a given end-effector location, there are generally two real inverse kinematics solution, one being the reflection of the other about a line connecting points O and P, is illustrated in Fig. 3.3

For the purpose of simulation of human being's motion, we have to constraint the work space of joint of KHR-1 biped robot and kinematical model into a valid sphere. In other words, when we have two possible inverse kinematics solutions, each one must be satisfied with the constraint of human being's motion, any invalid posture such as elbow up in Fig. 3.3, will be ignored in our biped robot gait generation procedure.

We adopted the inverse kinematics to solve the problem of two legs locomotion of biped robot. The original characteristic of kinematical model of KHR-1 biped robot is a spatial parallel type manipulator, is shown in Fig. 3.4, we can see the front leg with angles, θ_{1F} and θ_{2F}, back leg with angles, θ_{1B} and θ_{2B}. Based on the inverse kinematics, we can separate these two legs into two planar serial type manipulators, and then simplify the original characteristic of kinematical model.

Assuming the posture of front leg in arbitrary interval of time is given by defining the coordinate system, therefore, the end-effecotr, point H, is given, too. Notice that the end-effector of front leg is also the one of back leg, according to this correlation; one can find out the configuration of back leg and obtain the solutions of angles of θ_{1B} and θ_{2B} by inverse kinematics.

Q(CoM), end-effector

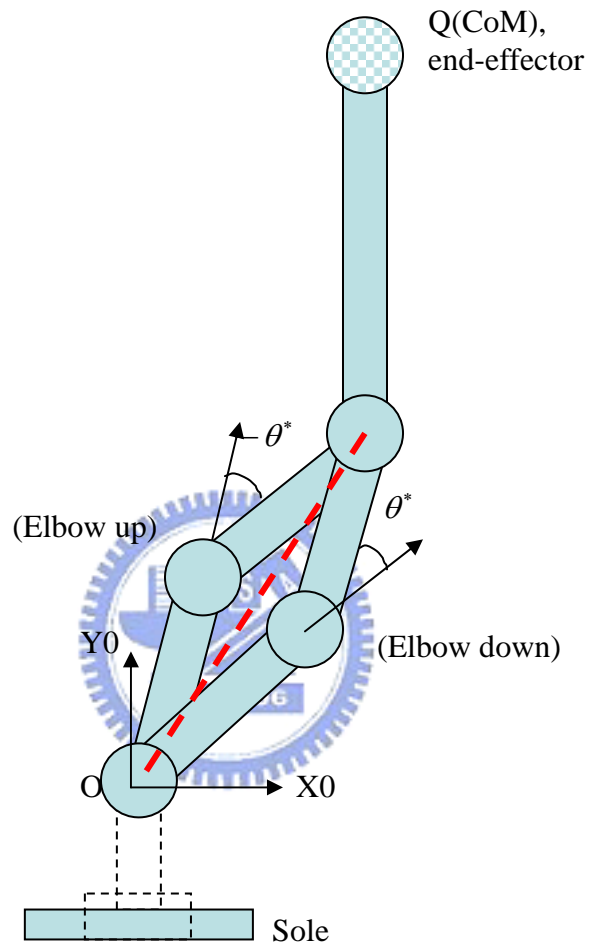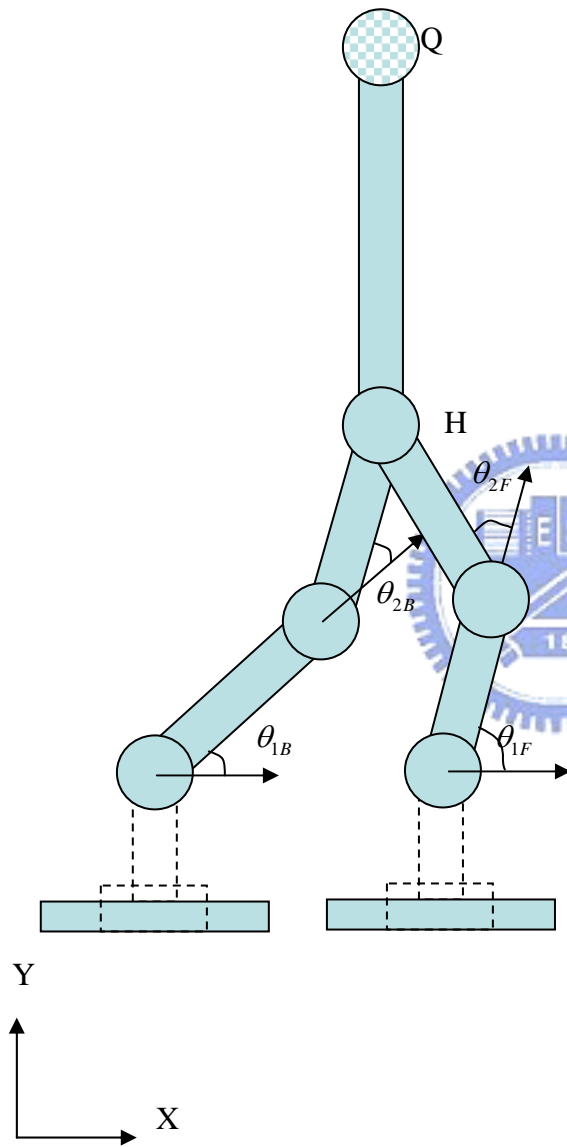θ^*

(Elbow up)

θ^*

Y0

(Elbow down)

O X0

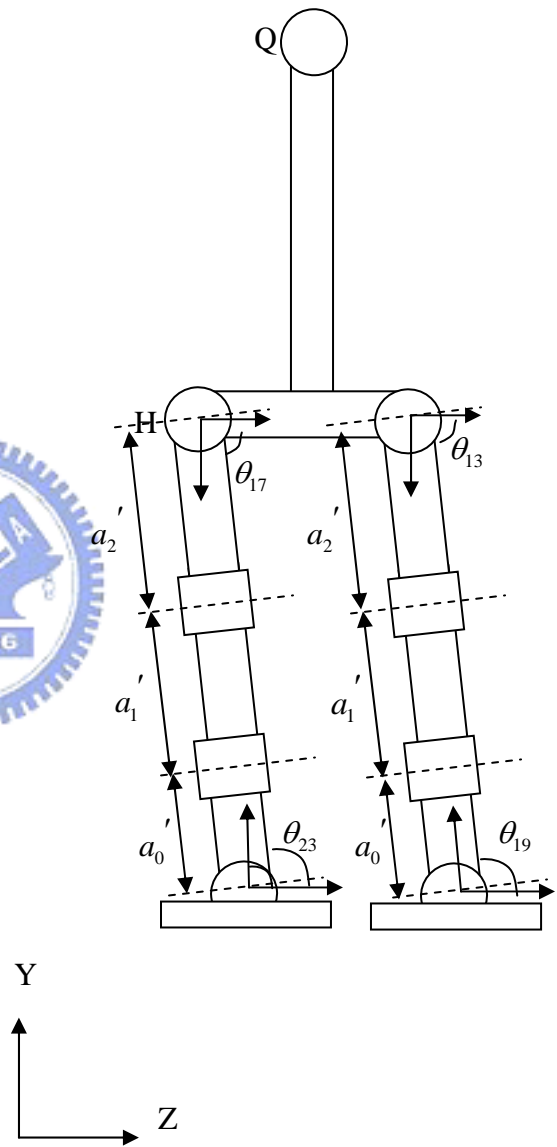Sole

Fig.3.3 Two possible inverse kinematics solution

Fig.3.4 Inverse kinematics implement for simplifying the kinematical model.
(a) X-Y plane
(b) Z-Y plane

3.5 ZMP (Zero-Moment Point) Algorithm

ZMP (Zero-Moment Point) algorithm was presented by M. Vukobratovich in 1970's. The ZMP algorithm has been presented over thirty five years. Its first practical demonstration was announced at Waseda University, Laboratory of Ichiro Kato in Japan in year 1984. It is also the first demonstration of dynamically balanced case of the WL-10RD robot which was the member of the robot family WABOT [13].

Referring to Fig. 3.5 (a), the ZMP is the point on the ground where the tipping moment, $M^P n$, acting on the biped, due to gravity and inertia forces, equals zero, the tipping moment being defined as the component of the moment that is tangential to the supporting surface. It should be noted that the term ZMP is not a perfectly exact expression because the normal component of the moment generated by the inertia forces acting on the biped is not necessarily zero. If we bear in mind, however, that ZMP abridges the exact expression "zero tipping moment point," then the term becomes perfectly acceptable [14].

The robot is subjected to a Ground Reaction Force (GRF), $\hat{R}$, at the point P, which is the center of pressure (CoP). Due to unilaterality of the GRF, P is always located within the convex hull of the foot support area. In Fig. 3.5 (b) left part, the GRF passes through the CoM at point G and consequently generates a zero moment. Thus $\dot{H}_G = 0$ and the robot will not be rotated. In Fig. 3.5 (b) right part, the GRF does not pass through the CoM thus generating a net clockwise moment around the CoM, i.e. $\dot{H}_G = GP \times \hat{R} \neq 0$. This implies the tendency of the robot to tip forward.

In current demonstrated example, based on the ZMP algorithm, the X-Z plane projection of zero moment point, Q', was constricted in the convex hull which was formed by single leg or two legs, the schematic area illustrated in Fig. 3.6 (a) and (b). Therefore, the point, Q in X-Y plane, Q' in Z-Y plane must be satisfied based on this theory so that the biped gait will be kept in the stable condition.
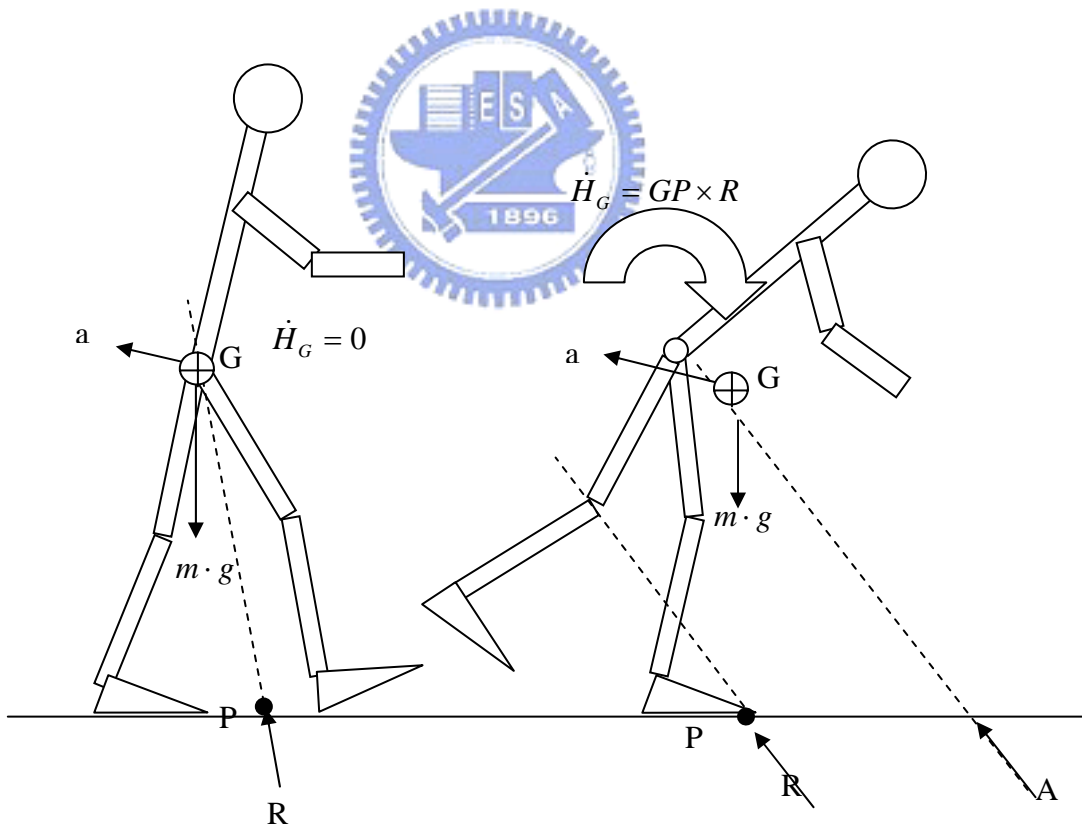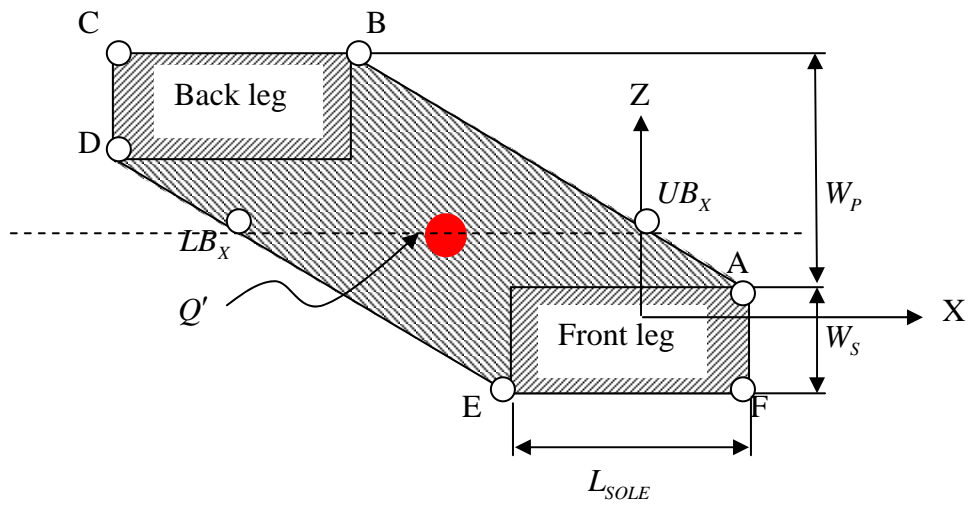
(a)
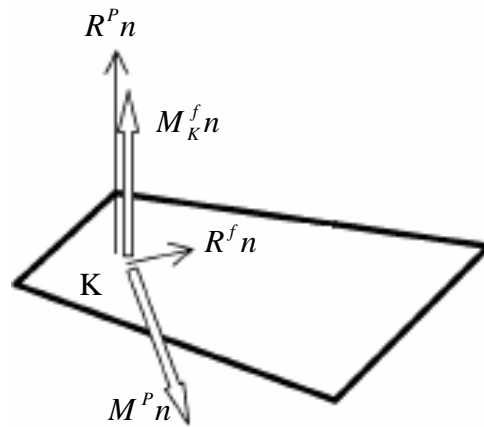
(b)

Fig.3.5 (a) The Single sole support area with tipping moment.
  (b) General configuration of a biped robot under interaction force/torque from ground and environment.
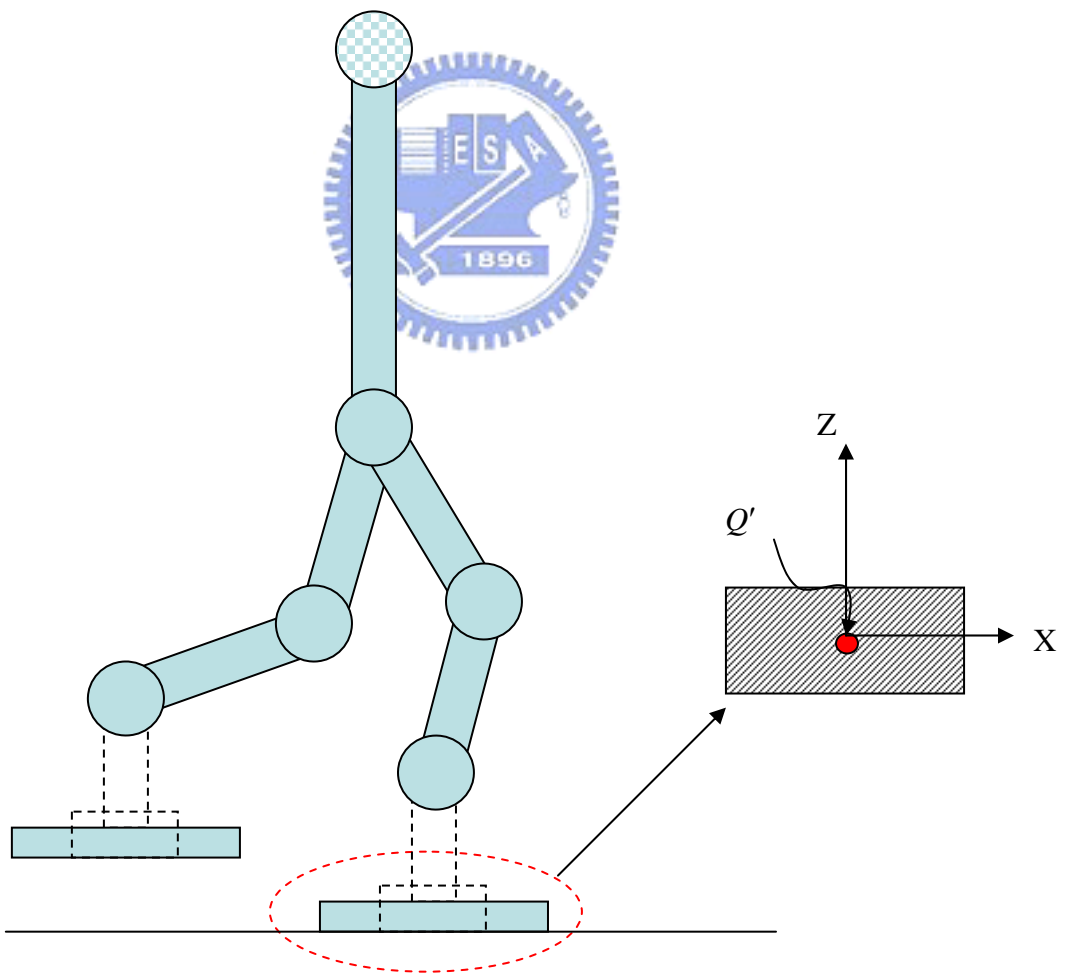
(a)

(b)

Fig.3.6 (a) Double support phase.
(b) Single support phase.

CHAPTER 4

Result of Simulation and Theoretical Analysis

4.1 Introduction

In this research we design a sequent biped gait which includes three envelopes (Fig. 1.1), the first envelope was defined as a robot or a human being is trying to approach to posture of standing from initial posture of squatting. The second envelope was defined as making first stride from initial posture of standing and the last envelope was defined as making another stride from the initial posture of previous stride.

Envelope two and three were connected as a cycle of walking motion, walk slowly, which is compared with a human being's action in the reality. We had been mentioned assumptions in chapter one, base on the static kinematics, in a specific locomotion which manipulate very slowly, however, in arbitrary interval of time, the robot can be kept in stable condition.

In this chapter we are going to present the result of experiments of KHR-1 robot locomotion. Notice the manipulation of KHR-1 robot with the joint trajectories was yielded from the main algorithms which were mentioned in chapter three. The presentation will be divided to two parts:

(1) Envelope one, two methods were implemented in the biped gait experimentation, the first method is only consider the effect of minimum combination of angular velocity through velocity ellipsoid, the second method is consider both the effects of minimum combination of angular velocity and minimum combination of joints torque through velocity ellipsoid and force ellipsoid. A combined estimate function, $e_1(t_i)$ and $e_2(t_i)$ were adopted to estimate the difference of these two methods.

(2) Envelope two and three, compare the sample motion which is developed by supplier,

KONDO Co., with the locomotion, walk slowly, which is developed by this research.

4.2 Introduction of Envelope One

We developed two methods to implement the manipulability ellipsoid algorithm and realize the biped robot gait. Method one is based on the effect of the minimum combination of angular velocity of each joint through angular velocity ellipsoid. Method two is based on effect of the combination of velocity of each joint through angular velocity ellipsoid and combination of joint torque through force ellipsoid. Through these two different methods we will find out the appropriate implementation of manipulability.

The transformation of postures can be divided to several segments, as shown in Table 4.1, each segment is the control point which defined as a node [8]. From node to node, the angular displacement in arbitrary interval will be decided by manipulability ellipsoid algorithm.

The definition of envelope one is from an initial posture, squatting, to goal posture, standing. In this envelope, the ZMP area constructed by both legs, double support phase, the projection of CoM, Q', will be constricted within this area in arbitrary interval of time or the robot could be tipped up by an unbalance torque.

The trajectory planning in envelope one is based on manipulability ellipsoid algorithm; the theory includes the unity end-effector velocity circle in end-effector force space and velocity ellipsoid in the joint torque space. We can find a coordinate to determine the velocity of end-effector in Cartesian coordinate which is corresponding to another coordinate on ellipsoid which determines joints rates. Because we have already known that the motion, squat to stand up, extend the body of robot in a continuously motion, we constraint the end-effector moves along the $V_x = 0$, and $V_y > 0$, then the half unity end-effector velocity circle and half velocity ellipsoid will be produced. In arbitrary instantaneous segment of robot motion, the graph of unity end-effector velocity circle and velocity ellipsoid is individual.

Table 4.1 Detail process of biped gait generation in envelope one.

Detail Process of Biped Gait Generation				
Status	Posture in X-Y Plane	Posture in Z-Y Plane	Angular Displacement	Range of Unity Circle of end-effector
Envelope 1			$\theta_{1F} = \theta_{1B} = 30$ $\theta_{2F} = \theta_{2B} = 105$ $\theta_{23F} = \theta_{19B} = 90$ $\theta_{17F} = \theta_{13B} = 90$	
			$\theta_{1F} = \theta_{1B} = 90$ $\theta_{2F} = \theta_{2B} = 0$ $\theta_{23F} = \theta_{19B} = 90$ $\theta_{17F} = \theta_{13B} = 90$	Front leg: $(V_X - V_Y)$ $\theta_{V(FRONT)} = 0 \sim 180$ Back leg: $(V_X - V_Y)$ $\theta_{V(BACK)} = 0 \sim 180$

(a)
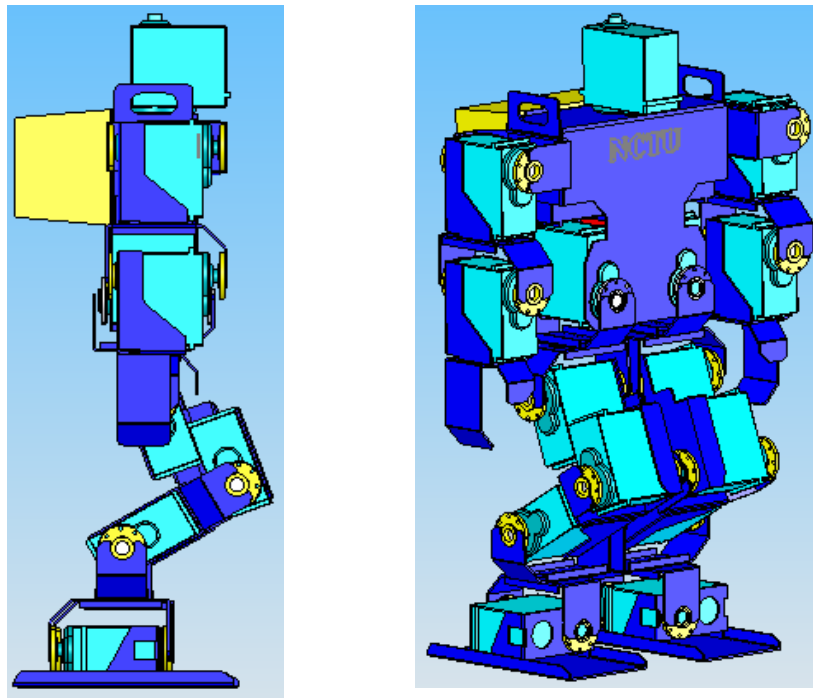
(b)
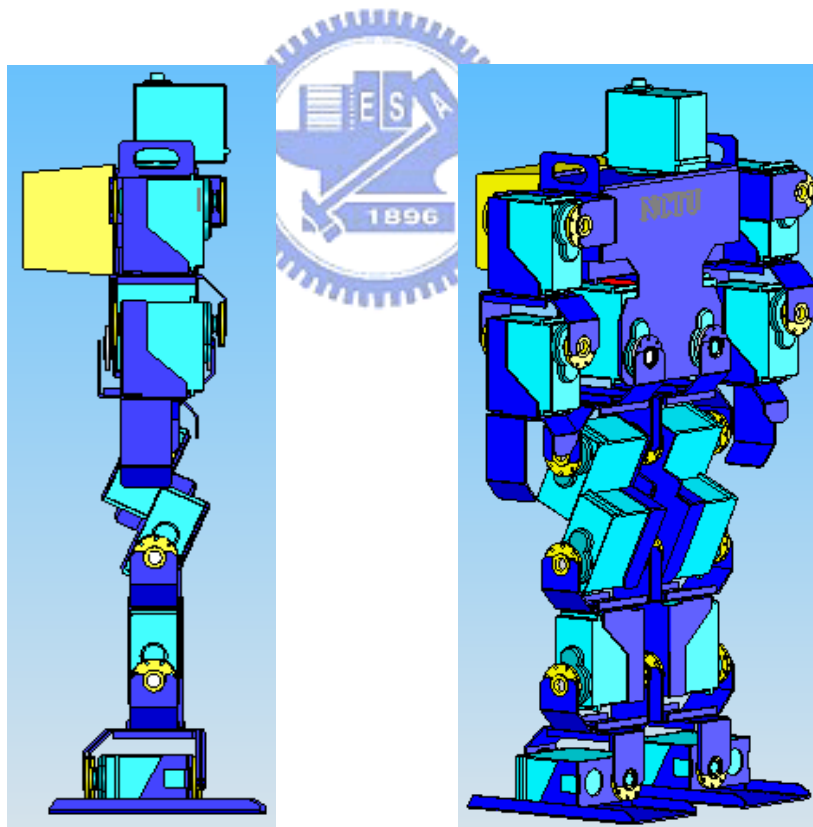
Fig.4.1 (a) Initial posture right view and 3-D view.
(b) Goal posture right view and 3-D view.

4.2.1 Compound Estimate Function in Envelope one

A compound estimate function, $e_1(t_i)$ and $e_2(t_i)$ is a criterion to estimate the two different methods for realizing the envelope one, where the $e_1(t_i)$ is associated with method one, and $e_2(t_i)$ is associated with method two. The definition of compound estimate function is combine the two parameters, combination of angular velocity of each joint and combination of joint torque, and give it a weight to avoid the situation of magnitude of two parameters are extremely differ from each other. In terms of obtain a stable condition of biped gait, the ideal condition is the angular displacement in arbitrary interval of time is determined by the minimum combination of angular velocity of each joint which is produced from last interval of time. We define the ideal stable condition as

$$C_{MIN,F} = \sqrt{\dot{\theta}_{1F}^2 + \dot{\theta}_{2F}^2} \tag{4.1}$$

$$C_{MIN,B} = \sqrt{\dot{\theta}_{1B}^2 + \dot{\theta}_{2B}^2} \tag{4.2}$$

Where the $C_{MIN,F}$ is determined for front leg and $C_{MIN,B}$ is determined for back leg. Because the manipulation of front and back legs are totally the same in envelope one, therefore we just need to consider the $C_{MIN,F}$ or $C_{MIN,B}$. In terms of reducing the energy consumption, the ideal condition in arbitrary interval of time is associated with the minimum combination of joint torque. We also can determine the ideal condition for reducing energy consumption as

$$F_{MIN,F} = \sqrt{\tau_{1F}^2 + \tau_{2F}^2} \tag{4.3}$$

$$F_{MIN,B} = \sqrt{\tau_{1B}^2 + \tau_{2B}^2} \tag{4.4}$$

Where the $F_{MIN,F}$ is determined for front leg and is determined for back leg. Because the manipulation of front and back legs are totally the same in envelope one, therefore we just need to consider the $F_{MIN,F}$ or $F_{MIN,B}$.

From Eq. (2.15) and (3.21), we can find out that the $C_{MIN,F}$, $C_{MIN,B}$, $F_{MIN,F}$, $F_{MIN,B}$ are all depend on the configuration of last interval of time. Therefore, we must consider these four parameters at the same time when a configuration in arbitrary time is determined suppose we want to yield a stable and effort-saving biped robot gait. Next, we can define the compound estimate function which is based on this idea

$$e_j(t_i) = \frac{\sqrt{\dot{\theta}_1^{\,2} + \dot{\theta}_2^{\,2}}}{\max \sqrt{\dot{\theta}_1^{\,2} + \dot{\theta}_2^{\,2}}} + \frac{\sqrt{\tau_1^{\,2} + \tau_2^{\,2}}}{\max \sqrt{\tau_1^{\,2} + \tau_2^{\,2}}}, \quad (j=1,\ 2) \tag{4.5}$$

Where j=1 determine the compound estimate function of method one, and j=2 determine the compound estimate function of method two. When numerator of $\sqrt{\dot{\theta}_1^{\,2} + \dot{\theta}_2^{\,2}}$ and $\sqrt{\tau_1^{\,2} + \tau_2^{\,2}}$ is smaller, then $e_j(t_i)$ will be smaller and yield a stable condition and effort-saving condition of biped robot gait. In this sense, $e_j(t_i)$ is the smaller the better. The angular displacement in arbitrary interval of time will be determined by the smallest $e_j(t_i)$. In envelope one, we are trying to compare the method one and method two, finally we will obtain a conclusion which is better than the other one. The compound estimate function of method one is

$$e_1(t_i) = \frac{\min \sqrt{\dot{\theta}_1^{\,2} + \dot{\theta}_2^{\,2}}}{\max \sqrt{\dot{\theta}_1^{\,2} + \dot{\theta}_2^{\,2}}} + \frac{\sqrt{\tau_1^{\,2} + \tau_2^{\,2}}}{\max \sqrt{\tau_1^{\,2} + \tau_2^{\,2}}} \tag{4.6}$$

Where the numerator of $\min \sqrt{\dot{\theta}_1^{\,2} + \dot{\theta}_2^{\,2}}$ is determined the minimum combination of angular velocity in arbitrary interval of time, and the $\sqrt{\tau_1^{\,2} + \tau_2^{\,2}}$ is corresponding to the same configuration which derive the $\min \sqrt{\dot{\theta}_1^{\,2} + \dot{\theta}_2^{\,2}}$.

4.2.2 Process Flows of Two Different Methods in Envelope One

We can find out the differences between method one and two from Fig. 4.2 and 4.3, here are the presentation of differences between these two methods:

(1) Method one: Determine the angular displacement of next interval of time through finding

out the minimum $\sqrt{\dot{\theta}_1^2 + \dot{\theta}_2^2}$. The angular displacement of next interval of time is

produced by the minimum $\sqrt{\dot{\theta}_1^2 + \dot{\theta}_2^2}$ of last interval of time. Therefore, the result of

angular displacement of arbitrary interval of time is independent of joint torque.

(2) Method two: Determine the angular displacement of next interval of time by considering

both $\sqrt{\dot{\theta}_1^2 + \dot{\theta}_2^2}$ and $\sqrt{\tau_1^2 + \tau_2^2}$, and the compound estimate function is based on

estimating $\sqrt{\dot{\theta}_1^2 + \dot{\theta}_2^2}$ and $\sqrt{\tau_1^2 + \tau_2^2}$ at the same time. Therefore, we can conclude the

angular displacement of next interval of time is determined by compound estimate

function. Notice that in method one, though the minimum $\sqrt{\dot{\theta}_1^2 + \dot{\theta}_2^2}$ can cause a stable

condition for robot gait, but the $\sqrt{\tau_1^2 + \tau_2^2}$ which correspond to minimum $\sqrt{\dot{\theta}_1^2 + \dot{\theta}_2^2}$ is

not necessarily the minimum choice which can reduce the energy consumption in the best

situation. On the other hand, method two is adopted a balanced decision for yielding the

stability and reducing energy consumption at the same time.

```
┌─────────────────────────────────────┐
│ (1) Define the initial configuration│
│   θ₁F = θ₁B, θ₂F = θ₂B               │
└─────────────────────────────────────┘
                 │
                 ▼
┌─────────────────────────────────────┐
│ (2) Jacobian matrix calculating     │
└─────────────────────────────────────┘
```

(1) Define the initial configuration
$$\theta_{1F} = \theta_{1B}, \theta_{2F} = \theta_{2B}$$

(2) Jacobian matrix calculating

(3) Velocity Ellipsoid

$$C_1 = \sqrt{\dot{\theta}_1^2 + \dot{\theta}_2^2}$$
$$C_2 = \sqrt{\dot{\theta}_1^2 + \dot{\theta}_2^2}$$
$$\vdots$$
$$C_{180} = \sqrt{\dot{\theta}_1^2 + \dot{\theta}_2^2}$$

(4) Force Ellipsoid

$$F_1 = \sqrt{\tau_1^2 + \tau_2^2}$$
$$F_2 = \sqrt{\tau_1^2 + \tau_2^2}$$
$$\vdots$$
$$F_{180} = \sqrt{\tau_1^2 + \tau_2^2}$$

(5) Find the
$$\min \sqrt{\dot{\theta}_1^2 + \dot{\theta}_2^2} \quad \text{and} \sqrt{\tau_1^2 + \tau_2^2}$$
which correspond to $\min \sqrt{\dot{\theta}_1^2 + \dot{\theta}_2^2}$

(6) Obtain $e_1(t_i)$

(7) Produce new angular displacement
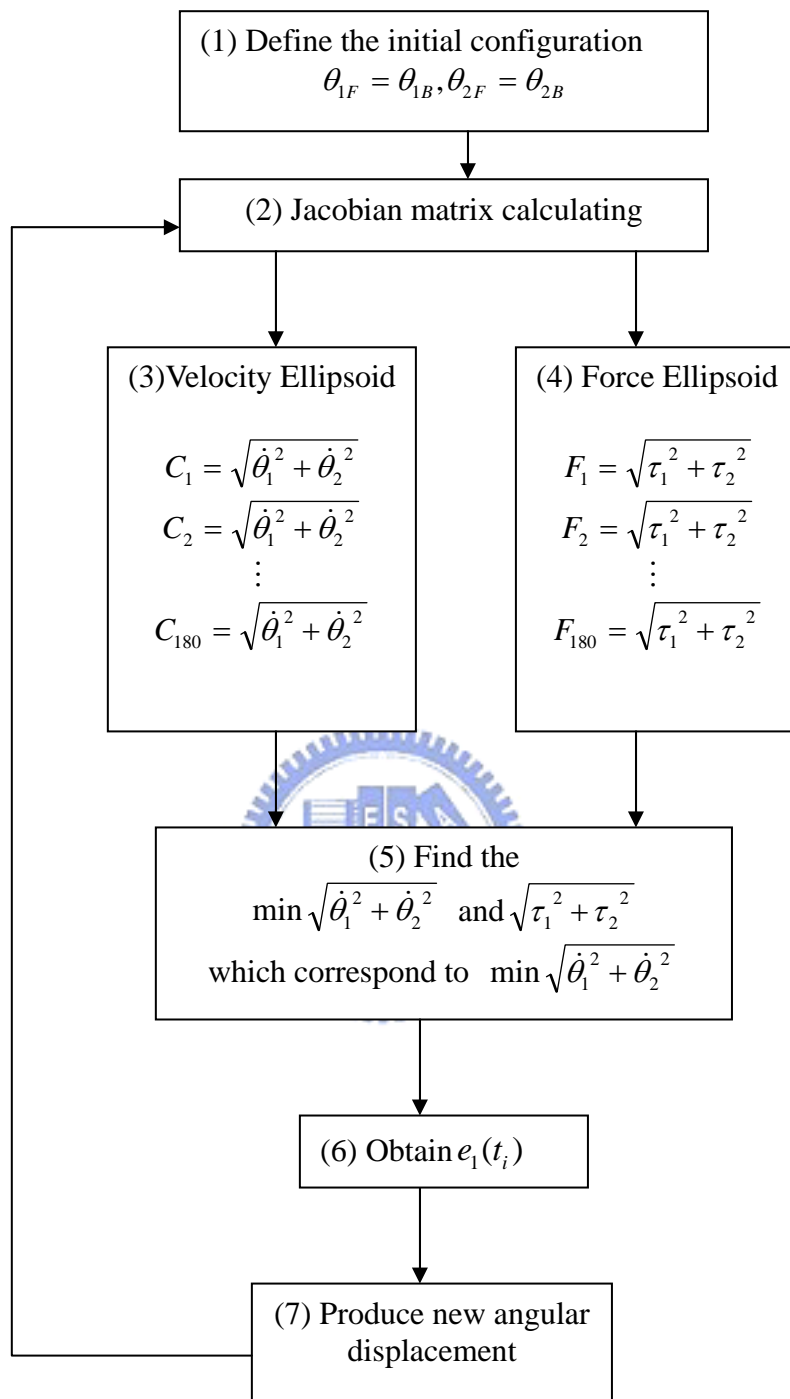
Fig 4.2 Process flow chart of method one on envelope one.

```
┌─────────────────────────────────────┐
│ (1) Define the initial configuration │
│   θ₁F = θ₁B, θ₂F = θ₂B                │
└─────────────────────────────────────┘
```

(1) Define the initial configuration
$$\theta_{1F} = \theta_{1B}, \theta_{2F} = \theta_{2B}$$

(2) Jacobian matrix calculating

(3) Velocity Ellipsoid

$$C_1 = \sqrt{\dot{\theta}_1^{\,2} + \dot{\theta}_2^{\,2}}$$
$$C_2 = \sqrt{\dot{\theta}_1^{\,2} + \dot{\theta}_2^{\,2}}$$
$$\vdots$$
$$C_{180} = \sqrt{\dot{\theta}_1^{\,2} + \dot{\theta}_2^{\,2}}$$

(4) Force Ellipsoid

$$F_1 = \sqrt{\tau_1^{\,2} + \tau_2^{\,2}}$$
$$F_2 = \sqrt{\tau_1^{\,2} + \tau_2^{\,2}}$$
$$\vdots$$
$$F_{180} = \sqrt{\tau_1^{\,2} + \tau_2^{\,2}}$$

(5) $e_{2,1}(t_i)$
$e_{2,2}(t_i)$
$\vdots$
$e_{180,2}(t_i)$

(6) Find minimum $e_2(t_i)$

(7) Find the $\dot{\theta}_1$, $\dot{\theta}_2$, τ_1, τ_2 corresponding to minimum $e_2(t_i)$

(8) Produce new angular displacement
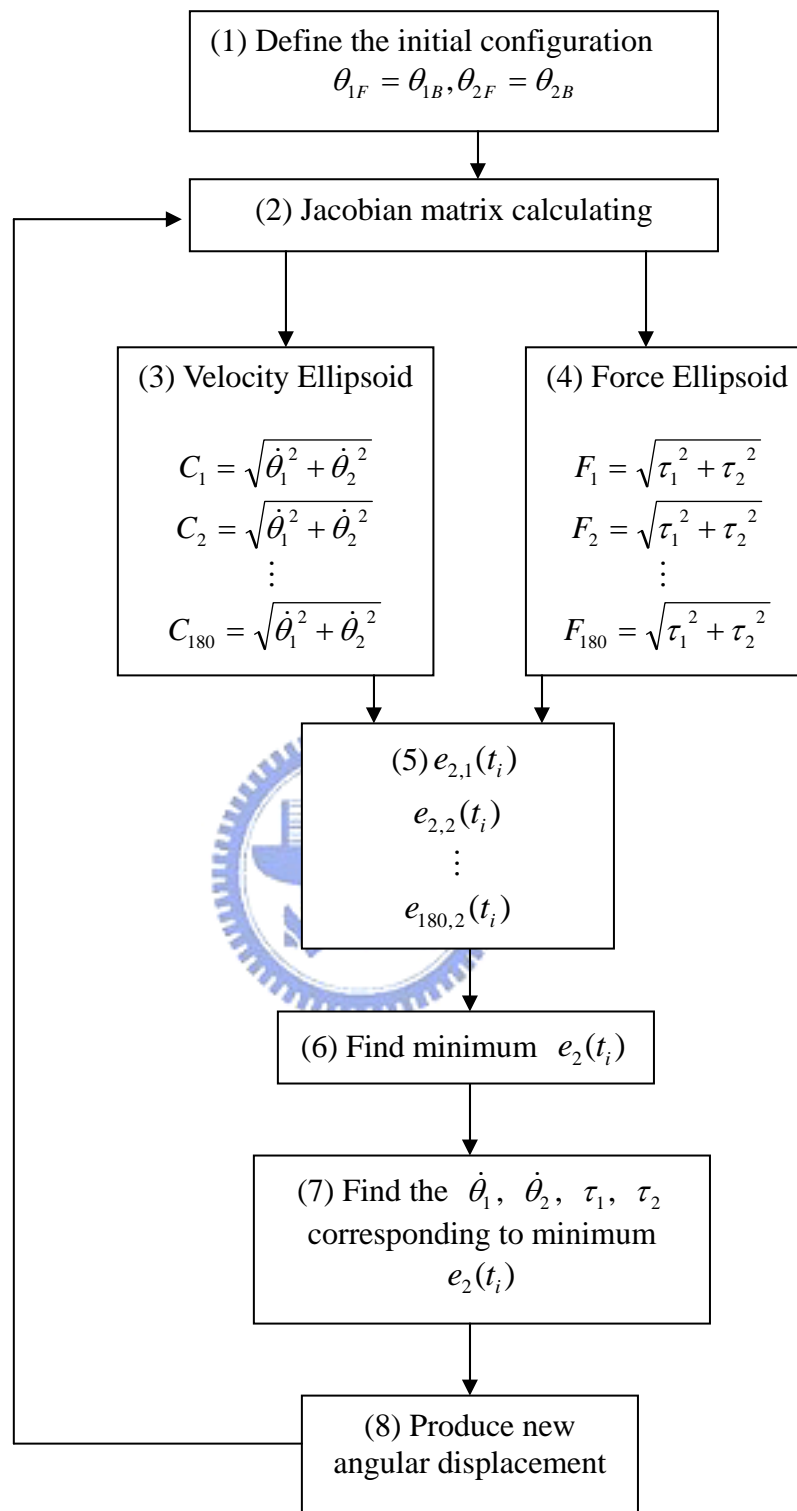
Fig 4.3 Process flow chart of method two on envelope one.

4.2.3 The Result of Simulation in Envelope One

We are going to present the differences between method one and two through several important parameters, joint locations, angular displacement, angular velocity, joint torque and compound estimate function.

In terms of angular displacement, in Fig. 4.4 (a) and (b), we can find out the variation of curve of angular velocity through method one and two is quite different. Besides, the tendency of X-Y distribution of angular velocity appear the method two is more smooth than method one, and this is a quite important information, in other words, the behavior of angular displacement through method two is more stable than method one. Furthermore, the period of method two is shorter than method one, it means, cost of time through method two is less than method one.

In terms of joint location variation, the result of these two methods is obviously different from each other. Curve of method two is more like a weight lifting player doing his motion with dumbbell and it is more like the way human being's motion.

In terms of joint torque, we can easily find out the summary of joint torque through method two is less than method one, in other words, the effort of reducing energy consumption through method two will be better than method one.

In terms of the most important criterion, compound estimate function, a better effort of method can be found out in Fig. 4.10 and Table 4.2. In most situations, the compound estimate function of method two is smaller than method one, therefore, the efficiency of approaching the purpose with stable and energy consumption at the same time through method two will be better than method one.

(a)
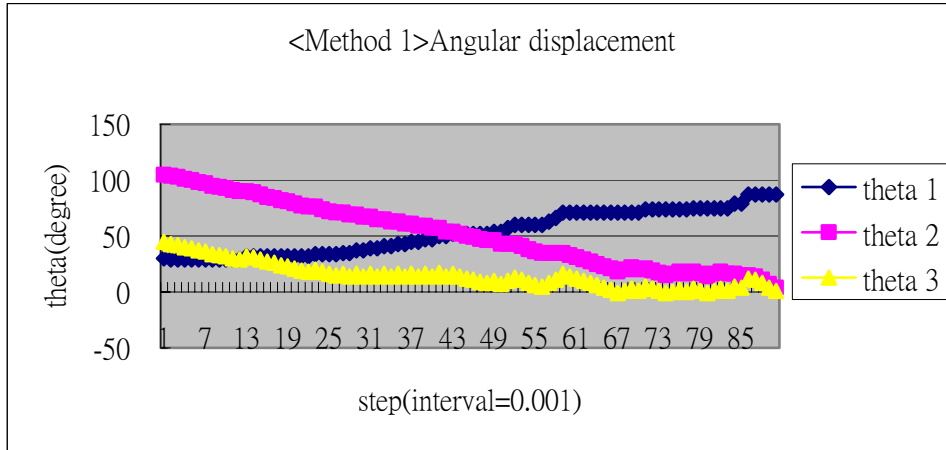
(b)
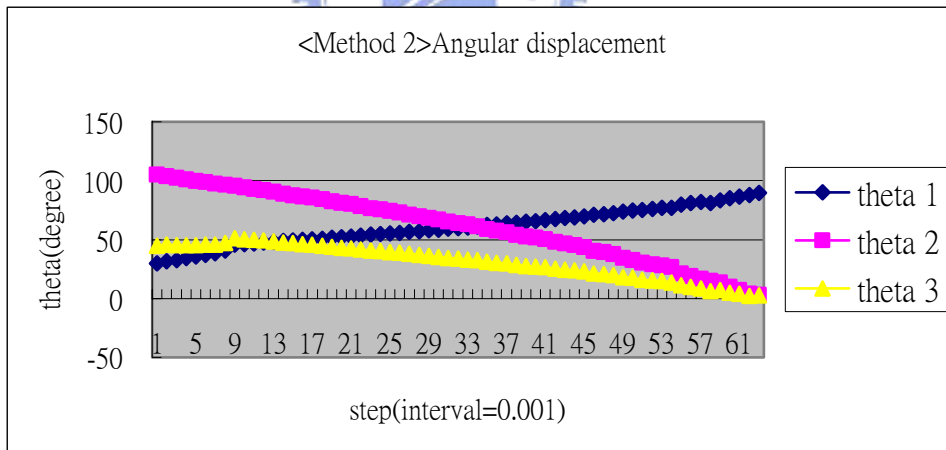
Fig. 4.4 (a) Angular displacement of method one.
(b) Angular displacement of method two.

(a)

<Method 1>X-Y ditribution of angular displacement

(b)

<Method 2>X-Y distribution of angular displacement
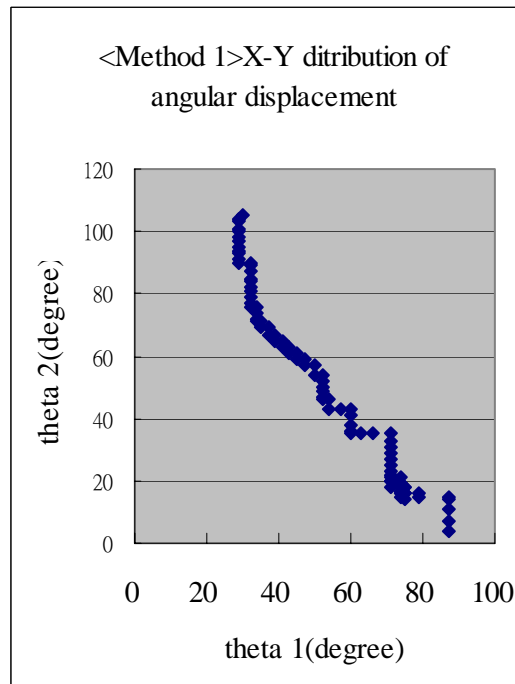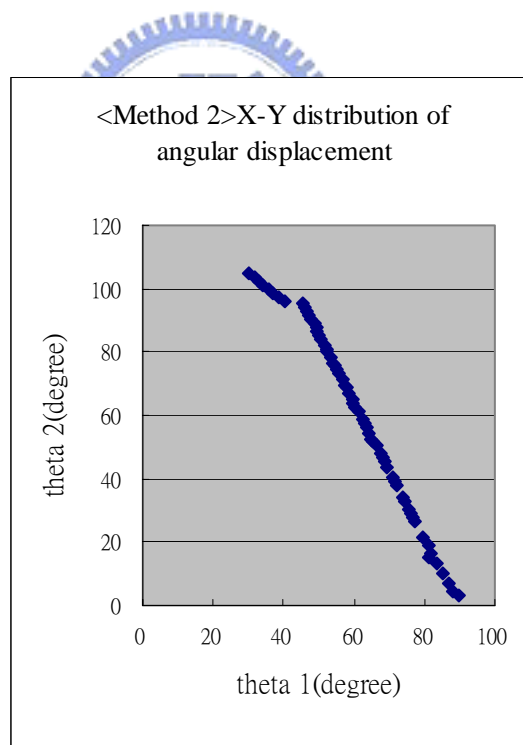
Fig. 4.5 (a) X-Y distribution of angular displacement of method one.
(b) X-Y distribution of angular displacement of method two.

(a)
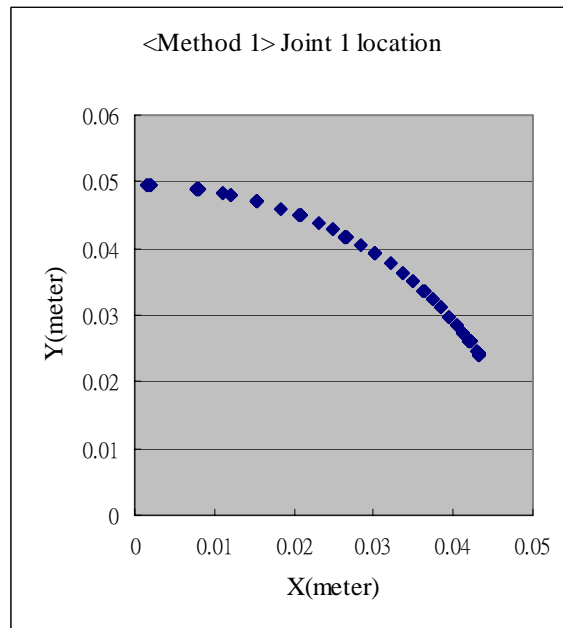
(b)
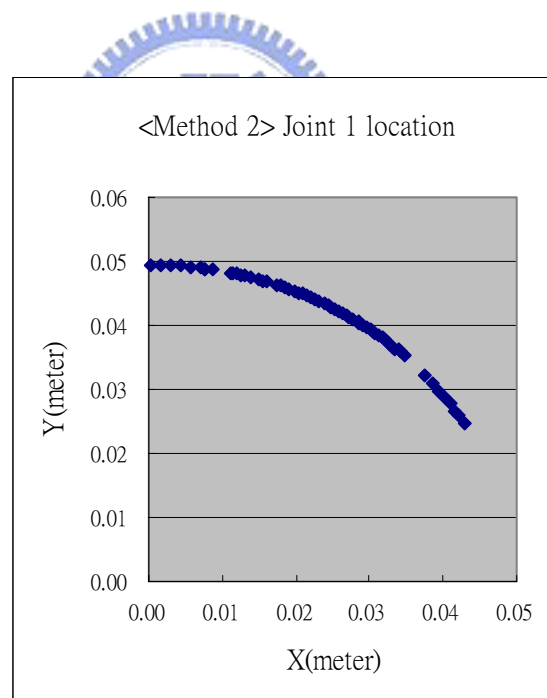
Fig. 4.6 (a) Joint one location of method one.
(b) Joint one location of method two.
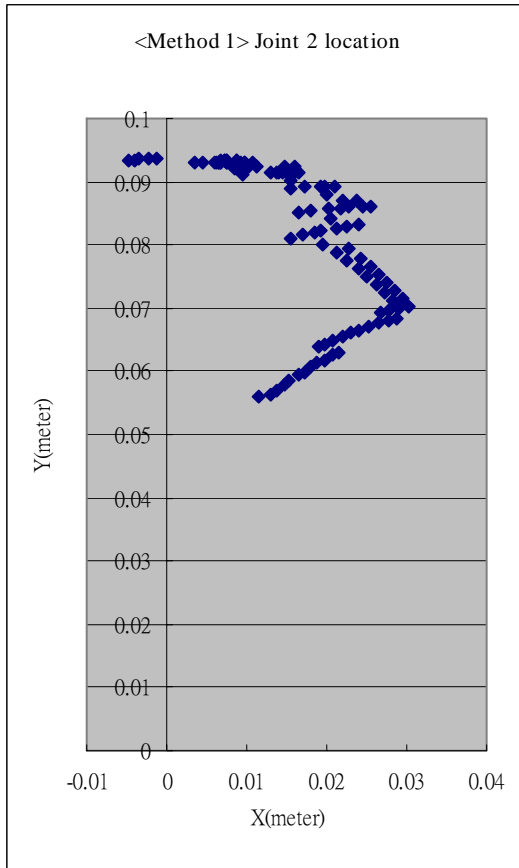
(a)　　　　　　　　　　　　　　　　　　　　(b)
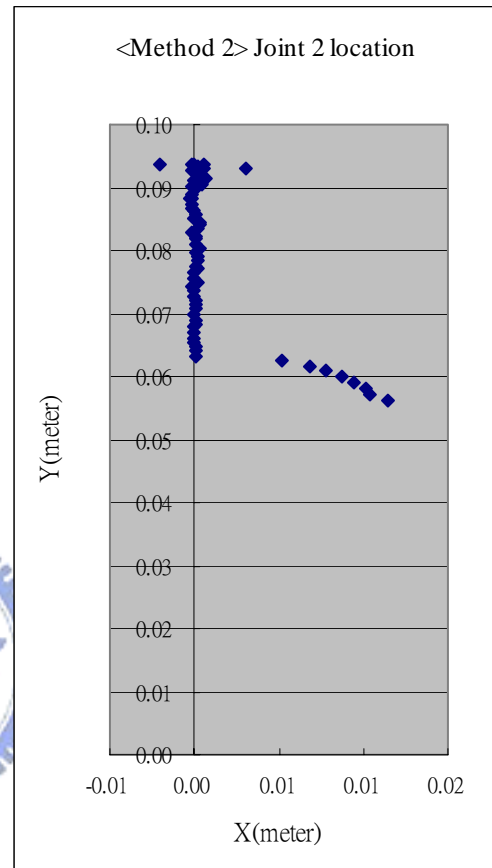
Fig. 4.7 (a) Joint two location of method one.
(b) Joint two location of method two.

(a)

(b)

(c)
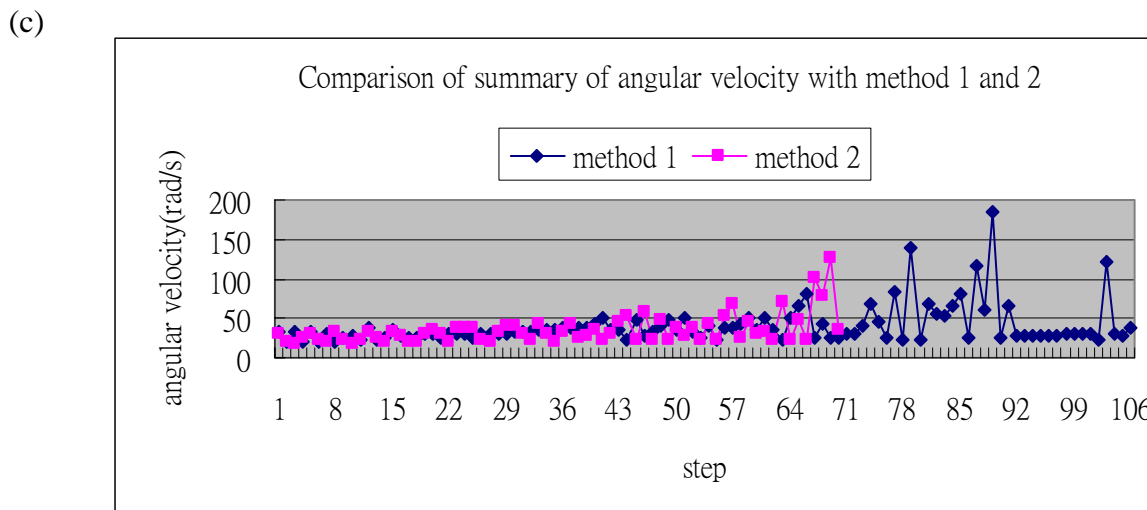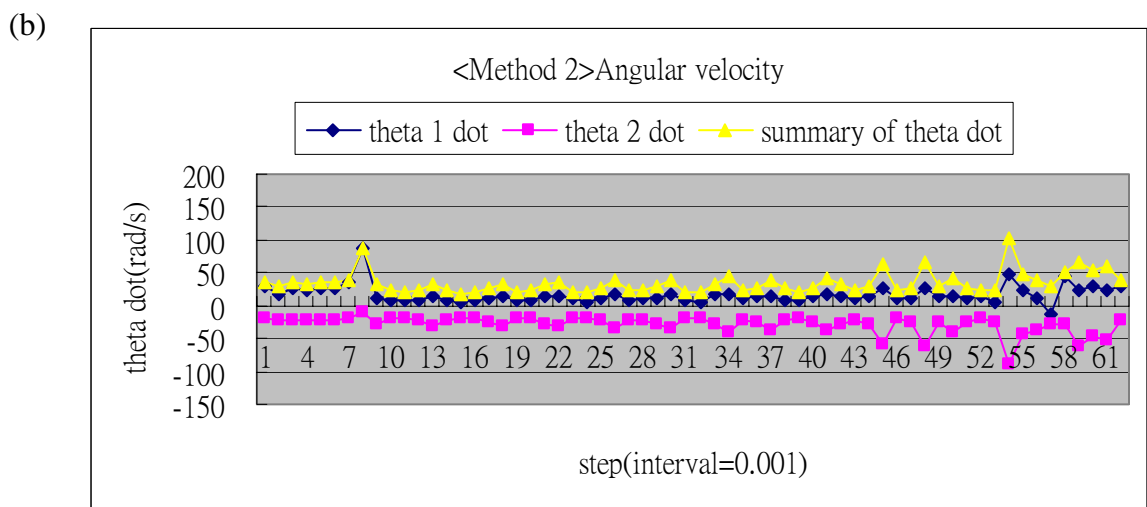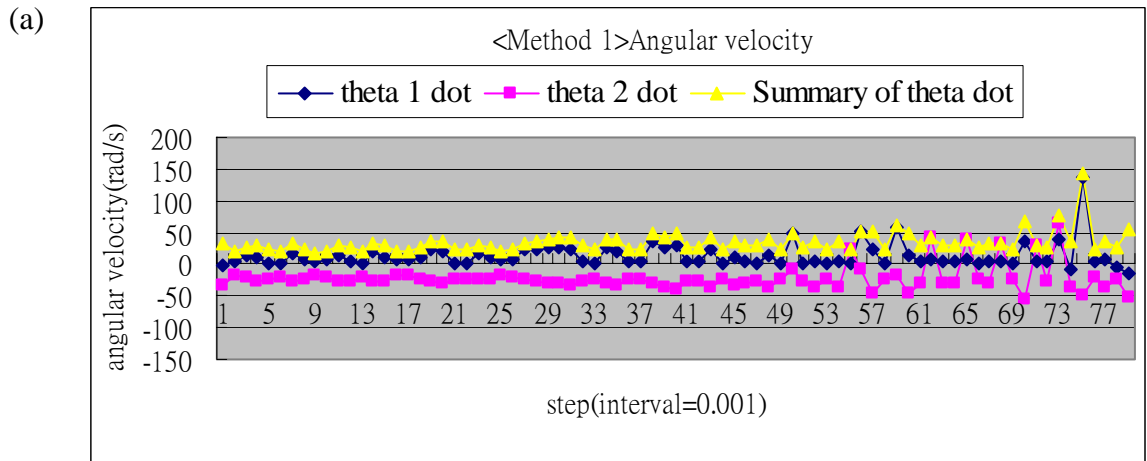
Fig. 4.8 (a) Angular velocity of method one.
(b) Angular velocity of method two.
(c) Comparison of angular velocity.

(a)
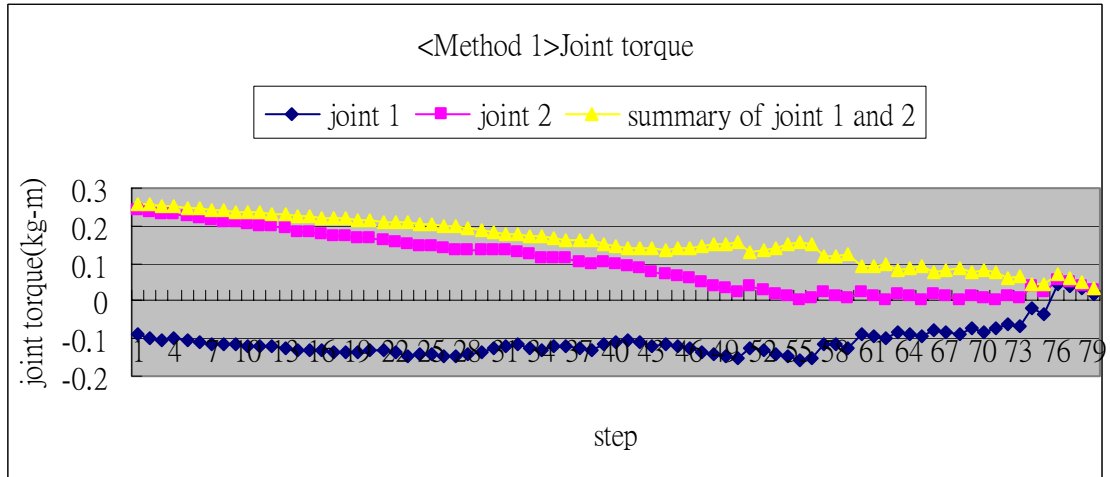
(b)
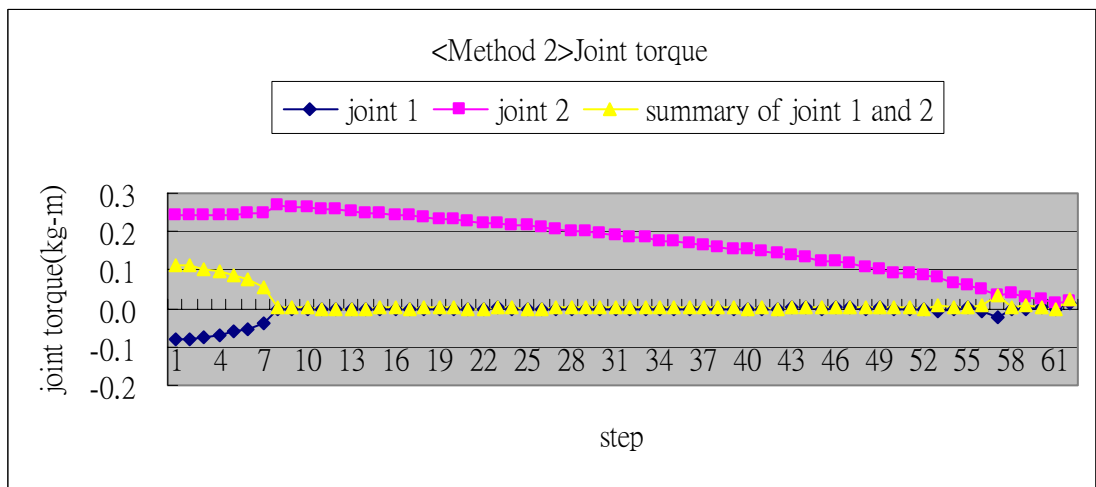
(c)
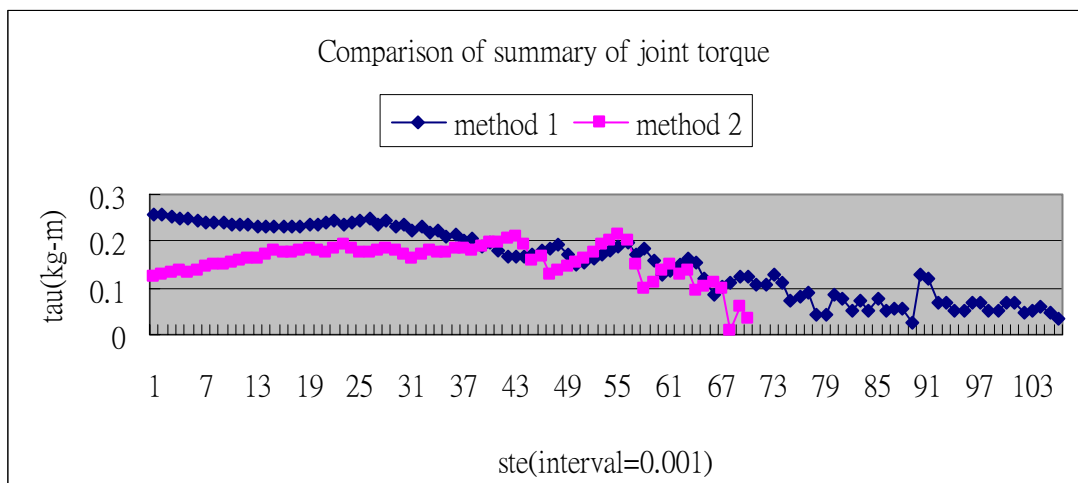
Fig. 4.9 (a) Joint torque of method one.
(b) Joint torque of method two.
(c) Comparison of Joint torque.
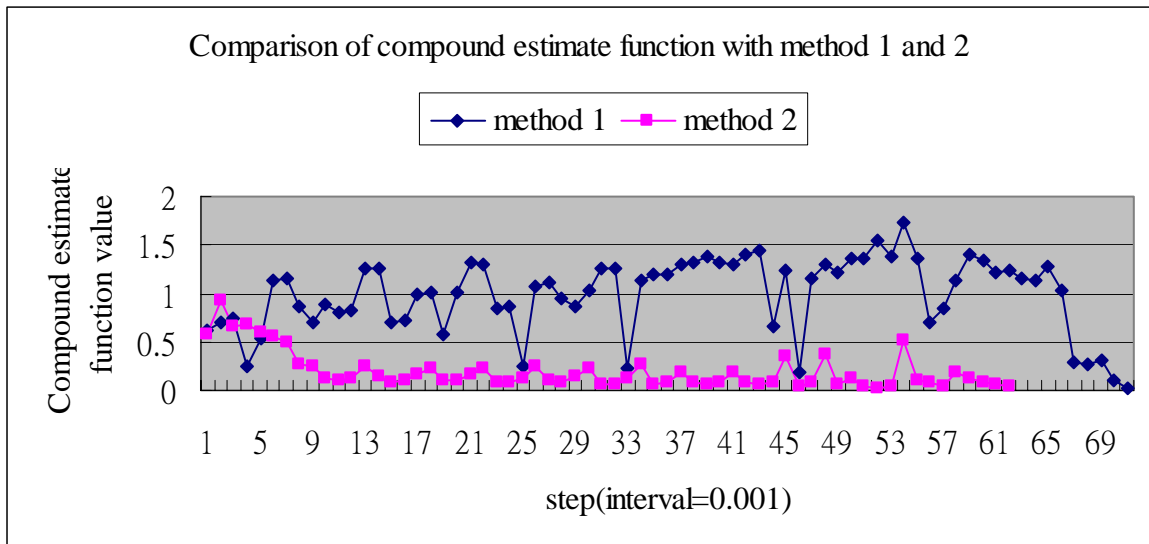
Fig. 4.10 Comparison of compound estimate function.

Table. 4.2 Comparison of method one and two.

Comparison of method one and two			
	Method 1*	Method 2*	Effect promoted
Summary of angular velocity (rad/s)	2478.101	2150.561	13.22%
Summary of joint torque (kg-m)	10.87964	0.78208	92.81%
Summary of compound estimate value	70.0806	11.827	
*Method 1: consider only the effective of minimum angular velocity combination. *Method 2: consider the compounds estimate function which include angular velocity and joint torque.			

(a)
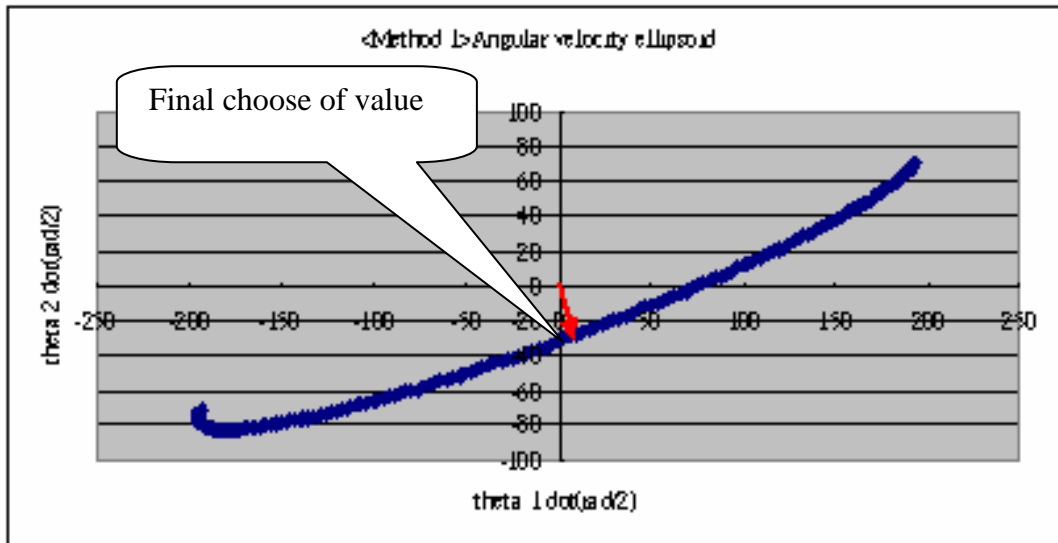
(b)
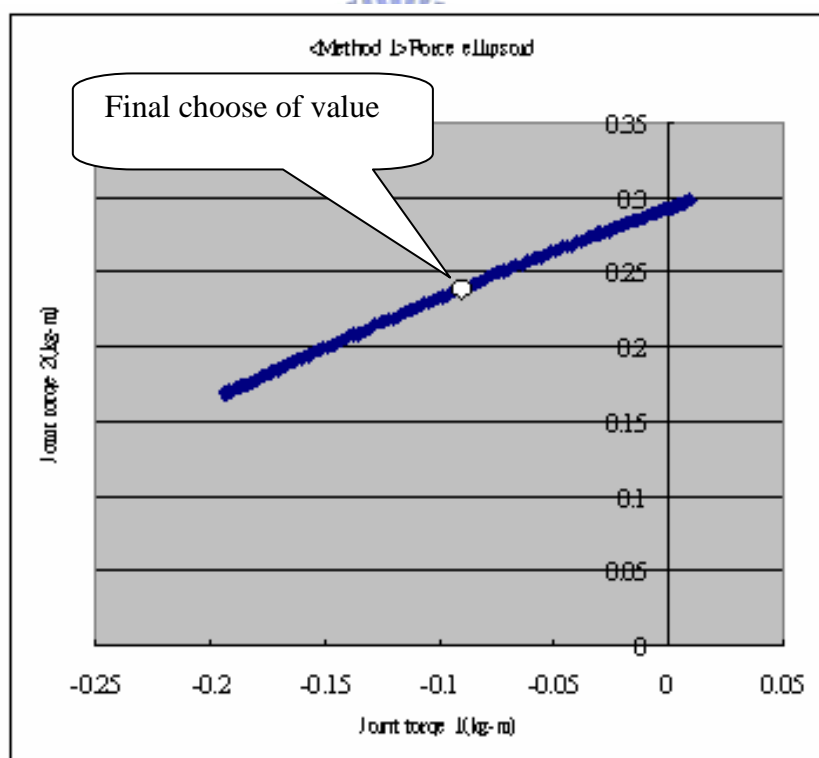
Fig. 4.11 Manipulability ellipsoid of method one in first interval.
(a) Angular velocity ellipsoid.
(b) Force ellipsoid.

(a)
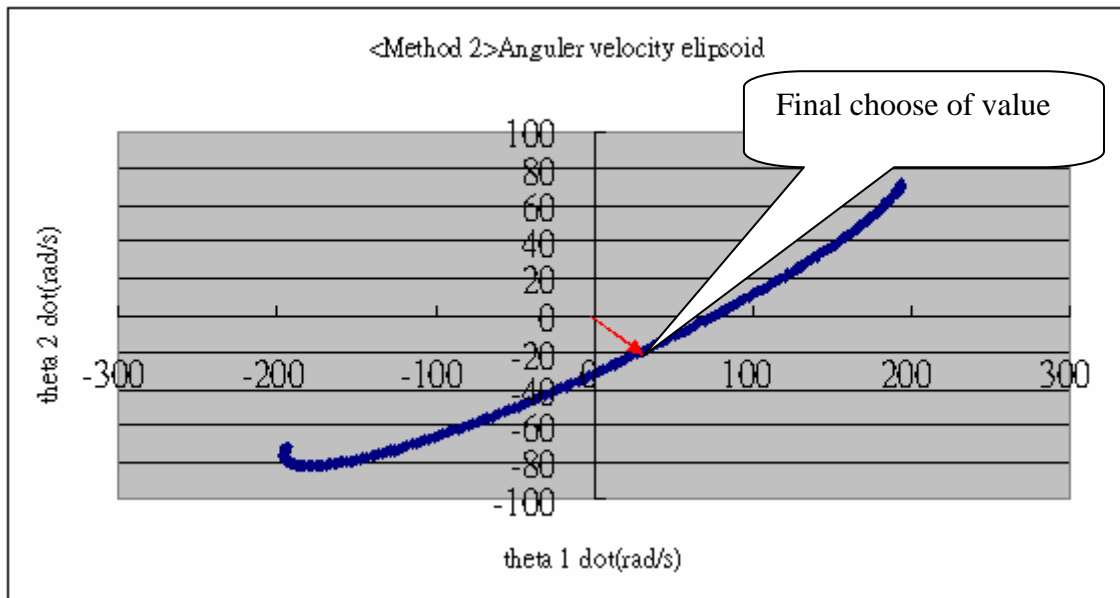
(b)
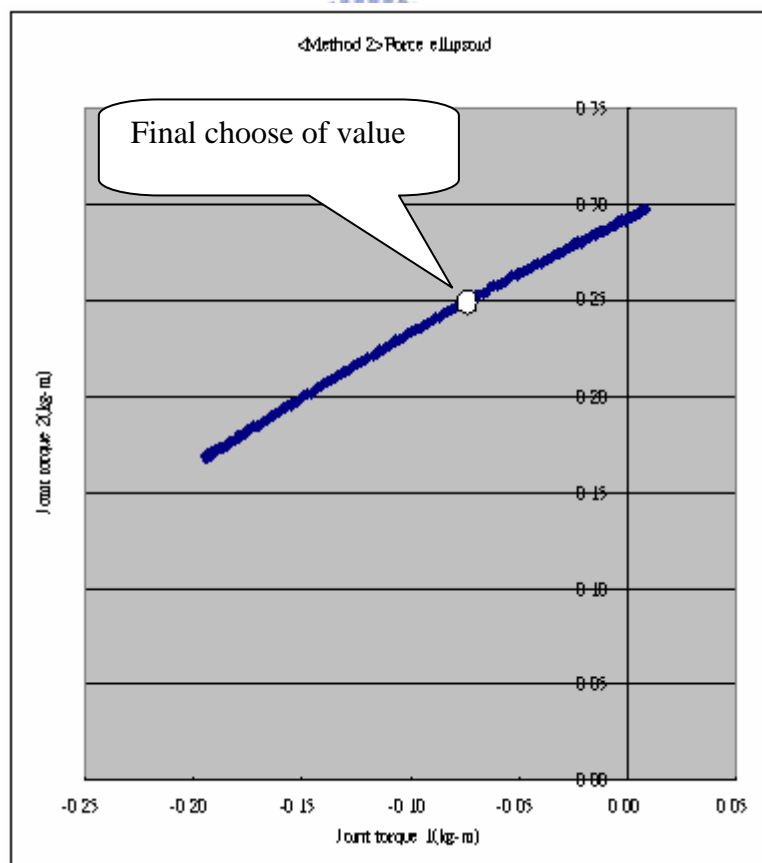
Fig. 4.12 Manipulability ellipsoid of method two in first interval.
(c) Angular velocity ellipsoid.
(d) Force ellipsoid.

4.3 Introduction of Envelope Two and Three

In our biped gait generation designing, the humanoid walking is the target for realizing by manipulability ellipsoid algorithm. The consequently motion of humanoid walking is shown as segment number two to sixteen in Fig. 4.13 and 4.14, and the parameters is listed in the Table 4.4 to 4.10. The characteristic of humanoid walking in this research can be concluding in several key points as below:

(1) Base on the static kinematics, the biped robot gait will be in the stable condition as long as the speed is in the low situation and without extremely high variation of angular velocity.

(2) A consequently biped robot gait can be divided into an arbitrary number of segments, each segment is a node as a control point, and we set the specific parameters such as configuration at each node, and connect arbitrary two nodes as a consequently process or a gait.

(3) Based on second point, we implement manipulability ellipsoidalgorithm, inverse kinematics, ZMP algorithm in the biped robot gait generation. Notice that the inverse kinematics was implemented only in the biped motion, landing (segment number five and eleven), which one leg is a support on ground, and another leg is from a initial posture, hung in the air, to a goal posture, touch the ground, and change the single support phase to double support phase. All nodes are in the constraint to satisfy the ZMP algorithm to yield a stable condition when biped robot is manipulating.

4.3.1 Process Flows of Envelope Two and Three

The correlation of manipulability ellipsoid and ZMP algorithm is shown in Fig. 4.15, the configuration in arbitrary interval of time is determined by manipulability ellipsoid, where the configuration include X-Y plane and Z-Y plane. When the configuration in X-Y plane and Z-Y plane were determined, the location of Q' must be checked if its location is within ZMP

area, which is defined by Fig. 3.5 (a) and (b). Suppose the location of Q' is satisfied with the ZMP area, then go to next process until finished the entire procedure, suppose the location is not satisfied with ZMP algorithm, then the configuration in Z-Y plane need to be modified until the condition is pass.

4.3.2 The Result of Simulation of Envelope Two and Three

From Fig. 4.16 (a) and (b), 4.17 (a) and (b), we can find out the variation of angular displacement and the location of ankle with both legs. We can classify the biped locomotion into several type situations, CoM moving, leg swing and landing. Notice that the CoM moving motion is for the purpose to maintain the balance either in double support condition or in single support condition. During the period of support area was changed, the support area which associate with the stability is extremely reducing to a small area, therefore, the constraint of location of CoM moving is much important. Arbitrary leg swing causes the location of ankle is changed, and the position of both leg will be exchanged to opposite one, then the original front leg exchange to back leg, and the back exchange to front leg.

From Fig. 4.18 (a) to (l) we can see the practical simulation of KHR-1 robot, the upper body of KHR-1 robot is always keep straight up, therefore the end-effector of link three of kinematical model of KHR-1 robot in X-direction will be the same as location of hip, point H. In this sense, we can simplify the kinematical model of KHR-1 robot to a two link serial type manipulator, and make the development of biped gait is easier.
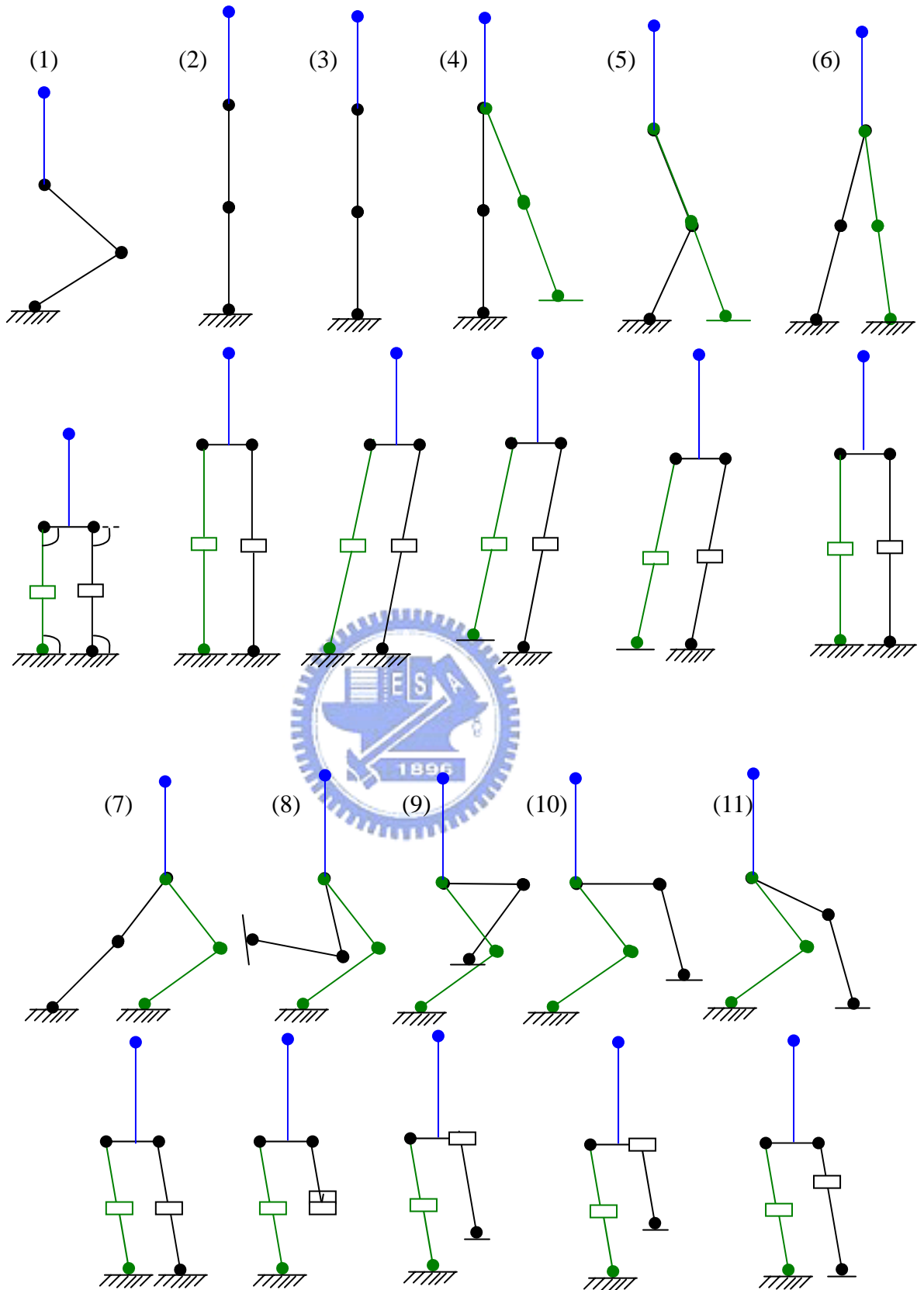
Fig. 4.13 Consequently locomotion of all envelopes.

(12)　(13)　(14)　(15)　(16)
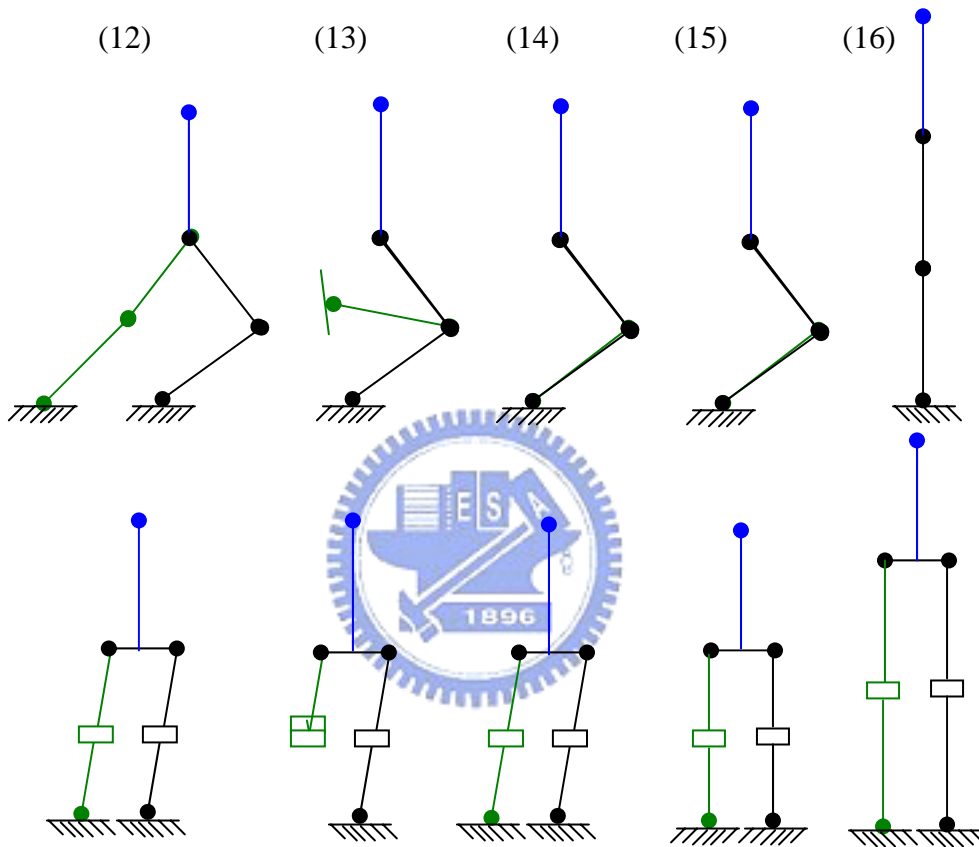
Fig. 4.14 Consequently locomotion of all envelopes.

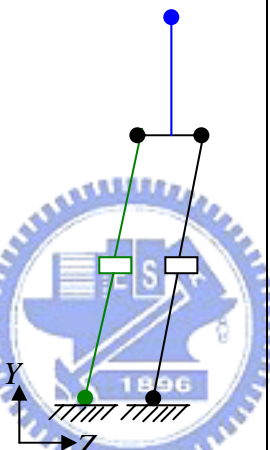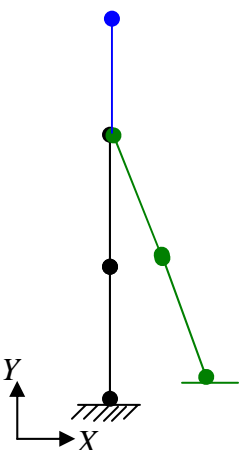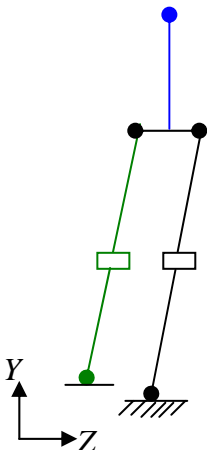Table 4.3 Detail process of biped gait generation in envelope two.
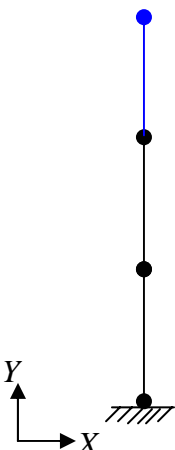
Detail Process of Biped Gait Generation in Envelope Two				
Status	Posture in X-Y Plane	Posture in Z-Y Plane	Angular Displacement	Range of Unity Circle of end-effector
Envelope 2			$\theta_{1F} = \theta_{1B} = 90$ $\theta_{2F} = \theta_{2B} = 0$ $\theta_{23F} = \theta_{19B} = 75$ $\theta_{17F} = \theta_{13B} = 105$	Front leg: $(V_Z - V_Y)$ $\theta_{V(FRONT)} = -90 \sim 0$ Back leg: $(V_Z - V_Y)$ $\theta_{V(BACK)} = -90 \sim 0$
			$\theta_{1F} = 133.1483$ $\theta_{2F} = 1$ $\theta_{1B} = 90$ $\theta_{2B} = 0$ $\theta_{23F} = \theta_{19B} = 75$ $\theta_{17F} = \theta_{13B} = 105$	Front leg: $(V_X - V_Y)$ $\theta_{V(FRONT)} = 0 \sim 90$

Table 4.4 Detail process of biped gait generation in envelope two.

Detail Process of Biped Gait Generation in Envelope Two				
Status	Posture in X-Y Plane	Posture in Z-Y Plane	Angular Displacement	Range of Unity Circle of end-effector
Envelope 2			$\theta_{1F} = 133.1483$ $\theta_{2F} = 1$ $\theta_{1B} = 48.5784$ $\theta_{2B} = 87.402$ $\theta_{23F} = \theta_{19B} = 75$ $\theta_{17F} = \theta_{13B} = 105$	Inverse kinematics for back leg
			$\theta_{1F} = 110$ $\theta_{2F} = 1$ $\theta_{1B} = 68.5011$ $\theta_{2B} = 2.2207$ $\theta_{23F} = \theta_{19B} = 90$ $\theta_{17F} = \theta_{13B} = 90$	Front leg: $(V_X - V_Y)$ $\theta_{V(FRONT)} = 0 \sim 90$ Front leg: $(V_Z - V_Y)$ $\theta_{V(FRONT)} = 90 \sim 180$ Back leg: $(V_Z - V_Y)$ $\theta_{V(BACK)} = 90 \sim 180$

Table 4.5 Detail process of biped gait generation in envelope three.

Detail Process of Biped Gait Generation				
Status	Posture in X-Y Plane	Posture in Z-Y Plane	Angular Displacement	Range of Unity Circle of end-effector
Envelope 3			$\theta_{1F} = 30.2536$ $\theta_{2F} = 106.7919$ $\theta_{1B} = 35.0228$ $\theta_{2B} = 2.072$ $\theta_{23F} = \theta_{19B} = 105$ $\theta_{17F} = \theta_{13B} = 75$	Front leg: $(V_X - V_Y)$ $\theta_{V(FRONT)} = -90 \sim 0$ Front leg: $(V_Z - V_Y)$ $\theta_{V(FRONT)} = -180 \sim -90$ Back leg: $(V_Z - V_Y)$ $\theta_{V(BACK)} = -180 \sim -90$
			$\theta_{1F} = 30.2536$ $\theta_{2F} = 106.7919$ $\theta_{23F} = \theta_{19B} = 105$ $\theta_{17F} = \theta_{13B} = 75$	Back leg: $(V_X - V_Y)$ $\theta_{V(BACK)} = 0 \sim 45$

Table 4.6 Detail process of biped gait generation in envelope three.

	Detail Process of Biped Gait Generation			
Status	Posture in X-Y Plane	Posture in Z-Y Plane	Angular Displacement	Range of Unity Circle of end-effector
Envelope 3			$\theta_{1F} = 30.2536$ $\theta_{2F} = 106.7919$ $\theta_{1B} = 70.6783$ $\theta_{2B} = 109.3218$ $\theta_{23F} = \theta_{19B} = 105$ $\theta_{17F} = \theta_{13B} = 75$	
			$\theta_{1F} = 30.2536$ $\theta_{2F} = 106.7919$ $\theta_{1B} = 112.5232$ $\theta_{2B} = 67.4768$ $\theta_{23F} = \theta_{19B} = 105$ $\theta_{17F} = \theta_{13B} = 75$	Back leg: $(V_X - V_Y)$ $\theta_{V(BACK)} = 0 \sim 90$

Table 4.7 Detail process of biped gait generation in envelope three.

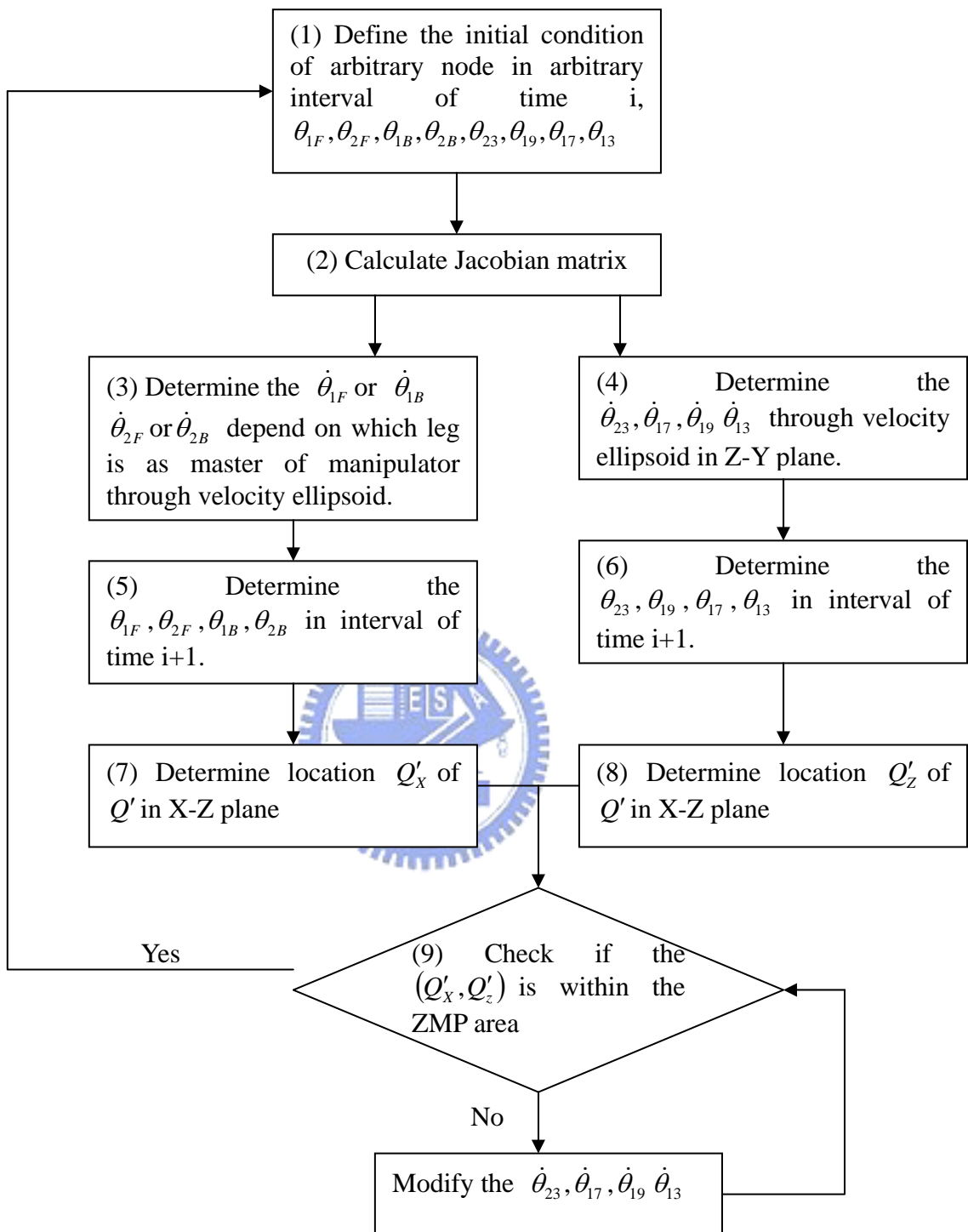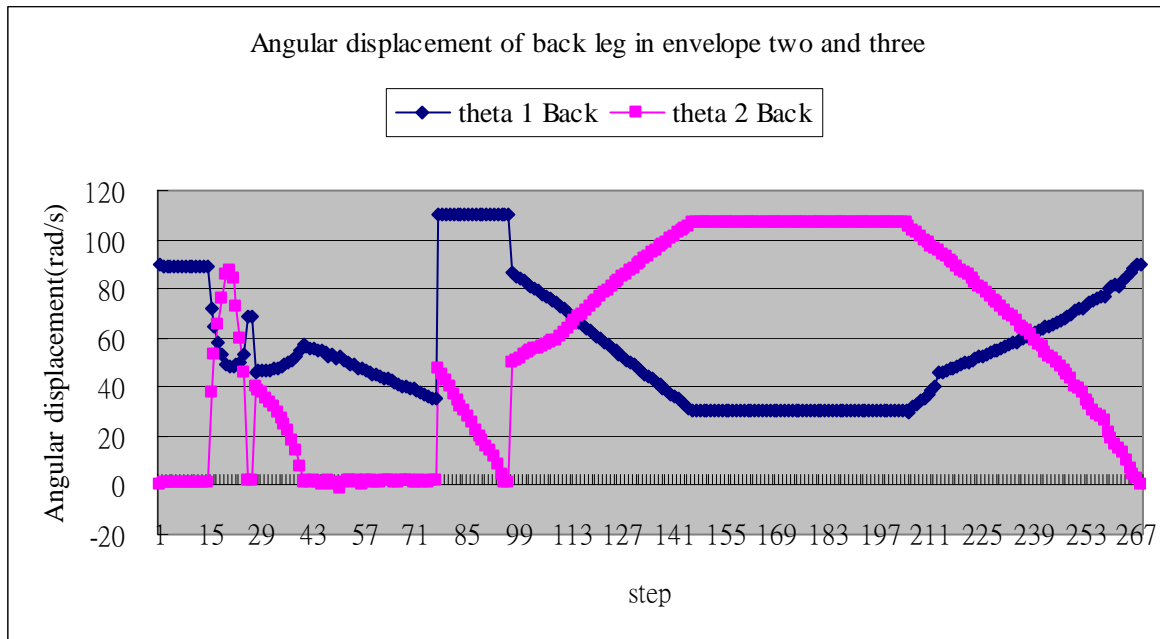| Detail Process of Biped Gait Generation				
Status	Posture in X-Y Plane	Posture in Z-Y Plane	Angular Displacement	Range of Unity Circle of end-effector
Envelope 3			$\theta_{1F} = 30.2536$ $\theta_{2F} = 106.7919$ $\theta_{1B} = 103.8462$ $\theta_{2B} = 67.4768$ $\theta_{23F} = \theta_{19B} = 105$ $\theta_{17F} = \theta_{13B} = 75$	Inverse kinematics for back leg
			$\theta_{1F} = 68.5011$ $\theta_{2F} = 2.2207$ $\theta_{1B} = 110$ $\theta_{2B} = 1$ $\theta_{23F} = \theta_{19B} = 90$ $\theta_{17F} = \theta_{13B} = 90$	Front leg: $(V_X - V_Y)$ $\theta_{V(FRONT)} = 0 \sim 90$ Front leg: $(V_Z - V_Y)$ $\theta_{V(FRONT)} = 0 \sim 90$ Back leg: $(V_Z - V_Y)$ $\theta_{V(BACK)} = 0 \sim 90$

Table 4.8 Detail process of biped gait generation in envelope three.

Detail Process of Biped Gait Generation				
Status	Posture in X-Y Plane	Posture in Z-Y Plane	Angular Displacement	Range of Unity Circle of end-effector
Envelope 3			$\theta_{1F} = 35.0228$ $\theta_{2F} = 2.072$ $\theta_{1B} = 30.2536$ $\theta_{2B} = 106.7959$ $\theta_{23F} = \theta_{19B} = 75$ $\theta_{17F} = \theta_{13B} = 105$	Front leg: $(V_X - V_Y)$ $\theta_{V(FRONT)} = -90 \sim 0$ Front leg: $(V_Z - V_Y)$ $\theta_{V(FRONT)} = -90 \sim 0$ Back leg: $(V_Z - V_Y)$ $\theta_{V(BACK)} = -90 \sim 0$
			$\theta_{1F} = 20.1544$ $\theta_{2F} = 116.9349$ $\theta_{1B} = 30.2536$ $\theta_{2B} = 106.7959$ $\theta_{23F} = \theta_{19B} = 75$ $\theta_{17F} = \theta_{13B} = 105$	Back leg: $(V_X - V_Y)$ $\theta_{V(BACK)} = 0 \sim 45$

Table 4.9 Detail process of biped gait generation in envelope three.

Status	Posture in X-Y Plane	Posture in Z-Y Plane	Angular Displacement	Range of Unity Circle of end-effector
Envelope 3			$\theta_{1F} = \theta_{1B} = 30$ $\theta_{2F} = \theta_{2B} = 105$ $\theta_{23F} = \theta_{19B} = 90$ $\theta_{17F} = \theta_{13B} = 90$	
			$\theta_{1F} = \theta_{1B} = 30$ $\theta_{2F} = \theta_{2B} = 105$ $\theta_{23F} = \theta_{19B} = 90$ $\theta_{17F} = \theta_{13B} = 90$	Front leg: $(V_X - V_Y)$ $\theta_{V(FRONT)} = 0 \sim 180$ Back leg: $(V_X - V_Y)$ $\theta_{V(BACK)} = 0 \sim 180$
			$\theta_{1F} = \theta_{1B} = 90$ $\theta_{2F} = \theta_{2B} = 0$ $\theta_{23F} = \theta_{19B} = 90$ $\theta_{17F} = \theta_{13B} = 90$	

Detail Process of Biped Gait Generation

Fig 4.15 Process Flows of Envelope Two and Three.

The flowchart contains the following boxes:

(1) Define the initial condition of arbitrary node in arbitrary interval of time i, $\theta_{1F}, \theta_{2F}, \theta_{1B}, \theta_{2B}, \theta_{23}, \theta_{19}, \theta_{17}, \theta_{13}$

(2) Calculate Jacobian matrix

(3) Determine the $\dot{\theta}_{1F}$ or $\dot{\theta}_{1B}$ $\dot{\theta}_{2F}$ or $\dot{\theta}_{2B}$ depend on which leg is as master of manipulator through velocity ellipsoid.

(4) Determine the $\dot{\theta}_{23}, \dot{\theta}_{17}, \dot{\theta}_{19}\ \dot{\theta}_{13}$ through velocity ellipsoid in Z-Y plane.

(5) Determine the $\theta_{1F}, \theta_{2F}, \theta_{1B}, \theta_{2B}$ in interval of time i+1.

(6) Determine the $\theta_{23}, \theta_{19}, \theta_{17}, \theta_{13}$ in interval of time i+1.

(7) Determine location Q'_X of Q' in X-Z plane

(8) Determine location Q'_Z of Q' in X-Z plane

(9) Check if the (Q'_X, Q'_z) is within the ZMP area

Yes

No

Modify the $\dot{\theta}_{23}, \dot{\theta}_{17}, \dot{\theta}_{19}\ \dot{\theta}_{13}$

83

Fig 4.16 (a) Angular displacement of front leg.
(b) Angular displacement of back leg.

(a)

Location of front ankle

(b)

Location of back ankle
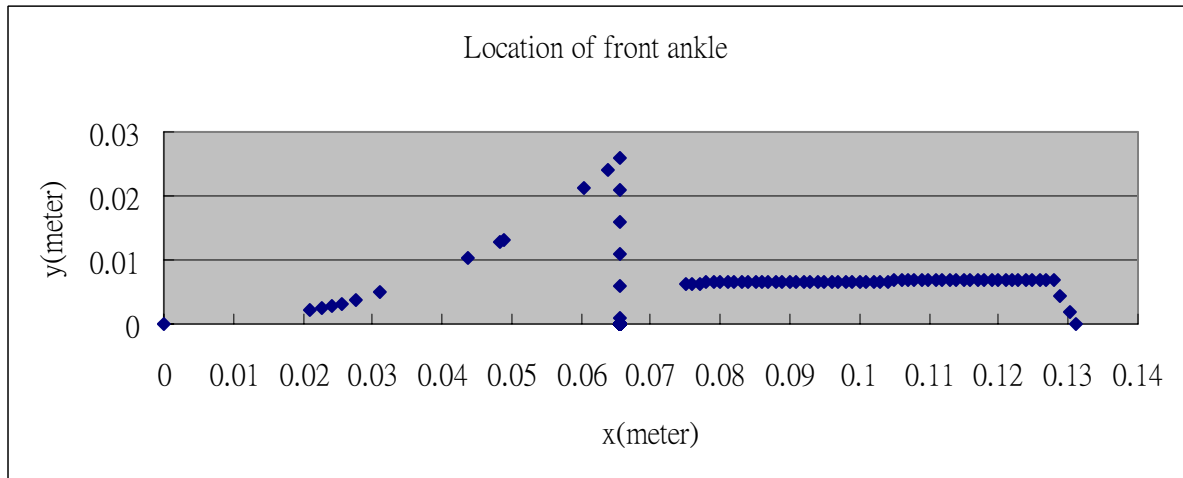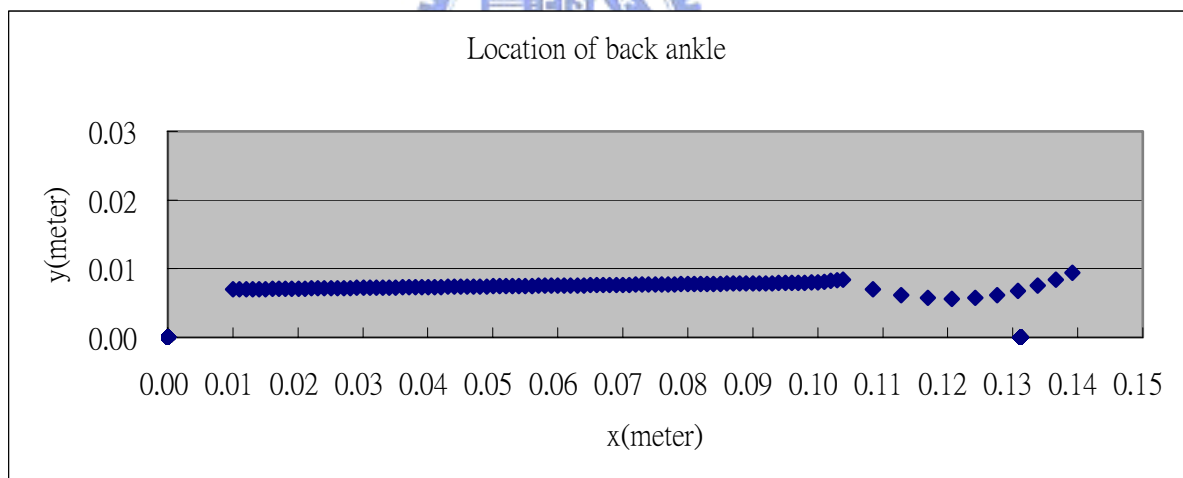
Fig 4.17 (a) Location of front ankle.
(b) Location of back ankle.

(a)
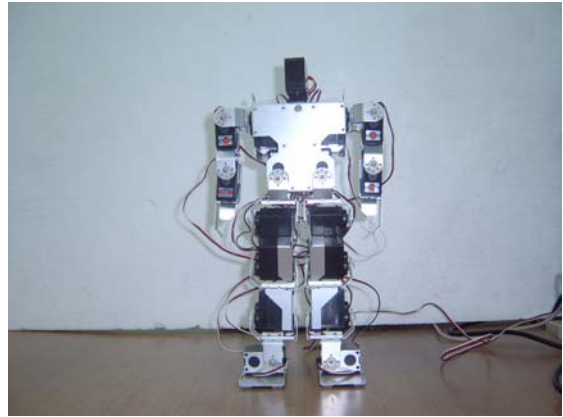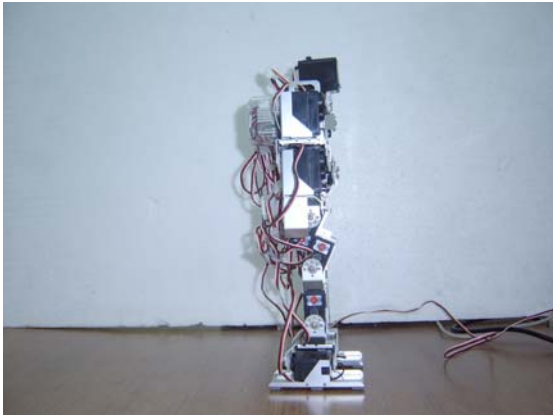
(b)
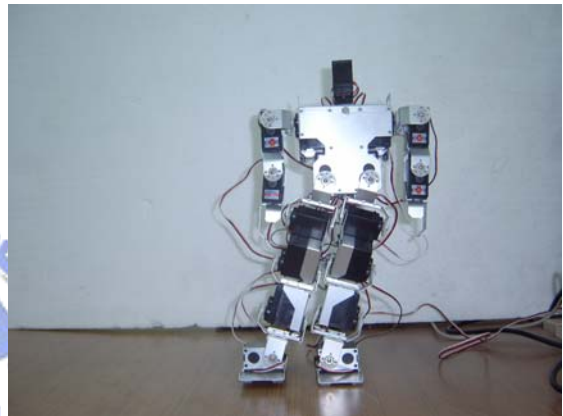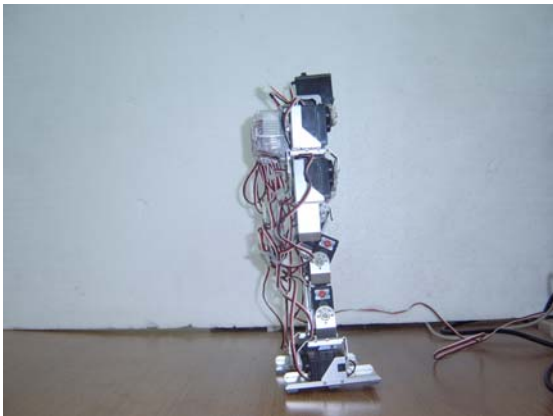
(c)
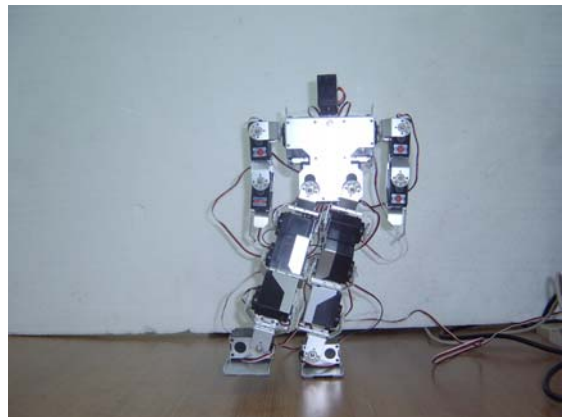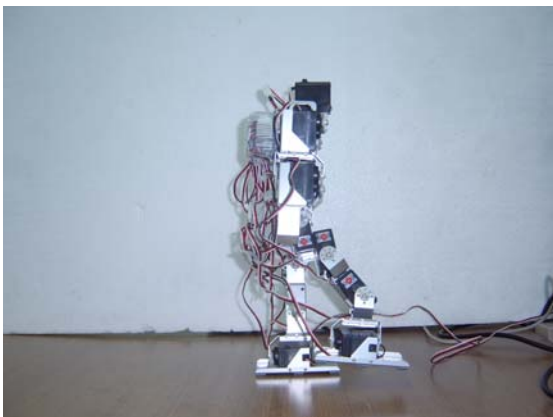
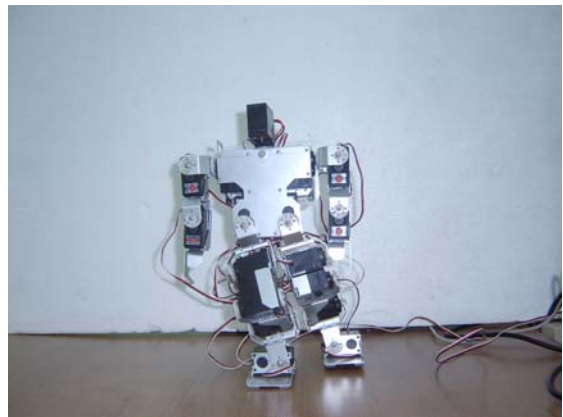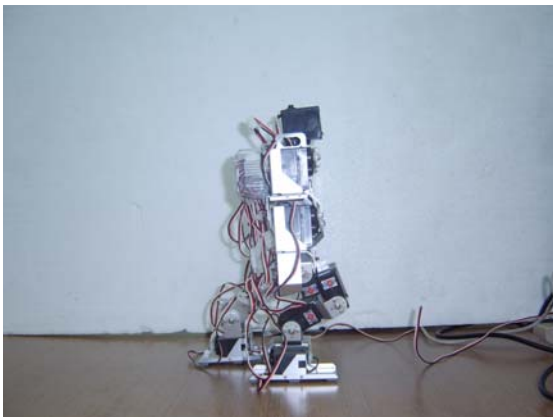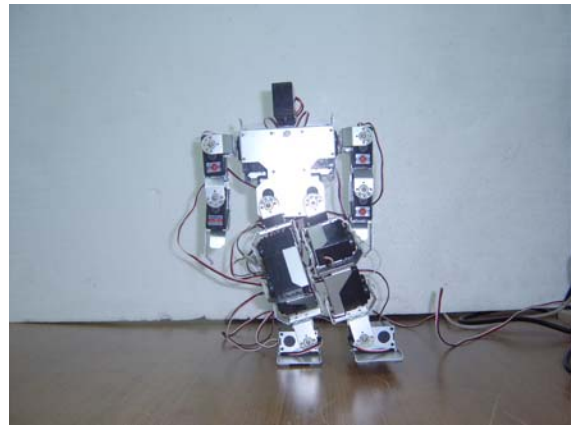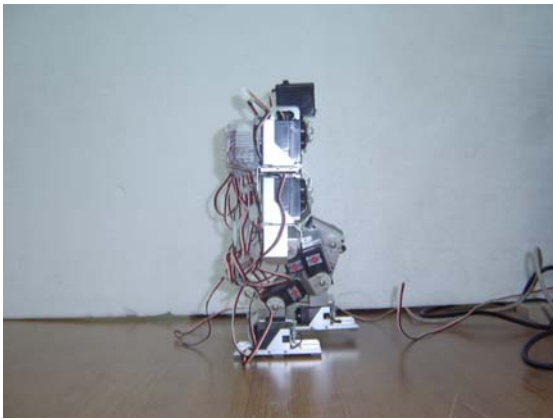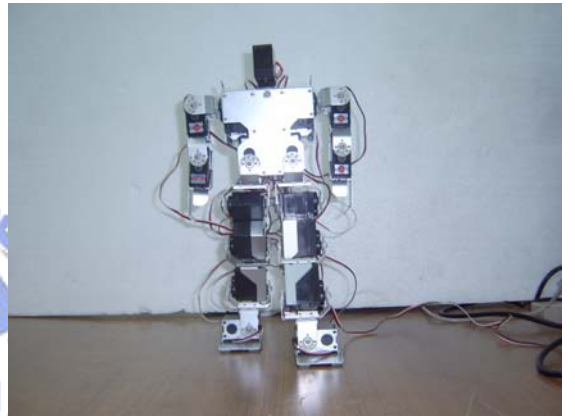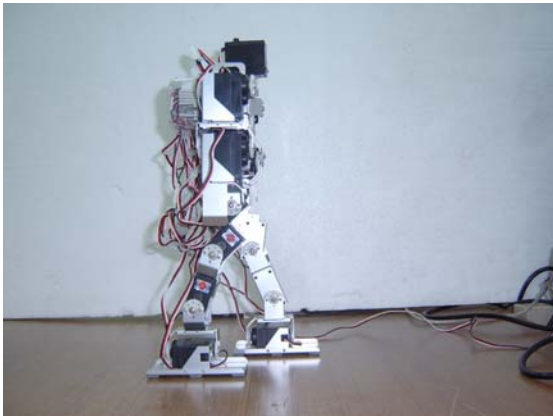Fig. 4.18 (1) Practical simulation of envelope two and three.

(d)
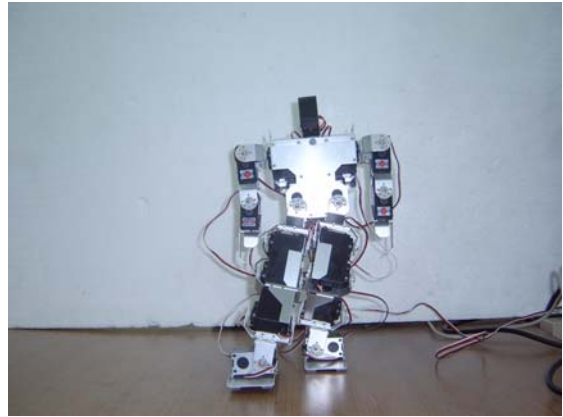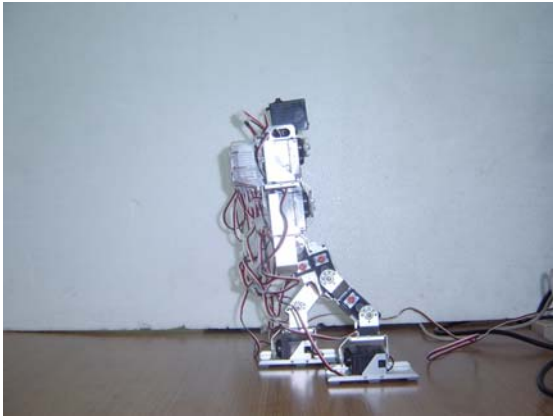
(e)
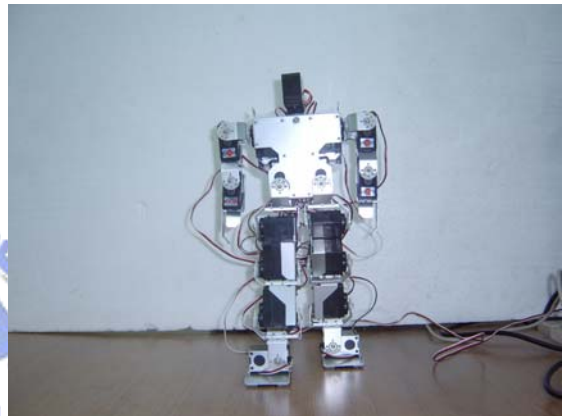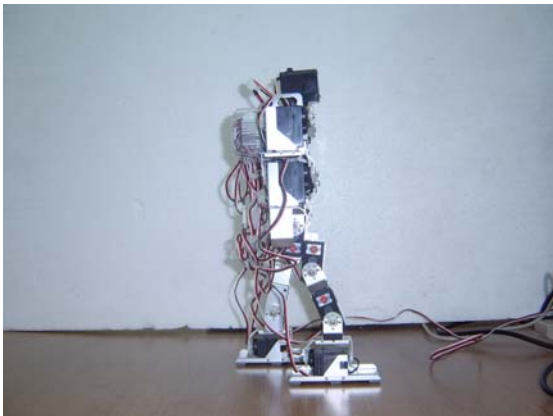
(f)

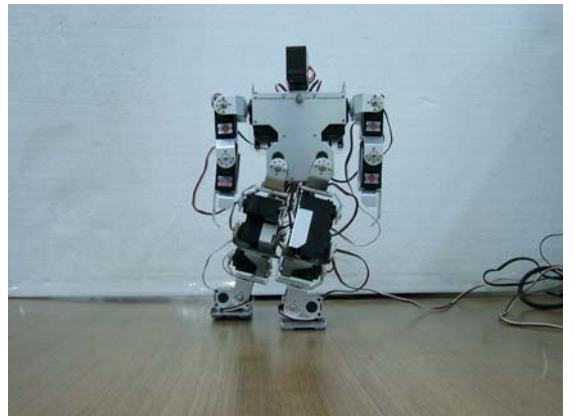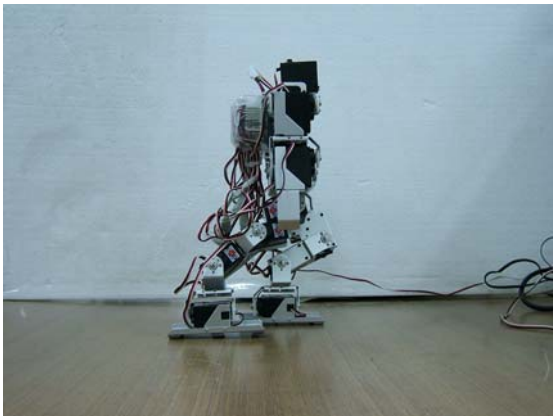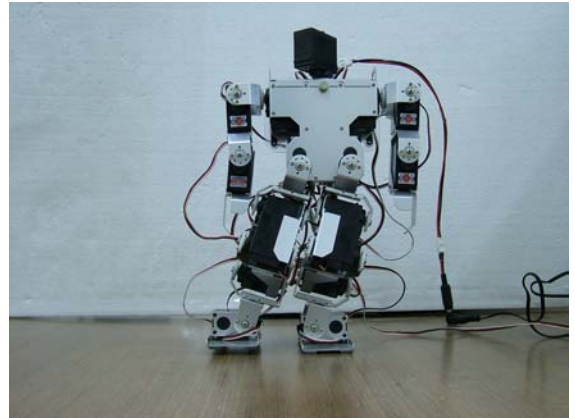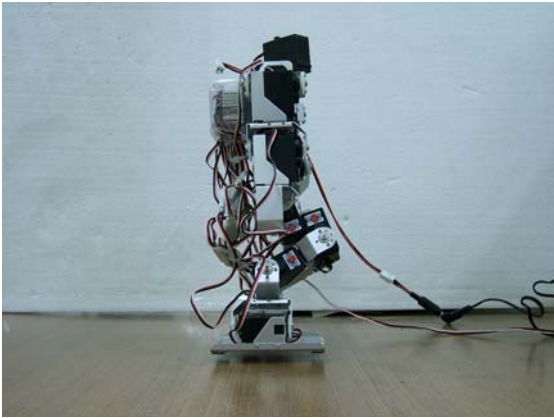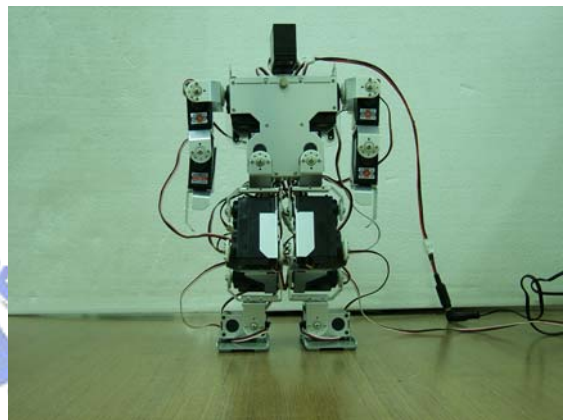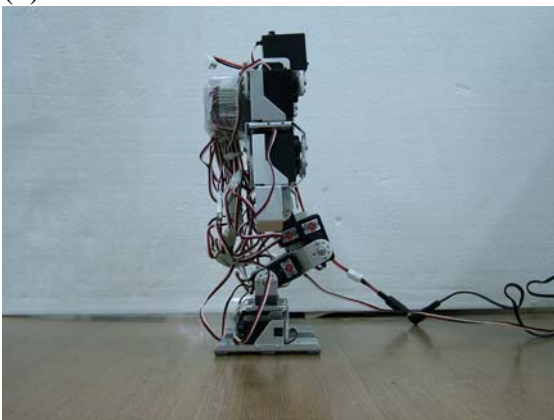Fig. 4.18(2) Practical simulation of envelope two and three.

(g)

(h)

(i)

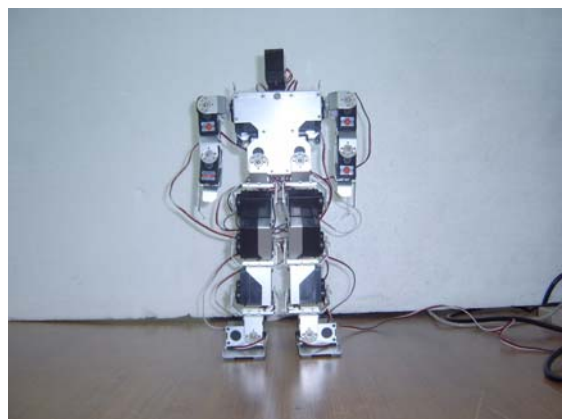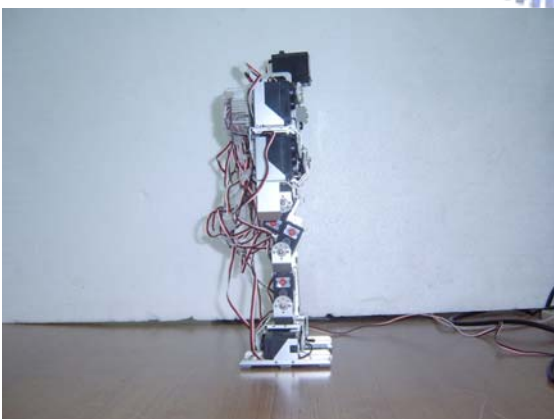Fig. 4.18 (3) Practical simulation of envelope two and three.

(j)

(k)

(l)

Fig. 4.18 (4) Practical simulation of envelope two and three.

CHAPTER 5

Conclusions and Future Work

The trajectory planning of biped robot is a significant study in biped robot research and implementation. In this thesis we proposed a gait generation method based on a manipulability ellipsoid algorithm to design a series of gait envelops, such as squat to stand, humanoid walking motion for KHR-1 biped robot. The object of the study are mainly simplifying the procedure of biped robot motion design, reducing the cycle-time of trajectory planning, and providing a stable and successfully trajectory data. Any point on the unity end-effector velocity circle in the proposed manipulability ellipsoid method represents the linear velocity of end-effector of a robot manipulator. And it can be mapped to a corresponding point which represents the angular velocity of each joint on the velocity ellipsoid.
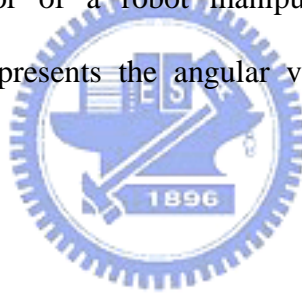
5.1 Conclusions

Several significant results of the current research are summarized and listed as follows.

(1) A new biped robot gait generation methodology is proposed, which can shorten and simplify the cycle time of gait planning of the locomotion of biped robot. Based on the manipulability ellipsoid algorithm, the proposed method can assist to generate the high stability motion gait. Zero-Moment point (ZMP) algorithm has also been introduced into the planning system as the stability criteria of joint trajectory generation for the KHR-1 biped robot instead of using try and error processes which is time consuming.

(2) Based on the manipulability ellipsoid algorithm, the output of joint torque will further be planed to reduce energy consumption in specific biped robot gait.

(3) A multilink biped robot with more than ten degree of freedoms has been assembled

and input with prescribed gait data. The verification of the microchip controlled biped walking robot via some typical gait envelopes has demonstrated its advantage and usefulness on the gait planning using the proposed methodology.

5.2 Future Work

The future research of biped robot gait will be extended from several aspects:

(1) The investigation of the characteristics of velocity ellipsoid in terms of dynamic parameters. The Lagrangian formulation of the dynamics model will be derived for assisting to the angular acceleration planning.

(2) The trajectory planning will be focused on complex and highly dynamic biped motion. The object of future research includes that designing the various complex biped motion such as high speed walking, running, non-symmetric motion in a shorter cycle-time.

(3) Zero-moment-point algorithm and global dynamics will be applied for planning the gait for dynamic motion.

(4) The simulation software such as ADAMS can be acted as a vehicle which simulate the robot system with some specific parameters and observe either the processes or results in numerical data and video for further evaluation on dynamics of the biped robot.

Reference

[1] Fujimoto, Y., "Trajectory generation of biped running robot with minimum energy consumption", Robotics and Automation, 4, pp. 3803 – 3808, April 2004.

[2] Tang, Z., Zhou, C., Sun, Z., "Trajectory Planning for Smooth Transition of a Biped Robot", Robotics and Automation, 2, pp. 2455 – 2460, September 2003.

[3] McGee, T. G., Spong, M. W., "Trajectory Planning and Control of a Novel Walking Biped", Control Applications, 5-7, pp. 1099 – 1104, September 2001.

[4] Chiacchio, P., Chiaverini, S., Sciavicco, L., Siciliano, B., "Global Task Space Manipulability Ellipsoids for Multiple Arms System", Robotics and Automation, 7, pp. 678 – 685, October 1991.

[5] Tao, J. M., Luh, J. Y. S., "Coordination of Two Redundant Robots", Robotics and Automation, 1, pp. 425 – 430, May 1989.

[6] Lee, J., "A Study on the Manipulability Measures for Robot Manipulators", Intelligent Robots and Systems, 3, pp. 1458 – 1465, September, 1997.

[7] Lee, K. M., Johnson, R., "Static Characteristics of an In-Parallel Actuated Manipulator for Clamping and Bracing Application", Robotics and Automation, 3, pp. 1408 – 1413, May 1989.

[8] Yamamoto, T., Kuniyoshi, Y., "Stability and controllability in a rising motion: a global dynamics approach", Intelligent Robots and System, 3, pp. 2467 – 2472, September 2002.

[9] Hirai, K., Hirose, M., Haikawa, Y., Takenaka, T., "The development of Honda humanoid robot", Robotics and Automation, 2, pp. 1321 – 1326, May 1998.

[10] Goswami, A., Kallem, V., "Rate of change of angular momentum and balance maintenance of biped robots", Robotics and Automation, 4, pp. 3785 – 3790, April 2004.

[11] Tsai, L. W., <u>Robot Analysis-The Mechanics of Serial and Parallel Manipulator</u>, John Wiley & Song, Inc., New York, 1999.

[12] Salisbury, J. K., <u>Kinematic and Force Analysis of Articulated Mechanical Hands</u>, Mechanical Engineering Department, Stanford University, Stanford, CA, 1982.

[13] Vukobratovich, M., Borovac, B., "Zero-Moment Point-Thirty Five Years of Its Life", <u>International Journal of Humanoid Robotics</u>, Vol. 1, No. 1, pp. 158-173, January 2004.

[14] Sardain, P., Bessonnet, G., "Forces Acting on a Biped Robot. Center of Pressure—Zero Moment Point", Vol. 34, No. 5, pp. 630 – 637, September 2004.